



Numerical Investigation of the Hydrodynamic Performances of Marine Propeller

Carlos Parra Contreras

Master Thesis

presented in partial fulfillment
of the requirements for the double degree:
"Advanced Master in Naval Architecture" conferred by University of Liege
"Master of Sciences in Applied Mechanics, specialization in Hydrodynamics,
Energetics and Propulsion" conferred by Ecole Centrale de Nantes

developed at "Dunarea de Jos" University of Galati
in the framework of the

"EMSHIP"
Erasmus Mundus Master Course
in "Integrated Advanced Ship Design"

Ref. 159652-1-2009-1-BE-ERA MUNDUS-EMMC

Supervisor : Prof.Mihaela Amoraritei, University "Dunarea de Jos" of Galati.

January 2013



Universität
Rostock



Traditio et Innovatio



Zachodniopomorski
Uniwersytet
Technologiczny
w Szczecinie

TABLE OF CONTENTS

ABSTRACT	6
1. INTRODUCTION	7
1.1. BRIEF LIST OF RESEARCHES	9
1.2. CFD ANALYSIS	10
1.2.1. 2D flow computation	10
1.2.2. 3D flow computation	10
2. THEORETICAL FRAMEWORK	11
2.1. PROPELLER CHARACTERISTICS	11
2.1.1 Propeller geometry	11
2.1.2 Open water characteristics	15
2.1.3 Behind-hull propeller characteristics	16
2.2. STANDARD SERIES DATA	17
2.2.1 Wageningen B-screw series	17
2.3. PROPELLER THEORIES	22
2.3.1 Momentum theory	22
2.3.2 Lifting-line methods	23
2.3.3 Lifting-surface method	25
2.3.4 Boundary element method/panel method	27
2.3.5 RANSE method	27
2.4. GOVERNING EQUATIONS OF CFD METHOD	28
2.4.1 Continuity equation: Mass conservation	28
2.4.2 The momentum Equation: Force Balance	28
2.4.3 Additional Equations for Turbulent Flow	29
3. METHODOLOGY: PROPELLER DESIGN	30
3.1. DEFINITION OF THE PROBLEM	32
3.2. FIRST STAGE: PRELIMINARY DESIGN	35
3.2.1 Propeller revolution rate (<i>rpm</i>)	36
3.2.2 Diameter of the propeller	36
3.1.3 Number of Blades <i>Z</i>	37
3.1.4 Pitch ratio <i>P/D</i>	38
3.1.5 Blade area ratio(<i>blade outline</i>)	38
3.1.6 Skew	39
3.1.7 The boss diameter	39
3.1.8 The radial distribution of loading	39
3.1.9 Expanded blade area ratio A_E/A_o	40
3.1.9 wake fraction <i>w(x)</i>	40
3.3. SECOND STAGE: DETAIL DESIGN PHASE	40
3.3.1 The lifting line theory with lifting surface corrections method	41
3.4. THIRD STAGE: ANALYSIS	58
3.4.1 Turbulence model	58
4. ANALYSIS AND RESULTS	59
4.1 DEFINITION OF THE PROBLEM	59
4.2. FIRST STAGE: PRELIMINARY DESIGN	62
4.2.1 Use of Wageningen-B series to obtain the optimum diameter <i>D</i>	62
4.3. SECOND STAGE: DETAIL DESIGN PHASE	68
4.3.1 Design of the non-dimension relations of the blade sections	68
4.3.2. Generation of the section geometry	71
4.3.3 Result of the lifting-line with surface corrections method	74
4.4. THIRD STAGE: ANALYSIS OF THE DESIGN	74

4.4.1 Numerical Analysis in 2D of the geometry of blade's sections in Fluent.....	74
4.4.2 Numerical Analysis in 3D of the entire propeller in Fluent	81
4.4.1 Generation of the 3D propeller and fluid domain.....	83
4.4.2 Setting up of the RANS analysis in Fluent	88
4.5. POST-PROCESSING AND RESULTS.....	88
4.5.1. Thrust and Torque for operational speed V_S	88
4.5.2. Analysis of the velocity and pressure field.....	90
4.5.3. Developpe of the K_T , K_Q and η_o Diagrams.	95
5. CONCLUSIONS	100
6. REFERENCES	101
APPENDIX A1	103

TABLE OF FIGURES

FIGURE 2.1 PROPELLER GEOMETRY, (BOOK: PRACTICAL SHIP HYDRODYNAMICS, BERTRAM)	11
FIGURE 2.2 HELICOIDAL SURFACE , (BOOK: PRACTICAL SHIP HYDRODYNAMICS, BERTRAM)	12
FIGURE 2.3 PITCH LINES , (BOOK: MARINE PROPELLERS AND PROPULSION, CARLTON)	13
FIGURE 2.4 OPEN-WATER PROPELLER DIAGRAM	16
FIGURE 2.5 FOIL REPRESENTED BY BOUND VORTEX AND TRAILING VORTICES.....	24
FIGURE 2.6 FOIL REPRESENTED BY A DISTRIBUTION OF HORSESHOE VORTICES.....	24
FIGURE 2.7 VORTEX SYSTEM OF A WING WITH CIRCULATION VARYING ALONG THE SPAN	25
(BASIC SHIP PROPULSION, GHOSE AND GOKARN).....	25
FIGURE 2.8 VORTEX-LATTICE ELEMENTS ALLOCATED ON A PROPELLER BLADE (PRACTICAL SHIP HYDRODYNAMICS,.....	26
FIGURE 3.1 THE PHASES OF PROPELLER DESIGN (CARLTON)	31
FIGURE 3.2 TYPICAL OPTIMUM OPEN-WATER EFFICIENCIES FOR DIFFERENT PROPELLER TYPES (SNAME.....	33
FIGURE 3.3 TYPICAL PROPELLER DESIGN POINT (CARLTON)	34
FIGURE 3.4 KRAMER'S THRUST COEFFICIENT CURVES (A PROPELLER DESIGN METHOD, 1955)	44
FIGURE 3.5 GOLDEIN FUNCTIONS (K) FOR FOUR-BLADED PROPELLERS (A PROPELLER DESIGN METHOD, 1955)	46
FIGURE 3.6 MINIMUM PRESSURE ENVELOPES FOR NACA-66	50
FIGURE 4.0 PREDICTION OF THE RESISTANCE OF THE SHIP.....	60
FIGURE 4.1 K_Q OVER J FOR A GIVEN P_D	63
FIGURE 4.2 INTERSECTIONS FOR K_Q CURVES	64
FIGURE 4.3 INTERSECTIONS FOR K_Q CURVES ZOOMED	65
FIGURE 4.4 OPTIMUM J AND MAXIMUM OPEN-WATER EFFICIENCY.....	66
FIGURE 4.5 FLOWCHART OF THE LIFTING LINE THEORY WITH SURFACE CORRECTIONS	70
FIGURE 4.6 GENERAL DEFINITION OF AN AEROFOIL SECTION	71
FIGURE 4.7 AEROFOIL SECTION DEFINITION.....	71
FIGURE 4.8 DEFINITION OF THE EDGES AT EACH RADIUS.	73
FIGURE 4.9 TYPICAL FLUID DOMAIN IN 2D FOR THE ANALYSIS OF AN AIRFOIL	75
FIGURE 4.10 BOUNDARY LAYER APPLIED TO THE AIRFOIL AT $R/R=0.2$	76
FIGURE 4.11 COMPLETE MESHING OF THE FLUID DOMAIN FOR AIRFOIL AT $R/R=0.2$	76
FIGURE 4.12 CONTOURS OF STATIC PRESSURE FOR EACH SECTION	78
FIGURE 4.13 THRUST AND TORQUE OF THE BLADE ELEMENT	79
FIGURE 4.14 DEFINITION OF AN ARBITRARY POINT P ON A PROPELLER BLADE SURFACE. (CARLTON)	82
FIGURE 4.15. GEOMETRY OF THE SINGLE BLADE GENERATED IN GAMBIT.	84
FIGURE 4.16. VOLUME CREATED OF THE SINGLE BLADE.....	85
FIGURE 4.17. FINAL VOLUME OF THE PROPELLER.....	85
FIGURE 4.18 SCHEME OF THE PROPELLER AND FLUID DOMAIN	86
FIGURE 4.19A FINAL MESHING OF THE FLUID DOMAIN AND THE PROPELLER	87
FIGURE 4.19B FINAL MESHING OF THE PROPELLER	87
FIGURE 4.20 REPORT OF THE FORCE IN THE "X" DIRECTION	89
FIGURE 4.21 CONVERGENCE AT ITERATION 740	89
FIGURE 4.22. REPRESENTATION OF THE MOMENTUM THEORY. (BERTRAM, 2000) WHERE U_A AND U_J ARE	91
FIGURE 4.23 DISTRIBUTION OF PRESSURE OVER THE FACE SIDE OF THE PROPELLER AT $J=0.53$	92
FIGURE 4.24 DISTRIBUTION OF PRESSURE OVER THE BACK SIDE OF THE PROPELLER $J=0.53$	92
FIGURE 4.25 IDEALIZED PRESSURE DISTRIBUTION OVER AN AEROFOIL WITHOUT TURBULENCE.	93
FIGURE 4.26 EFFECT OF THE PROPELLER ON THE VELOCITY SLIPSTREAM	94
FIGURE 4.28. K_T AND K_Q DIAGRAM COMPARING RANS METHOD AND WAGENINGEN-B SERIES CHART.	97

Declaration of Authorship

I declare that this thesis and the work presented in it are my own and have been generated by me as the result of my own original research.

Where I have consulted the published work of others, this is always clearly attributed.

Where I have quoted from the work of others, the source is always given. With the exception of such quotations, this thesis is entirely my own work.

I have acknowledged all main sources of help.

Where the thesis is based on work done by myself jointly with others, I have made clear exactly what was done by others and what I have contributed myself.

This thesis contains no material that has been submitted previously, in whole or in part, for the award of any other academic degree or diploma.

I cede copyright of the thesis in favour of the University of Galati "Dunarea de Jos".

Date: 21-01-2013

Signature

A handwritten signature in blue ink, consisting of several loops and a long horizontal stroke, followed by a period.

ABSTRACT

a) Objective:

The master thesis will be focused on 2D/3D numerical investigations of flow field around marine propeller. The problems will be solved using the commercial code: FLUENT. The propeller geometry is known. Aspects of flow field around propeller blades, including global hydrodynamic performance, velocity and pressure distributions will be analyzed.

b) Content (preliminary):

In the last few years, RANS codes have been rapidly integrated in the propeller design process and they are routinely used to predict marine propeller performances. The viscous flow around propeller blades can be derived from the fundamental equations of fluid flow, using adequate boundary conditions.

Numerical Investigation of the Hydrodynamic Performances of Marine Propeller in steady flow will be approached in two ways:

- 2D flow computation

Using lifting line theory with lifting surface corrections, the propeller blade sections, the resultant velocities and the angles of attack (at various radii), will be computed. These results will be used as input data for a 2D numerical investigation of flow field around blade profiles.

- 3D flow computation

The numerical simulation of 3D flow around marine propeller will be performed in two cases: first, the computational domain will be cylindrical, including all propeller blades. Second, the computational domain will include only one propeller blade and rotational periodic boundary conditions will be used to reduce mesh size.

Using incompressible RANS computations with different turbulence models, the flow around marine propeller will be numerically simulated to find out the pressure distribution on the blades and to define the propeller hydrodynamic characteristics.

1. INTRODUCTION

During the last decade the huge increase in power and ship speed for all kind of vessels has been demanding propulsion devices every time more efficient in order to absorb the minimum power, with minimum cavitation, noise and vibrations.

The design of a propeller operating in steady flow can be considered the first approach of the propeller performance, then the design should be followed by the study in non-uniform flow behind the ship taken as an iterative process to optimise the propeller efficiency with less restrictive constraints concerning cavitation, noise, vibrations, geometry and strength. The propeller is an important source of noise and the main source of vibration. For the performance of the ship, cavitation is related to noise and pressure pulses and bearings forces induced by propeller are related to vibrations.

A marine propeller has a very complex geometry, in that it has variable section profiles, chord lengths, and pitch angles. Also, in order to meet the heavy loads required for today's high-speed vessels, it should be operated at high speeds of rotation, which ensues higher skewness in the propeller design. All of these make the propeller flow one of the most challenging problems in computational fluid dynamics (CFD) and many researchers and designers have relied on experimental techniques and simplified numerical methods, such as vortex lattice methods and boundary element methods, so far.

Nowadays, model tests provide very accurate results regarding the flow around the propeller. In addition to the global forces and moments due to the rotating propeller, it is now possible to observe the detailed flow field with the turbulence quantities, thanks to the improvement of non-intrusive experimental techniques, such as the Laser Doppler Velocimetry (LDV) or Particle Image Velocimetry (PIV). Nevertheless, it is still necessary to have sophisticated test facilities, additionally, it takes big amount of time and money to analyze only one propeller model.

The numerical simulation approaches for marine propeller geometries have been studied for decades. The inviscid potential flow method based on the lifting surface vortex lattice method was successfully applied to many propeller geometries and is still popular among field designers. The same type of approach has been continuously improved in terms of the effects

of wake alignment and cavitation. Nonetheless, this approach requires in many cases cumbersome procedures and a considerable amount of preliminary knowledge, such as proper location of the trailing wake vorticity.

Since the of 90's, CFD methods solving the Reynolds-averaged Navier-Stokes (RANS) equations have been introduced and increasingly applied to various marine propeller geometries and off-design conditions. The propeller blade tip vortex flow was also studied using CFD methods. Most of the studies show great advancement of CFD technologies and feasibilities of the approaches for marine propeller flows. It is acknowledged that, however, some issues need to be addressed for more practicable procedures.

In the past, propeller design was totally based on design charts. These charts were created by fitting theoretical models to data derived from actual model or full size tests and therefore their number was limited. Nowadays, propeller design is based almost completely on computer tools. Traditional propeller diagrams, such as for the Wageningen B-series, have been numerically adapted into polynomial expressions allowing easy interpolation and optimization within the traditional propeller geometries. This is still very common as starting point for modern propeller design. At this point is very important to clarify the use of the word "optimization", as the propeller design is an iterative process to optimize the efficiency of a propeller subjected to several constraints concerning cavitation, geometry, strength, etc.. Then a "formal" optimization is practically impossible for modern propellers as the description of the final geometry regards some hundred offsets and the evaluation of the efficiency based on numerical hydrodynamics codes requires considerable time. Thus, while the word "optimization" will be used, it may concern just like to a good solution satisfying the given constraints.

According to the works of professor Amoraritei and the actual procedures related to the design of propeller can be carried out in three main stages: *preliminary design*, *design* and *analysis*. Once the design point is chosen and the main parameters are fixed, the problem is to design a propeller with specified performances for given conditions.

In preliminary design stage, a propeller of optimal efficiency is determined using the design charts based on model tests with series of propellers (such as the Wageningen B-series). The

main characteristics of the propeller such as diameter, number of blades, rotation rate, etc. are fixed and this is a *starting point* for the propeller design using the circulation theory: lifting line and lifting surface theory.

The second step, *design*, known like "indirect" problem, can be done using the lifting line theory and the objective is to find the blade geometry for a specified distribution of blade loading over the radius (wake adapted propeller).

In the analysis stage the propeller can be evaluated in several ways: computational analysis, experimental model tests and full scale tests. The analysis requires the detailed geometry of propeller, the effective wake distribution and operational conditions of the propeller. The experimental tests in towing tanks and tunnel cavitation are expensive, time consuming and for this reason analytical and numerical methods have been developed and used for the study of the propeller's behaviour in off design conditions. The objectives of this stage are the evaluation of the hydrodynamic performances of propeller in steady and unsteady flow. Then, for a steady analysis, we can obtain:

- calculation of the open water characteristics
- calculation of the pressure distribution on propeller blades operating in uniform flow or in a radially varied circumferential mean flow

1.1. Brief list of researches

1992: Kodama used a RANS equation method with structural mesh technique[3]. This method has some difficulties such as: restriction of results only in steady state and open water, also because of blade's geometry complication. They couldn't predict the current near the tip of blades accurately.

2002: Funeno simulated the current around a highly skewed propeller via unstructured mesh [4]. He got good correspondence experiment data for steady state and unsteady flow, but this method was complicated and time consuming.

2002: Martinez simulated the propeller via k-epsilon turbulent method in open water in steady state condition. Totally, the results were acceptable but there was approximately 30% error in prediction of torque coefficient [6].

2003: Takekoshi simulated the propeller via standard k-omega turbulent method in open water and steady state conditions [7]. He used the propeller symmetry and simulated only one blade, comparing to the experimental tests, he got 15 percent or error.

2004: Rhee simulated 2D propeller model in unsteady state flow[8]. He used the sliding mesh method for displaying the propeller rotation and turbulent flow of standard k- ω . Its error in comparison with experimental method was approximately 13 percent.

2006: Amoraritei (UGAL) with RANS method, an unstructured tetrahedral mesh for the control volume, RNG k- ϵ turbulence model and moving reference frame(MRF) modeled in FLUENT, she got differences about 5 percent with the experimental data[9].

2010: Amoraritei (UGAL) performed the analysis using FLUENT with k- ϵ Standard turbulence model with 2nd order convective discretization and then compared with analytical results and got difference less than 1.2% for thrust and less than 2.2% for torque[10].

1.2. CFD Analysis

After that the geometry is complete it is possible to continue with the third stage called analysis or also called "direct" problem to evaluate the propeller in all conditions and the objectives are to obtain the pressure distributions on the propeller surfaces and evaluate the hydrodynamic performances of propeller in off-design conditions, for instance K_Q and K_T for different advance ratios J .

1.2.1. 2D flow computation

Using the data from the lifting line method with lifting surface correction, which is the complete geometry of blade sections, the resultant velocity and angle of attack at various radii, we can perform a numerical simulation and analysis of flow around the blade profile regarding the pressure distributions on propeller blades under a radially varied circumferential mean flow.

1.2.2. 3D flow computation

The numerical simulation of 3D flow around propeller will be performed with a Computational domain is cylindrical and it includes all the blade propeller surfaces.

2. THEORETICAL FRAMEWORK

In the present chapter, the theoretical background of Lifting Line theory and lifting surface theory will be explained and also CFD for solving three dimensional (3D) fluid flow problems is introduced. The CFD code is extended from different solver techniques, discussing influences and impacts on the fluid flow simulation. But first I will introduce the propeller characteristics.

2.1. Propeller characteristics

The performance characteristics of a propeller will be divided into *open water* and *behind-hull* properties. In the case of open water characteristics, these relate to the description of the forces and moments acting on the propeller when operating in a uniform fluid stream and The behind-hull characteristics are those generated by the propeller when operating in a mixed wake field behind the ship.

2.1.1 Propeller geometry

The propeller geometry is given in technical drawings following a special convention, or in thousands of offset points or spline surface descriptions, similar to the ship geometry. The complex propeller geometry is usually characterized by a few parameters.

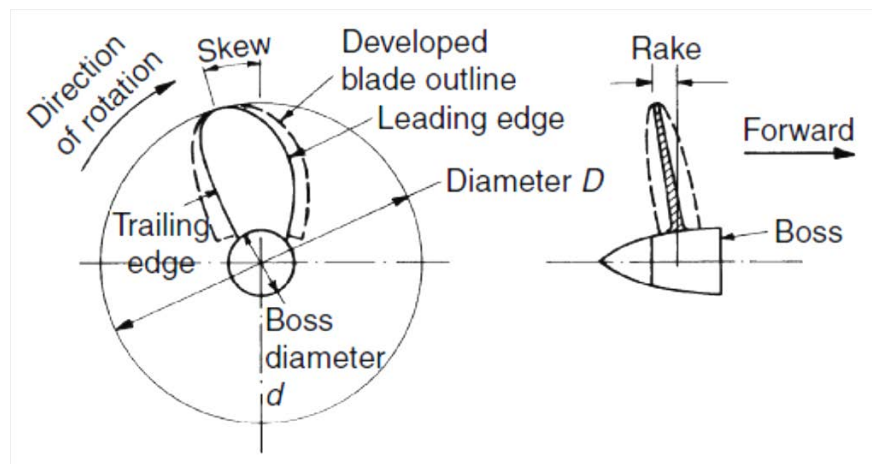


Figure 2.1 Propeller geometry, (Book: Practical Ship Hydrodynamics, Bertram)

- propeller diameter D
- boss (or hub) diameter d
- propeller blade number Z :

The blade number Z is an important parameter for propeller-induced vibration. In general, odd numbers Z feature better vibration characteristics than even numbers. High blade numbers reduce vibration problems (due to less pronounced pressure peaks), but increase manufacturing costs.

- propeller pitch P

A propeller may be approximated by a part of a helicoidal surface which in rotation screws its way through the water. A helicoidal surface is generated as follows. Consider a line AB perpendicular to a line AA_0 as shown in Fig. 2.2. AB rotates around the axis of AA_0 with uniform angular velocity while moving along AA_0 with uniform speed. AB then forms a helicoidal surface. Its pitch is the distance AA_0 . A propeller with a flat face and radially constant pitch would trace out a helicoidal surface. In reality, ship propellers often have neither a radially constant pitch nor a flat face. Then averaging in a circumferential direction creates a flat reference line to define the pitch as a function of the radius. Again averaging in a radial direction may define an average pitch P used to describe the propeller globally. Alternatively, the pitch at one radial position, typically $0.7R$ or $0.35D$, is taken as a single value to represent the radial pitch distribution.

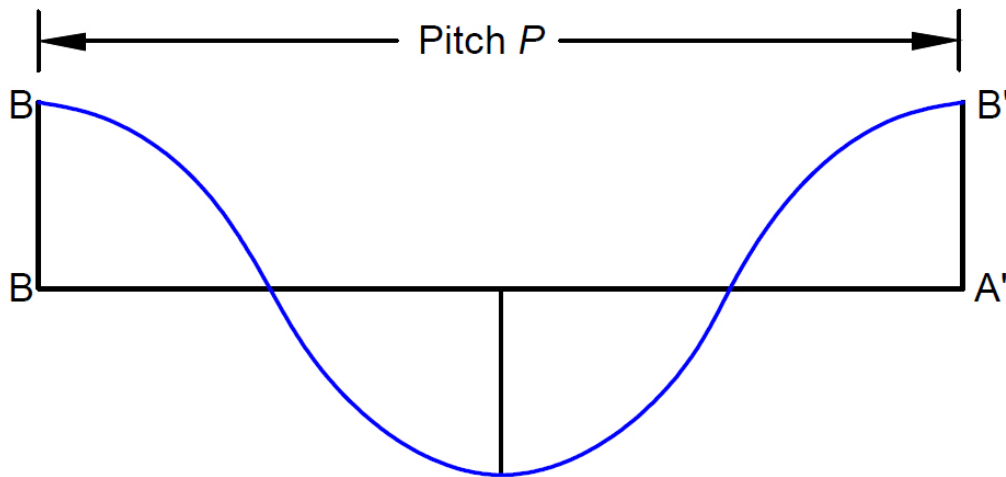


Figure 2.2 Helicoidal surface , (Book: Practical Ship Hydrodynamics, Bertram)

The important pitch terms with which the analyst needs to be thoroughly conversant are as follows:

1. nose–tail pitch,
2. face pitch,
3. effective or ‘no-lift’ pitch,
4. hydrodynamic pitch.

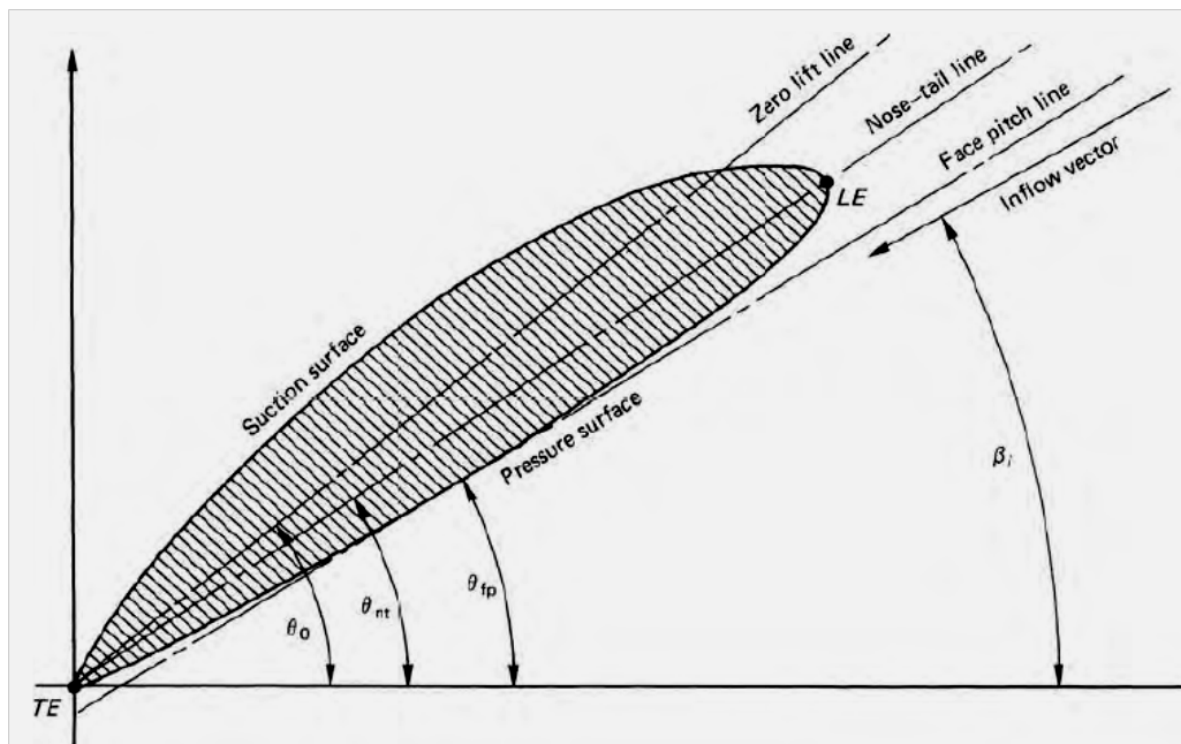


Figure 2.3 Pitch Lines , (Book: Marine propellers and propulsion, Carlton)

The effective pitch line of the section corresponds to the conventional aerodynamic no-lift line and is the line that if the incident water flowed along, zero lift would result from the aerofoil section. The effective pitch angle (θ_0) is greater than the nose–tail pitch angle by an amount corresponding to the three-dimensional zero lift angle of the section. As such this is a fundamental pitch angle since it is the basis about which the hydrodynamic forces associated with the propeller section are calculated. Finally, the hydrodynamic pitch angle (β_i) is the angle at which the incident flow encounters the blade section and is a hydrodynamic inflow rather than a geometric property of the propeller: neither this angle nor the effective pitch

angle would, however, be expected to be found on the propeller drawing in normal circumstances.

- disc area $A_0 = \pi \cdot D^2/4$
- projected area A_P
- expanded blade area A_E
- skew (back): is usually expressed as the circumferential displacement of the propeller tip made non-dimensional by the propeller diameter.
- rake i_G : is the tilted face respect to the normal plane on the propeller shaft, usually backwards to increase the clearance between the blade tip and the hull.

Normally some of this characteristics are given as non-dimensional ratios:

$$d/D$$

$$A_E/A_0$$

$$P/D$$

$$i_G$$

- extended blade area ratio A_E/A_0 :

Typical A_E/A_0 are between 0.3 and 1.5. Area ratios above 1 mean overlapping blades which are expensive to manufacture. A_E/A_0 is chosen such that the blade load is kept low enough to avoid unacceptable cavitation. Therefore A_E/A_0 increases with propeller load (thrust per propeller area A_0). The propeller efficiency decreases with A_E/A_0 since the increased area also increases frictional losses. Larger A_E/A_0 also often demand higher blade numbers to avoid too small side ratios for the blades.

2.1.2 Open water characteristics.

Thrust T and torque Q are usually expressed as functions of rpm n in non-dimensional form as:

$$K_T = \frac{T}{\rho \cdot n^2 \cdot D^4} \quad (2.1)$$

$$K_Q = \frac{Q}{\rho \cdot n^2 \cdot D^5} \quad (2.2)$$

The force T is made non-dimensional by the propeller disk area times the stagnation pressure based on the circumferential speed, omitting a factor $\pi^2/8$. The moment Q is made non-dimensional by the additional length D , i.e. the propeller diameter.

The advance number J is defined as $J = V_A/(nD)$.

$$J = \frac{V_A}{n \cdot D} \quad (2.3)$$

with:

$$V_A = V_S \cdot (1 - w) \quad (2.4)$$

V_A is the average inflow speed to the propeller, V_S the speed of the ship and w the wake coefficient. The propeller open-water efficiency is derived from thrust and torque coefficients and the advance number:

$$\eta_0 = \frac{T \cdot V_A}{2\pi \cdot n \cdot Q} = \frac{K_T \cdot \rho \cdot n^2 \cdot D^4}{K_Q \cdot \rho \cdot n^2 \cdot D^5} \cdot \frac{V_A}{2\pi \cdot n} = \frac{K_T}{K_Q} \cdot \frac{J}{2\pi} \quad (2.5)$$

K_T , K_Q , and η_0 are displayed over J . The curves are mainly used for propeller optimization and to determine the operation point (rpm, thrust, torque, power) of the ship. While the use of diagrams in education is still popular, in practice computer programs are almost exclusively used in propeller design.

Another important open-water parameters are the thrust loading coefficient and power coefficient:

$$C_{Th} = \frac{T}{\rho V_A^2 D^2 \frac{\pi}{8}} \quad (2.6)$$

$$C_P = \frac{P_D}{\rho V_A^3 D^2 \frac{\pi}{8}}$$

This coefficient makes the thrust non-dimensional with the propeller disk area times stagnation pressure based on the propeller inflow velocity.

The open-water diagrams are based on stationary flow. They are only suited for the case when the ship moves steadily ahead. The following figure shows a typical propeller diagram. K_T and K_Q decrease monotonously with J . The efficiency η has one maximum.

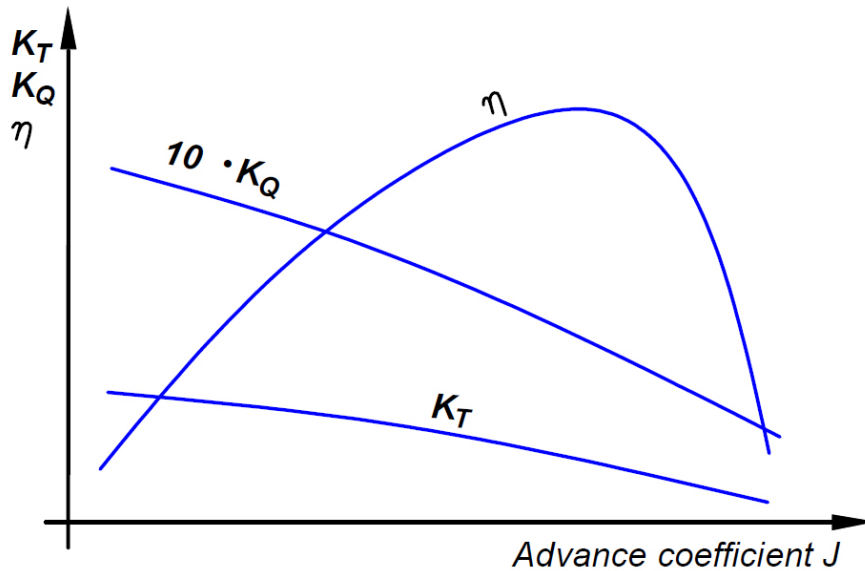


Figure 2.4 Open-water Propeller diagram

2.1.3 Behind-hull propeller characteristics

The behind-hull propeller characteristics, so far as powering is concerned, have been traditionally accounted for by use of the term relative rotative efficiency η_r . This term, which was introduced by Froude, accounted for the difference in power absorbed by the propeller when working in a uniform flow field at a given speed and that absorbed when working in a mixed wake field having the same mean velocity:

$$\eta_R = \frac{\text{power absorbed in open water of speed } Va}{\text{power absorbed in mixed wake field of mean velocity } Va} \quad (2.7)$$

Normally the correction defined by this efficiency parameter is very small since η_R is usually close to unity unless there is some particularly abnormal characteristic of the wake field. Typically, one would expect to find η_R in the range $0.96 < \eta_R < 1.04$.

As a consequence of this relationship the behind-hull efficiency (η_B), that is the efficiency of the propeller when working behind a body, is defined as:

$$\eta_B = \eta_o \eta_R = \frac{\eta_R \cdot K_T \cdot J}{2\pi K_Q} \quad (2.8)$$

2.2. Standard series data

The principal aim in performance systematic propeller tests is to provide a data base to help the designer understand the factors which influence propeller performance and the inception and form of cavitation on the blades under various operating conditions.

Then, a second purpose is to provide design diagrams, or charts, which will assist in selecting the most appropriate dimensions of actual propellers to suit full-size ship applications for the first stage of propeller design: *Preliminary design and starting point*.

2.2.1 Wageningen B-screw series

The Wageningen series is a general purpose, fixed pitch, non-ducted propeller series which is used extensively for design and analysis purposes. The Wageningen B Propeller Series are used by designers and engineers worldwide. These series comprise the open water characteristics of conventional fixed pitch propellers with various numbers of blades and blade area ratios.

The extent of the series in terms of a blade number versus blade area ratio matrix is shown in Table 2.1 from which it may be seen that the series numbers some 20 blade area–blade number configurations.

Blade number (Z)	Blade area ratio A_E / A_O					
2	0.30					
3	0.35	0.50	0.65	0.80		
4	0.40	0.55	0.70	0.85	1.00	
5	0.45	0.60	0.75			1.05
6		0.50	0.65	0.80		
7		0.55	0.70	0.85		

Table 2.1 Extent of the Wageningen B-screw series(Book: **Marine propellers and propulsion, Carlton**)

This is perhaps the most extensive and widely used propeller series. The series was originally presented in a set of papers presented by Troost in the late 1940s and, amongst many practitioners, is still referred to as the ‘Troost series’.

The results of the fairing exercise reported by Oosterveld defined the way for detailed regression studies on the performance characteristics given by this model series. Oosterveld and van Oossanen reported the results of this work in which the open water characteristics of the series are represented at a Reynolds number 2×10^6 by polynomials in the following form:

$$K_Q = \sum_{n=1}^{47} C_n (J)^{S_n} (P/D)^{t_n} (A_E/A_O)^{u_n} (Z)^{v_n} \quad (2.9)$$

$$K_T = \sum_{n=1}^{39} C_n (J)^{S_n} (P/D)^{t_n} (A_E/A_O)^{u_n} (Z)^{v_n} \quad (2.10)$$

The coefficients C , s , t , u , v can be found in the table 2.2

To extend this work further so, that propeller characteristics can be predicted for other Reynolds numbers within the range 2×10^6 to 2×10^9 a set of corrections of the following form was derived:

$$\begin{Bmatrix} K_T(Rn) \\ K_Q(Rn) \end{Bmatrix} = \begin{Bmatrix} K_T(Rn = 2 \times 10^6) \\ K_Q(Rn = 2 \times 10^6) \end{Bmatrix} + \begin{Bmatrix} \Delta K_T(Rn) \\ \Delta K_Q(Rn) \end{Bmatrix}$$

where

$$\begin{aligned} \Delta K_T = & 0.000353485 \\ & -0.00333758 (A_E/A_O) J^2 \\ & -0.00478125 (A_E/A_O)(P/D)J \\ & +0.000257792(\log Rn - 0.301)^2 \cdot (A_E/A_O) \cdot J^2 \\ & +0.0000643192(\log Rn - 0.301) \cdot (P/D)^6 \cdot J^2 \\ & -0.0000110636(\log Rn - 0.301)^2 \cdot (P/D)^6 \cdot J^2 \\ & -0.0000276305(\log Rn - 0.301)^2 \cdot Z \cdot (A_E/A_O) \cdot J^2 \\ & +0.0000954(\log Rn - 0.301) \cdot Z \cdot (A_E/A_O) \cdot (P/D) \cdot J \\ & +0.0000032049(\log Rn - 0.301) \cdot Z^2 \cdot (A_E/A_O) \cdot (P/D)^3 \cdot J \end{aligned}$$

$$\begin{aligned} \Delta K_Q = & -0.000591412 \\ & +0.00696898(P/D) \\ & -0.0000666654 \cdot Z \cdot (P/D)^6 \\ & +0.0160818(A_E/A_O)^2 \\ & -0.000938091(\log Rn - 0.301) \cdot (P/D) \\ & -0.00059593(\log Rn - 0.301) \cdot (P/D)^2 \\ & +0.0000782099(\log Rn - 0.301) \cdot 2 \cdot (P/D)^2 \\ & +0.0000052199(\log Rn - 0.301) \cdot Z \cdot (A_E/A_O) \cdot J^2 \\ & -0.00000088528(\log Rn - 0.301) \cdot 2 \cdot Z \cdot (A_E/A_O) \cdot (P/D)J \\ & +0.0000230171(\log Rn - 0.301) \cdot Z \cdot (P/D)^6 \\ & -0.00000184341(\log Rn - 0.301) \cdot 2 \cdot Z \cdot (P/D)^6 \\ & -0.00400252(\log Rn - 0.301) \cdot (A_E/A_O)^2 \\ & +0.000220915(\log Rn - 0.301) \cdot 2 \cdot (A_E/A_O)^2 \end{aligned}$$

And the following table shows the coefficient for the formulas (2.9) and (2.10).

Table for Coefficients for KT - polynomial						Table for Coefficients for KQ - polynomial					
n	C	s	t	u	v	n	C	s	t	u	v
1	0.00880496	0	0	0	0	1	0.0037937	0	0	0	0
2	-0.20455400	1	0	0	0	2	0.0086523	2	0	0	0
3	0.16635100	0	1	0	0	3	-0.0322410	1	1	0	0
4	0.15811400	0	2	0	0	4	0.0034479	0	2	0	0
5	-0.14758100	2	0	1	0	5	-0.0408811	0	1	1	0
6	-0.48149700	1	1	1	0	6	-0.1080090	1	1	1	0
7	0.41543700	0	2	1	0	7	-0.0885381	2	1	1	0
8	0.01440430	0	0	0	1	8	0.1885610	0	2	1	0
9	-0.05300540	2	0	0	1	9	-0.0037087	1	0	0	1
10	0.01438810	0	1	0	1	10	0.0051370	0	1	0	1
11	0.06068260	1	1	0	1	11	0.0209449	1	1	0	1
12	-0.01258940	0	0	1	1	12	0.0047432	2	1	0	1
13	0.01096890	1	0	1	1	13	-0.0072341	2	0	1	1
14	-0.13369800	0	3	0	0	14	0.0044384	1	1	1	1
15	0.00638407	0	6	0	0	15	-0.0269403	0	2	1	1
16	-0.00132718	2	6	0	0	16	0.0558082	3	0	1	0
17	0.16849600	3	0	1	0	17	0.0161886	0	3	1	0
18	-0.05072140	0	0	2	0	18	0.0031809	1	3	1	0
19	0.08545590	2	0	2	0	19	0.0158960	0	0	2	0
20	-0.05044750	3	0	2	0	20	0.0471729	1	0	2	0
21	0.01046500	1	6	2	0	21	0.0196283	3	0	2	0
22	-0.00648272	2	6	2	0	22	-0.0502782	0	1	2	0
23	-0.00841728	0	3	0	1	23	-0.0300155	3	1	2	0
24	0.01684240	1	3	0	1	24	0.0417122	2	2	2	0
25	-0.00122960	3	3	0	1	25	-0.0397722	0	3	2	0
26	-0.03177910	0	3	1	1	26	-0.0035002	0	6	2	0
27	0.01860400	1	0	2	1	27	-0.0106854	3	0	0	1
28	-0.00410798	0	2	2	1	28	0.0011090	3	3	0	1
29	-0.00060685	0	0	0	2	29	-0.0003139	0	6	0	1
30	-0.00498190	1	0	0	2	30	0.0035985	3	0	1	1
31	0.00259830	2	0	0	2	31	-0.0014212	0	6	1	1
32	-0.00056053	3	0	0	2	32	-0.0038364	1	0	2	1
33	-0.00163652	1	2	0	2	33	0.0126803	0	2	2	1

34	-0.00032879	1	6	0	2	34	-0.0031828	2	3	2	1
35	0.00011650	2	6	0	2	35	0.0033427	0	6	2	1
36	0.00069090	0	0	1	2	36	-0.0018349	1	1	0	2
37	0.00421749	0	3	1	2	37	0.0001125	3	2	0	2
38	0.00005652	3	6	1	2	38	-0.0000297	3	6	0	2
39	-0.00146564	0	3	2	2	39	0.0002696	1	0	1	2
						40	0.0008327	2	0	1	2
						41	0.0015533	0	2	1	2
						42	0.0003027	0	6	1	2
						43	-0.0001843	0	0	2	2
						44	-0.0004254	0	3	2	2
						45	0.0000869	3	3	2	2
						46	-0.0004656	0	6	2	2
						47	0.0000554	1	6	2	2

Table 2.2 Coefficients for the polynomials form of K_T and K_Q for $Rn=2 \times 10^6$

2.3. Propeller theories

Many models aimed at describing the action of the marine propeller tend to solve the potential flow problem, subject to viscous constraints, defined by the propeller operating at a particular advance and rotational speed. In one case, the design problem, the aim is to define the required blade geometry for a given set of operating conditions; and in the other, the analysis problem, which is the inverse of the design problem, the geometry is defined and the resulting load and flow condition is calculated. The models of propeller action normally fall into one of five categories

- Momentum or blade element models.
- Lifting line models.
- Lifting surface models.
- Boundary element models.
- Computational fluid dynamic models.

2.3.1 *Momentum theory*

The propeller is reduced to an actuator disk which somehow creates a pressure jump in the flow. Thrust and corresponding delivered power are expressed by increased velocities in the propeller plane and the contracted wake downstream of this plane. This simple model is unsuited for propeller design, but popular as a simple propeller model in RANSE ship computations and useful in understanding, some basic concepts of propeller flows. It is simple and fast specially to achieve the ideal efficiency η_i , but it doesn't model the rotative and viscous losses.

Momentum theory models the propeller as a simple actuator disk accelerating the flow in the axial direction by somehow creating a pressure jump in the propeller plane. The propeller is then seen as a continuous circular disk with infinite blades and $A_E/A_0 = 1$. The model is not enough accurate, but allows some valuable insight into the global mechanisms of a propeller.

2.3.2 Lifting-line methods

Lifting-line approaches are still popular in propeller design as a preliminary step, Propeller blade is reduced to radially aligned straight vortices (lifting lines). The lifting line model is perhaps the simplest mathematical model of propeller action in that it assumes the aerofoil blade sections to be replaced by a *single line vortex* whose strength varies from section to section (varies over the radius). Free vortices are scattered in the flow. Suitable for initial design of propellers, rotative losses reflected in model; viscous losses incorporated by empirical corrections. In the other hand, cross-sections found, but angle of incidence and camber require corrections; no simple way to consider skew.

The *single line vortex*, which is a continuous line in the radial direction about which vortices act, is termed the lifting line, and is normally considered to pass through the aerodynamic centre of the sections.

Lifting-line methods still form a vital part of practical propeller design. They find the radial distribution of loading optimum with respect to efficiency as a first step to determine the corresponding blade geometry. Alternatively, the radial distribution of loading may be specified to determine the corresponding blade geometry (Lerbs (1952, 1954)). If unrealistic or too demanding pressure distributions are specified, either no solution is found or the error in framework of the theory is so large that the solution does not yield a realistic result.

Since the Lifting-line methods were adopted from lifting-line theory for straight foils, it is necessary to briefly review the lifting-line theory for straight foils.

A straight line of vorticity creates lift orthogonal to the direction of the vortex line and the direction of the inflow, (Fig. 2.5). Helmholtz's first and second laws state:

1. The strength of a vortex line is constant along its length.
2. A vortex line must be closed, it cannot end in the fluid.

As a consequence, the vortex lines on a foil are bent downstream at the end of the foil.

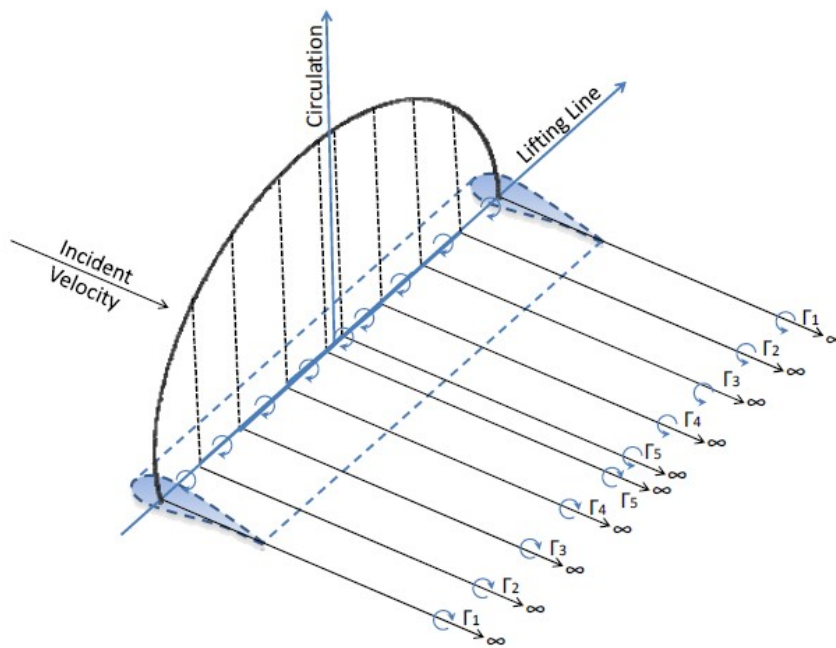


Figure 2.5 Foil represented by bound vortex and trailing vortices

In reality, the lift and thus the vorticity (vortex strength) are not constant over the foil span. This can be considered by approximating the continuous lift by a number of discrete constant vortex segments. Each of these will then produce trailing vortices (Fig. 2.6). In sum, the vortex segments form a 'lifting line' of (stepwise) variable vorticity. The trailing vortices induce a flow at the foil which is downward for positive lift. This velocity is therefore called downwash and changes the effective inflow angle experienced by each section of the foil.

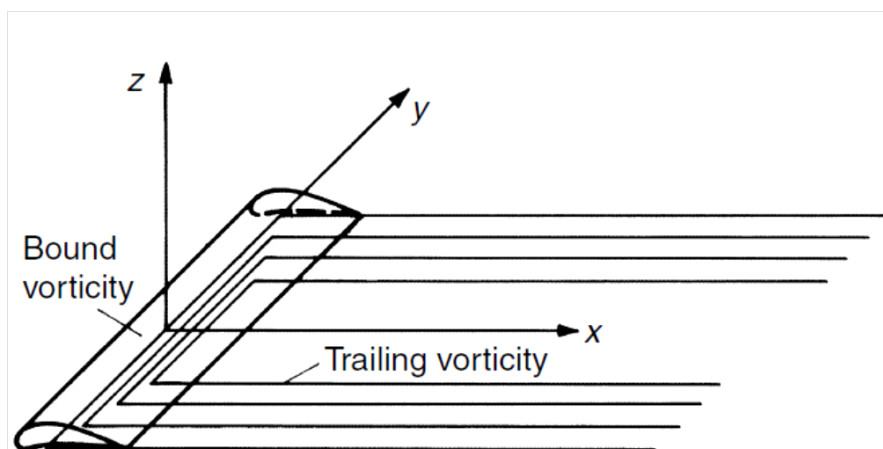


Figure 2.6 Foil represented by a distribution of horseshoe vortices

For propellers, each blade is represented by one lifting line extending from hub to blade tip. Typically the lifting lines are straight with skew and rake being neglected at this point in the analysis.

The vortex system of a propeller is similar to that of a wing as described in the following figure 2.7

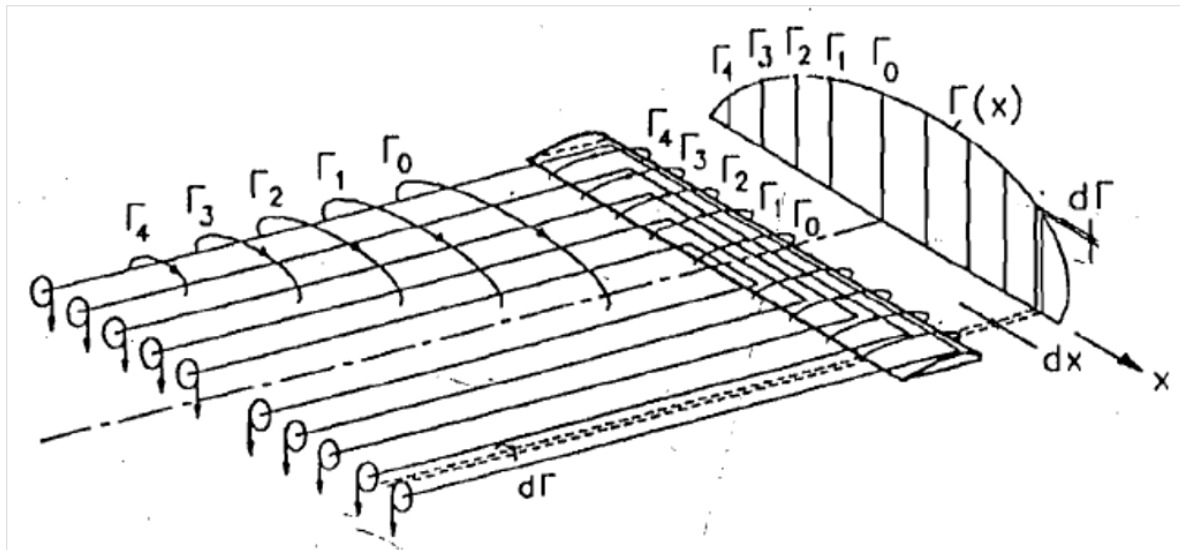


Figure 2.7 Vortex System of a Wing with Circulation Varying along the Span
(**Basic Ship Propulsion**, Ghose and Gokarn)

Each blade of the propeller is represented by a bound vortex or lifting line of strength varying along the length of the blade, and a vortex sheet is shed from the trailing edge. Since the propeller revolves about its axis while simultaneously advancing along it, this trailing vortex sheet has an helicoidal shape, and there are as many such vortex sheets as there are blades in the propeller.

2.3.3 Lifting-surface method

Propeller blade is reduced to a grid of horseshoe vortices; pressure distribution on the blade follows from Bernoulli's law from the induced velocities; pressure distribution yields forces and moments for the whole propeller. The Blade modelled three dimensionally and corrections are only necessary for viscous effects, also get good convergence to grid independent solutions with grid refinement.

The second generation of lifting-surface used vortex lattice which can handle arbitrary blade geometries, but neither consider the true blade thickness, nor the propeller hub.

A complete vortex-lattice method (VLM) can be established on the basis of the lifting-line method just described. The lifting-line model was used to find a circulation Γ that corresponds to a given resultant flow direction at the lifting line and is able to provide the predetermined (design) thrust. With a vortex lattice instead of a lifting line, a model for the material blade is inserted. One can now really investigate whether a given geometry corresponds to a desired thrust, a task that is beyond the scope of a lifting-line theory.

In a vortex-lattice system (Figure 2.8). The flow is generated by spanwise and (dependent) streamwise line vortices. Control points are positioned inside the loops of the vortex system. For steady flow, the vortex elements in the wake have the same strength in each spanwise segment. The vertical vortex lines then cancel each other and a semi-infinite horseshoe vortex results. The most downstream control point is located at the trailing edge behind the last streamwise vortex which is a very robust measure to enforce the Kutta condition.

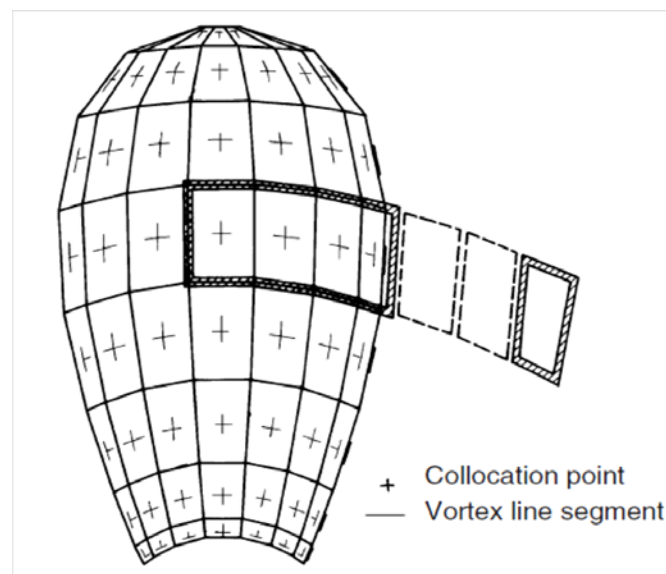


Figure 2.8 Vortex-lattice elements allocated on a propeller blade (Practical Ship Hydrodynamics, **Bertram**)

Lifting-surface methods arrange the vortex and source elements on the mean chord surface of the blade. Following Bernoulli's law, the pressure can be computed from the velocities. This yields pressure distributions which usually reproduce the actual pressure distributions quite

well except for a narrow region at the leading edge which may extend to a length of approximately twice the nose radius.

2.3.4 Boundary element method/panel method

Exact formulation of the potential theory problem with source or dipole panels, without simplifications besides the potential flow assumption. The Programming is complex, especially for the Kutta condition; relatively large number of dipole and/or source panels necessary and flow near propeller tip still not well captured.

2.3.5 RANSE method

During the last decade considerable advances have been made in the application of computational fluid dynamics to the analysis and design of marine propellers.

A number of approaches for modelling the flow physics have been developed. Typically for the analysis of the flow around cavitating and non-cavitating propellers these approaches are the Reynolds Averaged Navier–Stokes (RANS) method, Large Eddy Simulation (LES) techniques, Detached Eddy Simulations (DES) and Direct Numerical Simulations (DNS).

Of these methods the RANS codes appear to have found most favor because the computational times are rather lower than for the other methods.

If structured curvilinear grids are used in the modeling process this may result in a large number of cells which, in turn, may produce a complicated and time-consuming grid generation process. This has led to unstructured grids being favored since these can easily handle complex geometries and the clustering of grid cells in regions of the flow where large parameter gradients occur.

2.4. Governing equations of CFD Method

CFD method is fundamentally based on the governing equations of fluid dynamics which represent the mathematical enunciation of the "*conservation laws of physics*", where the following physical laws are assumed:

- ✓ Mass is conserved for the fluid.
- ✓ Newton's second law, the rate of change of momentum equals the sum of forces acting on the fluid.
- ✓ First law of thermodynamics, the rate of change of energy equals the sum of rate of heat addition to and the rate of work done on the fluid.

2.4.1 Continuity equation: Mass conservation

The following conservation law related to fluid flow matter may neither be created nor be destroyed, is possible to be expressed in the Cartesian coordinate system as follow:

$$\frac{\delta \rho}{\delta t} + \frac{\delta(\rho u)}{\delta x} + \frac{\delta(\rho v)}{\delta y} + \frac{\delta(\rho w)}{\delta z} = 0 \quad (2.11)$$

This equation is known as the **partial differential form** of the *continuity equation*, also called the *conservation form*. Where the fluid velocity V at any point in the flow field is described by the local velocity components u , v , and w which are, in general, functions of location (x , y , z) and time (t).

2.4.2 The momentum Equation: Force Balance

Newton's second law of motion states that the sum of forces that is acting on the fluid element equals the product between its mass and acceleration of the element. The conservation of momentum is the application of the *Newton's second law*. In an inertial frame of reference, the general form of the equations of fluid motion is:

$$\rho \left(\frac{\delta v}{\delta t} + v \cdot \nabla v \right) = -\nabla p + \nabla \cdot T + f \quad (2.12)$$

Also known as **Navier-Stokes equations** (in vector form), where v is the flow velocity, ρ is the fluid density, p is the pressure, T is the stress tensor, and f represents body forces (per unit volume) acting on the fluid.

Taking into account the fact that the fluid to be analyzed is incompressible the Navier-Stokes equations can be written as follows:

$$\rho \left(\frac{\delta v}{\delta t} + v \cdot \nabla v \right) = -\nabla p + \mu \nabla^2 v + f \quad (2.13)$$

The shear stress term $\nabla \cdot T$ becomes the useful quantity $\mu \nabla^2 v$ (∇^2 is the vector Laplacian) when the fluid is assumed incompressible, homogeneous and Newtonian, where μ is the (constant) dynamic viscosity.

2.4.3 Additional Equations for Turbulent Flow

First, we must define the term Turbulence. It is well known that small disturbances associated with disturbances in the fluid streamlines of a laminar flow can eventually lead to a chaotic and random state of motion, a turbulent condition. These disturbances may originate from the free stream of the fluid motion, or induced by the surface roughness, where they may be amplified in the direction of the flow, in which case turbulence will occur. The start of turbulence depends on the ratio of the inertia force to viscous force, which is indicated by the Reynolds number. At low Reynolds number, inertia forces are smaller than the viscous forces. At high Reynolds number, the inertia forces are sufficiently large to amplify the disturbances, and a transition to turbulence occurs, the motion becomes intrinsically unstable with the velocity and all other flow properties are varying in a random and chaotic way.

3. METHODOLOGY: Propeller design

Nowadays, propeller design relies mostly on computer tools. Some of the traditional propeller diagrams, such as for the Wageningen B-series of propellers, have been transformed into polynomial expressions, as mentioned in Chapter 2, allowing easy interpolation and optimization within the traditional propeller geometries being a still popular starting point for modern propeller design. Then, the design is followed by a succession of ever more sophisticated analysis programs to modify and fine-tune the propeller geometry.

The design is not a linear process but a continuous loop made up of a number of phases, each of which interacts on the other and is completed only when they all have been satisfied. The initial phase is the "*definition of the problem*," which may be modified as the design process is continued. This is followed by the "*preliminary design phase*" or "synthesis phase of the design," which involves the development of the basic design derived from the fundamental knowledge available to the designer. This in turn is followed by the "*detail design phase*" and finally the "*analysis and optimization phase of the design*." The latter two phases are a loop unto themselves as they attempt to meet all of the design requirements in a well balanced design. Sometimes, they also interact with the initial phase and modify the definition of the problem.

The final phase is the "*evaluation of the design*." For marine propulsors, this occurs during the initial sea trials conducted at the end of the ship-building period. If the design fails to meet all of the requirements, it is necessary to return to an earlier phase to determine the reasons for the failure and the modifications required.

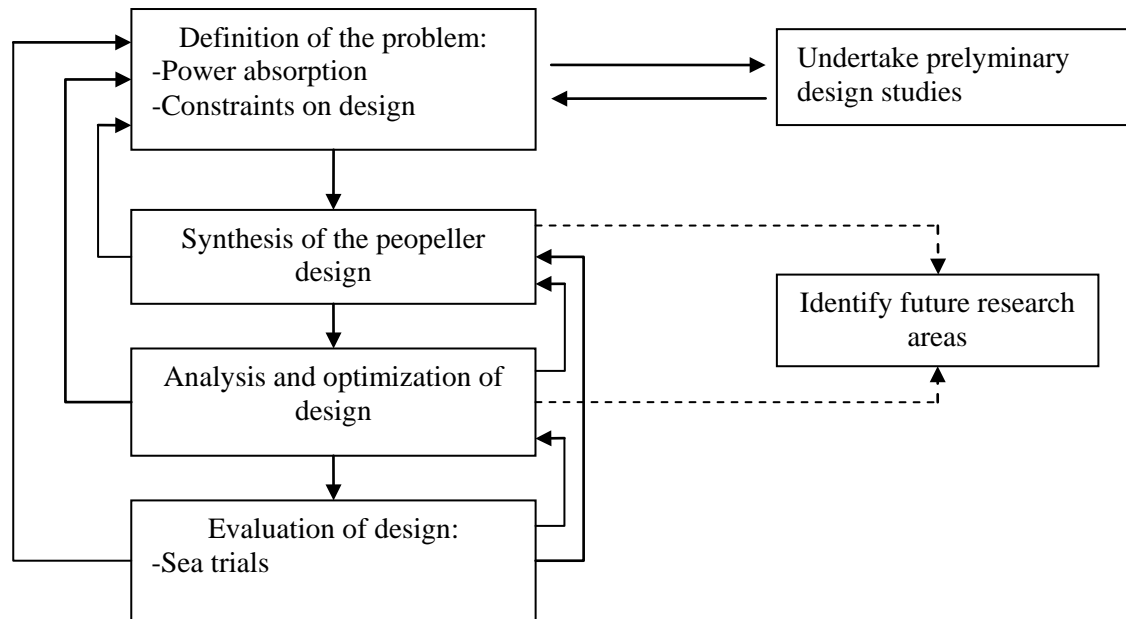


Figure 3.1 The phases of propeller design (Carlton)

The definition of the problem is mainly the specification of the design point, or points in the case of controllable pitch propellers, for the propeller together with the constraints which are applicable to that particular design or the vessel to which it is to be fitted.

Following the production of the design specification the synthesis of the design can commence. This design will be for the propeller type agreed during the specification stage, because it is very likely that some preliminary propeller design studies will have been conducted during the design specification phase. At that time propeller type, blade number and so on are most likely to have been chosen. As a consequence, during the synthesis phase the basic design concept will be worked up into a detailed design proposal typically using, for advanced designs, a wake adapted lifting line with lifting surface correction capability. The choice of method, however, will depend on the designer's own capability and the data available, and may, for small vessels, be an adaptation of a standard series propeller which may work in a perfectly satisfactory manner from the cost-effectiveness point of view.

The design that results from the synthesis phase, will then pass into the analysis and optimization phase. This phase may contain elements of both theoretical analysis and model testing. The theoretical analysis will vary, depending upon the designer's capabilities, from adaptations of lifting-line analysis procedure through to unsteady lifting surface, vortex lattice

or boundary element capabilities to finally analyze the model with RANS method using in our case the commercial code Fluent.

3.1. Definition of the problem

The selection of the design basis starts with a consideration of the mission profile for the vessel. Each vessel has a characteristic mission profile which is determined by the owner to meet the commercial needs of the particular service under the economic conditions prevailing. It must be recognized that the mission profile of a particular ship may change throughout its life, depending on a variety of circumstances. Normally, the client or the owner of the ship specifies within small margins what power P_D has to be delivered at what speed V_s and what is the rpm of the (selected) main engine.

In addition to satisfying the mission profile requirements it is also necessary that the propeller and engine characteristics match, not only when the vessel is new but also after the vessel has been in service for some years. Some factors which affects the choice of propulsor are:

- Role of vessel
- Special requirements
- Initial installation costs
- Running costs
- Maintenance requirements
- Service availability
- Legislative requirements

Besides purely geometric propeller features, a number of other factors influence the power absorption characteristics. Typical of these factors are sea conditions, wind strength, hull condition in terms of roughness and fouling, and, of course, displacement.

For instance, if the propeller is designed to operate at the Maximum Continuous Rate (MCR) condition when the ship is clean and in a light displacement with favorable weather, such as might be found on a trial condition, then the ship will not be able to develop full power in

subsequent service when the draughts are deeper and the hull fouls or during bad weather, hence the propeller is normally based on a Normal Continuous Rate (NCR) of between 85 per cent and 90 per cent of the MCR conditions, as you can see in the Figure3.3

When the ship includes a shaft generator, the power to supply the generator P_G is deducted from the NCR. Then, the rotational speed for the propeller design was fixed such that the power absorbed by the propeller in service, together with the generator power when in operation, could absorb the MCR of the engine at 100 per cent rpm.

Based on optimum open water efficiency and propeller power coefficient, van Manen(1966) developed a graph (Figure 3.2) to compare a variety of propeller forms based on the results of systematic series data.

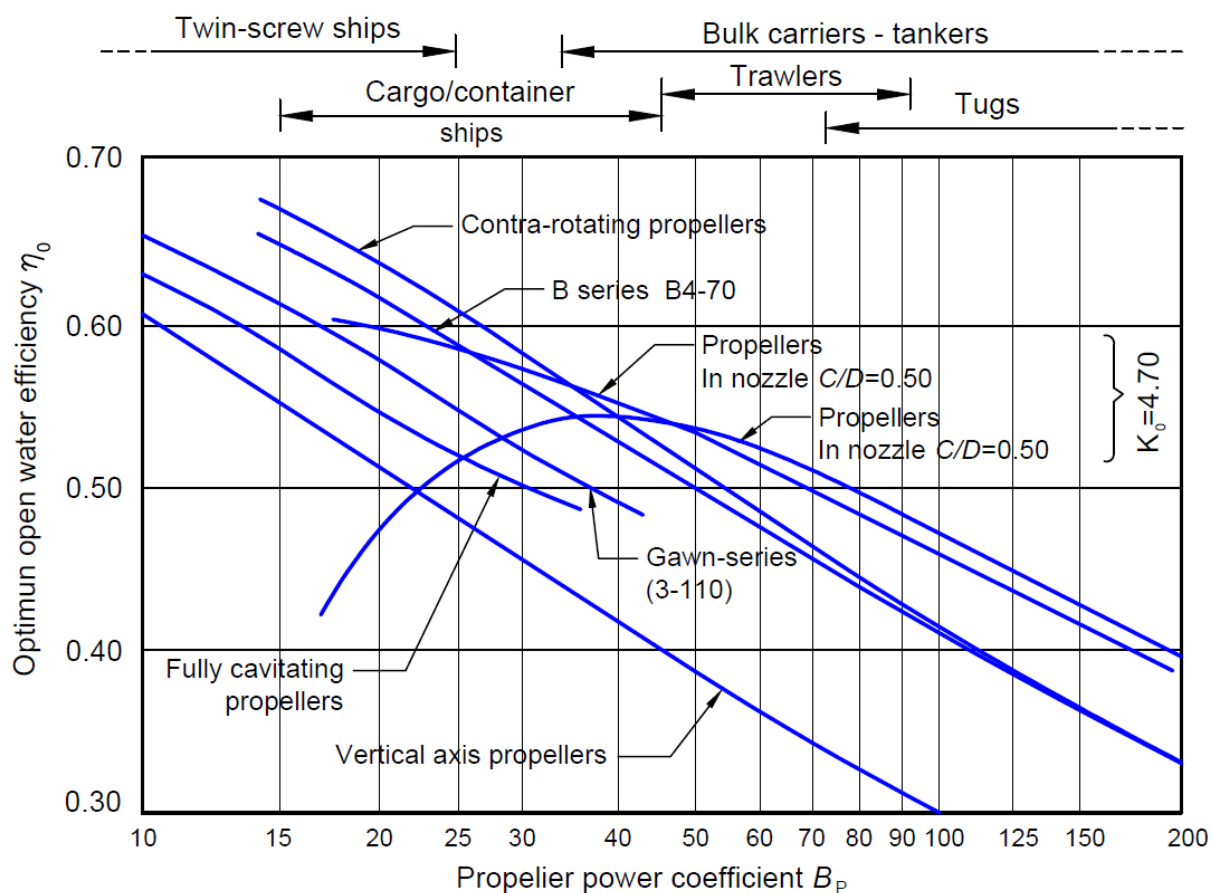


Figure 3.2 Typical optimum open-water efficiencies for different propeller types (SNAME **Propulsion** 2010)

The foregoing figure shows the highest obtainable open water efficiency for the different types of propeller as a function of the power coefficient B_p

$$B_p = \frac{P_D^{0.5} N}{V_a^{2.5}} \quad (3.1)$$

where B_p is calculated in British units of British horsepower, rpm and knots

In design terms, where no shaft generators exist to absorb power it is normally assumed that P_D is between 98 and 99 per cent of the value of P_S depending on the length of the line shafting and the number of bearings. When a gearbox is installed, then P_S usually lies between 96 and 98 per cent of the value of P_B , depending on the gearbox type.

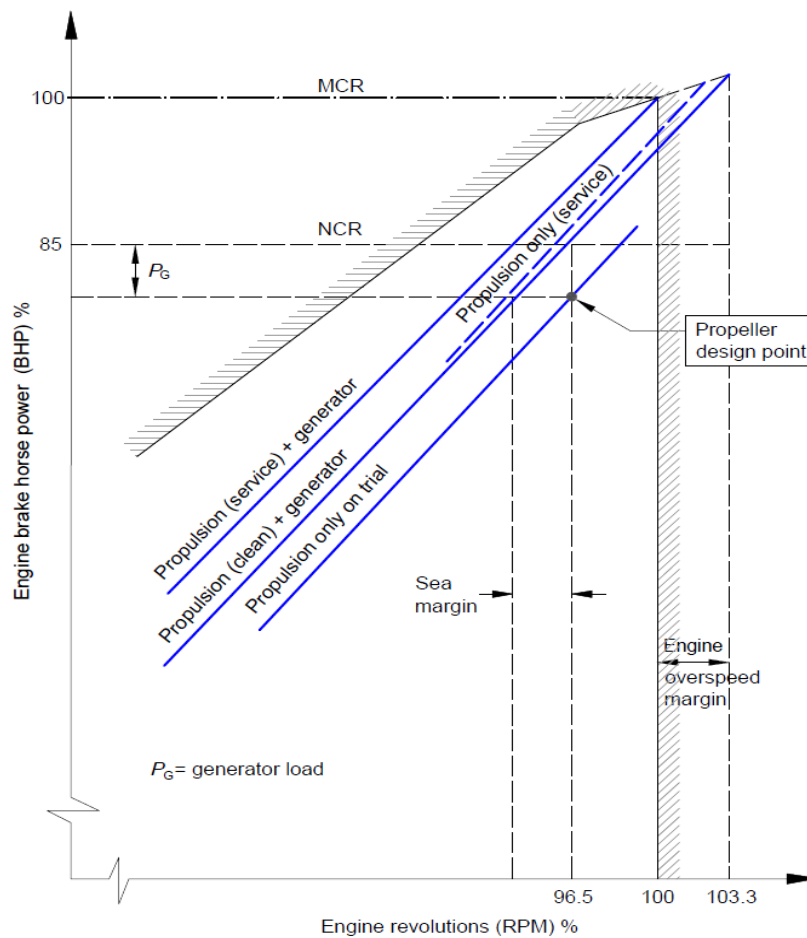


Figure 3.3 Typical Propeller design point (Carlton)

3.2. First stage: Preliminary design

In preliminary design stage, a propeller of optimal efficiency is determined using the design charts based on model tests with series of propellers (such as the Wageningen B-series). The main characteristics of the propeller such as diameter, number of blades, rotation rate, etc. are fixed and this is a *starting point* for the propeller design using the circulation theory: lifting line and lifting surface theory. The performance of these older propellers (Wageningen B-series) is insufficient for today's expectations and the propeller thus determined will only be used as a starting point for the actual design.

It should be pointed out that the modern calculation methods provide for much greater flexibility in the design of propellers as compared to the use of data from systematic propeller series (charts) as produced in the past by MARIN (Wageningen series), Troost (1937-38), (1939-40), (1950-51), Oosterveld & van Oossanen (1975), Admiralty Experiment Works (Gawn series), Gawn (1937, 1953), SSPA (SSP A standard series), Lindgren & Bjarne (1967) and DTRC (Admiral Taylor series), Taylor (1933). The use of these series restricts one to the fixed geometry, section characteristics and hub radius employed and does not allow for distributions in the inflow to the propeller disc as experienced in the wake behind a ship. Moreover, they do not include skew as a parameter as can be incorporated in lifting-line and lifting-surface theories.

The preliminary design of a marine propeller is almost invariably carried out by one of two methods. The first of these is based on experimental data derived from model propeller open-water tests and the second on circulation theory.

For a given ship, whose hull shapes and sizes are known, the propeller can be designed to:

- Absorb minimum power P_D , (the most common case for commercial ships)
- or to develop the required Thrust T at certain ship speed V , (typical in Tugs propeller design)

And there are two types of design problems for free running propellers related with P_D as the initial data:

- Given the propeller diameter and the ship speed, design the optimum propeller to minimize the power required, and determine the corresponding propeller rpm.
- Given the engine power and propeller rpm, design the optimum propeller to maximize the ship speed.

For the present Thesis my case the problem fit in the second type.

3.2.1 Propeller revolution rate (rpm)

In many cases, this parameter is selected previously to the propeller design and may not be a part of the preliminary design. A reduction of the RPM tends to be beneficial as the local section velocities become smaller. Vibration considerations may restrict the allowable range of RPM as the rotational speed and the number of blades together determine the frequency of unsteady forces. The rotational speed should be chosen, if possible, to be sufficiently different from resonant frequencies of the hull, shafting, and propulsion machinery.

3.2.2 Diameter of the propeller

The selection of the propeller diameter is dependent on numerous considerations of which the optimum propeller efficiency is usually the first.

The maximum diameter is usually limited by the geometry of the aperture. A further limiting factor is imposed by propeller-induced unsteady hull forces, which decrease with increasing clearance. The propeller efficiency usually increases with increasing diameter.

The diameter of the propeller is influenced by the propeller rpm, a lower rpm resulting in a higher optimum diameter and a higher efficiency. The maximum propeller diameter is limited by the need to maintain adequate clearances between the propeller and the hull and rudder. Typical values of the minimum clearances are required by a classification society

By using a series data to obtain the propeller diameter D for a propeller when absorbing a certain delivered power P_D and a rotational speed N and in association with a ship speed V_s , it is first necessary to determine a mean design Taylor wake fraction (w_T) from either experience, published data or model test results. From this the mean speed of advance V_a can be determined as $V_a = (1 - w_T)V_s$. This then enables the power coefficient B_p to be:

$$B_p = \frac{P_D^{0.5} N}{V_a^{2.5}} \quad (3.1)$$

and then, from a " $B_p - \delta_{OPT}$ " design chart, the value of δ_{OPT} is then read-off from the appropriate 'constant δ line' at the point of intersection of this line and the maximum efficiency line for required B_p value.

Now, it is possible to obtain the optimum diameter D_{OPT} by using the following formula:

$$D_{OPT} = \frac{\delta_{OPT} V_a}{N} \quad (3.2)$$

Now, in my case I don't have the " $B_p - \delta_{OPT}$ " design chart, so in this case it is possible to realize the process manually replacing B_p by K_Q/J^5 and δ by J for different P/D curves, as you will see in the next Chapter.

3.1.3 Number of Blades Z

From the wake field analysis it is known that the blade number affects the unsteady force levels. Therefore, the permissible levels of the exciting forces may influence the number of blades. In the other hand, efficiency considerations also have their impact on the choice of the number of blades: the optimum open-water efficiency (without any other restrictions) decreases with increasing Z . Increasing the number of blades and keeping the same blade area ratio and thickness-to-chord ratio will lead to a significantly reduced section modulus and an increased stress level. Near the blade tips, an increased blade area may be necessary in that case.

3.1.4 Pitch ratio P/D

The pitch ratio of a propeller governs the power that it will absorb in given; operating conditions, i.e. speed of advance and rpm: the higher the pitch ratio the higher the delivered power at a constant advance coefficient. The effect of pitch ratio on propeller rpm is given approximately by the following empirical relationships due to van Manen (1957):

$$\begin{aligned} \frac{\delta n/n}{\delta(P/D)/(P/D)} &= 1 && \text{at constant torque} \\ \frac{\delta n/n}{\delta(P/D)/(P/D)} &= 1.5 && \text{at constant power} \\ P + D &= \text{constant} && \text{at constant power and rpm} \end{aligned} \tag{3.3}$$

3.1.5 Blade area ratio(*blade outline*)

It is selected basically from considerations of cavitation. A certain minimum blade area being necessary to ensure that even if cavitation occurs it is within acceptable limits. Unduly large blade area ratios cause a reduction in propeller efficiency due to an increase in blade section drag.

Decreasing the blade area (or the chord) increases the efficiency because of the decreased frictional drag. This tendency holds up to the point where strength requirements cause the thickness to- chord ratio to become too large with an associated increase in form drag.

Very low expanded blade area ratios (below 0.3) may lead to difficulties in generating adequate astern thrust. A small increase in blade area ratio may be made to keep propeller blade stresses within permissible limits without an increase in the blade thickness fraction.

3.1.6 Skew

Concurrent with the development of the blade outline, the amount of skew must also be delineated. Highly skewed propellers, with skew greater than about 25 to 30 degrees, have the following advantages:

- Decrease in propeller-induced unsteady bearing forces and moments
- Decrease in propeller-induced unsteady pressure forces
- Decreased susceptibility to cavitation when operating in a wake

The cost of these advantages are:

- Decreased backing efficiency
- More difficulty in manufacture
- Strength-related problems for very high skew and for backing conditions

Concerning the open-water performance, Boswell (1971) and Cumming, Morgan, and Boswell (1972) found that skew has insignificant influence on efficiency for the ahead condition. Backing efficiency, on the other hand, shows large reductions with skew

3.1.7 The boss diameter

The boss diameter ratio of fixed pitch propellers usually lies between 0.15 and 0.20, values outside this range fall into a drop in propeller efficiency. The minimum permissible boss diameter, however, depends upon the diameter of the propeller shaft.

3.1.8 The radial distribution of loading

The variation of circulation with radius upon which the radial distribution of thrust depends is normally made optimum for the given average wake at each radius. In some cases, however, the loading may be decreased towards the blade tips to reduce cavitation, blade stresses and

propeller induced hull vibration. Departures from the optimum load distribution are naturally accompanied by a loss in efficiency.

3.1.9 Expanded blade area ratio A_E/A_o

It is selected basically from considerations of cavitation, a certain minimum blade area being necessary to ensure that even if cavitation occurs it is within acceptable limits. One criterion which may be used to determine the expanded blade area required to avoid cavitation is due to Keller (1966):

$$\frac{A_E}{A_o} = \frac{(1.3 + 0.3Z)T}{(p_o - p_v)D^2} + k \quad (3.4)$$

where k is a constant, equal to 0 for high speed twin screw ships such as naval vessels with transom sterns, 0.1 for twin screw ships of moderate speed with cruiser sterns and 0.2 for single screw ships

3.1.9 wake fraction $w(x)$

For a "wake adapted" propeller, it is necessary to know the mean effective circumferential wake fraction $w(x)$ as a function of the non-dimensional radius $x = r/R$.

3.3. Second stage: Detail design phase

The second step, *design*, known like "indirect" problem, can be done using the lifting line theory with lifting surface corrections (Circulation Theory) and the objective is to find the blade geometry for a specified distribution of blade loading over the radius (wake adapted propeller). In lifting line theory, propeller is replaced by a vortex system and the induced velocities in the propeller plane can be calculated without knowing propeller geometry. In a first stage known as hydrodynamic design, the circulation, the induced velocities, the resultant velocity and the hydrodynamic pitch at the various radii are calculated. In lifting line theory

the induced velocities are evaluated only on a single line. Since the propeller blades are surfaces, have finite thickness and operate in viscous flow, the angle of attack and chamber are corrected taking into account the lifting surface, thickness and viscous effects. Once the design is completed, the propeller is analyzed in all operating conditions: this is the third stage *analysis*, as well as known like "direct" problem and the objectives are to find the pressure distributions on propeller surfaces and to evaluate the hydrodynamics performances of propeller in off-design conditions.

3.3.1 The lifting line theory with lifting surface corrections method

The Circulation Theory may be used to design a propeller in detail to obtain a prescribe distribution of loading along the radius, a pitch distribution matching the mean circumferential wake at each radius and blade section shapes that fulfill desired cavitation and strength requirements.

Circulation theory methods are used for the design of propellers that are prone to have cavitation problems and work in very non-uniform velocity fields. In such cases, these theoretical design methods offer significant advantages regarding efficiency and cavitation over methods based on experimental propeller methodical series data using cavitation charts. At this point the following quantities or information must be known from the preliminary design calculation using methodical series data:

- V : Speed of the ship
- T : Propeller thrust
- D : Propeller diameter
- Z : Number of blades
- A_E/A_0 : An estimated expanded blade area ratio
- h : The depth of immersion of the shaft axis
- n : Propeller revolution rate
- $w(x)$: The mean effective circumferential wake fraction, for $x=r/R$

Now, the procedure will be explained in order, according to the methods proposed in the books *A propeller design method* by M.K. Eckhardt, W.B. Morgan, 1955 and the *Basic ship propulsion* by J.P. Ghose and R.P. Gokan, 2004.

(1) The difference between effective and nominal wake must be corrected as follow:

$$1 - w(x) = \frac{1 - \bar{w}}{1 - \bar{w}_{nom}} [1 - w_{nom}(x)] \quad (3.5)$$

where:

\bar{w} :is the effective wake fraction determined through a self-propulsion test using thrust identity

$w_{nom}(x)$:is the mean nominal circumferential wake fraction at radius x determined through a wake survey

\bar{w}_{nom} :is the volumetric mean nominal wake fraction given by:

$$1 - \bar{w}_{nom} = \frac{2}{1 - x_b^2} \int_{x_b}^1 [1 - w_{nom}(x)] x dx \quad (3.6)$$

with:

X_b :being the non-dimensional boss radius.

Then, the mean velocity of advance of the propeller is:

$$\bar{V}_A = (1 - \bar{w}) V \quad (3.7)$$

(2) Now, the thrust loading coefficient must be determined as follow:

$$C_{TL} = \frac{T}{\frac{1}{2} \rho A_o \bar{V}_A^2} \quad (3.8)$$

where $A_o = \pi D^2/4$ is the disc area of the propeller, and the advance ratio:

$$\lambda = \frac{\bar{V}_A}{\pi n D} \quad (3.9)$$

(3) One may then estimate the ideal thrust loading coefficient (i.e. for an inviscid fluid):

$$C_{TLi} = (1.02 \text{ to } 1.06) C_{TL} \quad (3.10)$$

At the same time one may make an initial estimate of the average drag-lift ratio, $\tan \gamma$ for the whole propeller, using the following relation:

$$\tan \gamma = \frac{0.4}{Z} \frac{A_E}{A_O} - 0.02 \quad (3.11)$$

and then obtain:

$$C_{TLi} = \frac{C_{TL}}{1 - 2\lambda \tan \gamma} \quad (3.12)$$

(4) Estimation of the ideal efficiency η_i of the propeller. By using the Kramer diagram (Figure 3.4), which gives η_i as a function of C_{TLi} , λ and Z . In order to select the best η_i the iterative process described in the following to determine the hydrodynamic pitch angles to be determined at the various radii x :

$$\tan \beta = \frac{[1 - w(x)] V}{2 \pi n r} = \frac{[1 - w(x)] V}{\pi n D x} \quad (3.13)$$

$$\tan \beta_I = \frac{1}{\eta_i} \tan \beta \left[\frac{1 - \bar{w}}{1 - w(x)} \right]^{\frac{1}{2}} \quad (3.14)$$

or

$$\tan \beta_I = \frac{1}{\eta_i} \tan \beta \left[\frac{1 - \bar{w}}{1 - w(x)} \right]^{\frac{3}{4}} \quad (3.15)$$

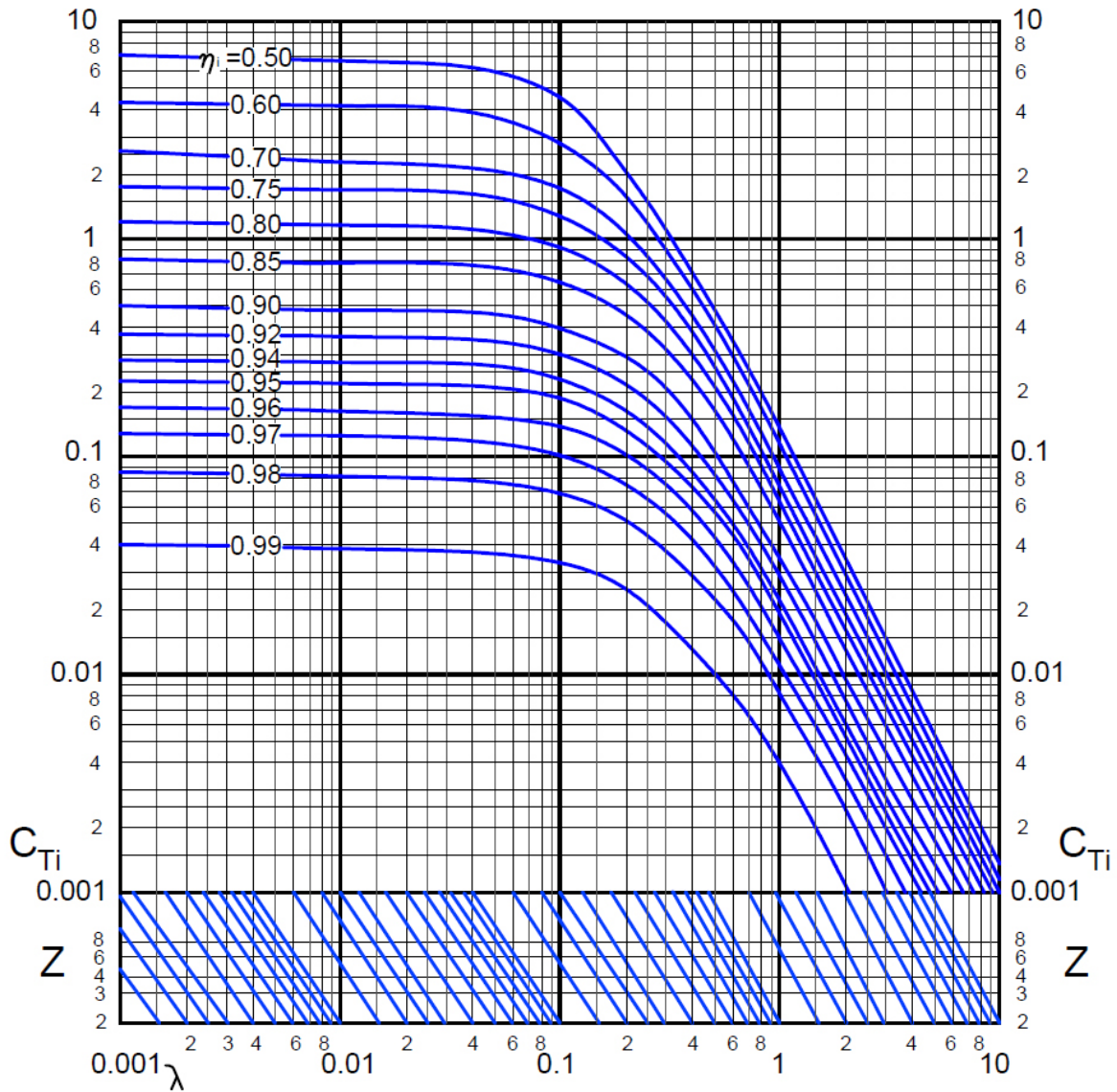


Figure 3.4 Kramer's Thrust coefficient curves (A propeller design method, 1955)

The latter two equations (3.14) and (3.15) are the optimum criteria for wake adapted propellers proposed by Lerbs (1952) and by van Manen (1955) respectively. and the aim is making the product of the ideal efficiency and the hull efficiency constant over the radius.

(5) In order to decrease the risk of cavitation, it is necessary to decrease the loading on the blades near the tip. To obtain this it is necessary reduce the values of β_I from the previous equations (3.14) and (3.15) using an appropriate pitch distribution factor for each radius. A typical radial distribution of hydrodynamic pitch to give reduced loading over the outer radii

has been suggested by O'Brien (1962) and is given in Table 3.2, which establish the ratio of the tangent of the hydrodynamic pitch angle at a non-dimensional radius x to that at $0.7R$. The loading on the blades may also be reduced at the inner radii to minimize hub vortex cavitation.

Radial Distribution of Hydrodynamic Pitch Angle for Reduced Thrust Loading at Outer Radii		
$0.2 \leq x \leq 0.4$	$\frac{\tan \beta_I(x)}{\tan \beta_I(0.7)} =$	$1.11 - 0.1x$
$0.4 \leq x \leq 0.6$	$\frac{\tan \beta_I(x)}{\tan \beta_I(0.7)} =$	$1.03 + 0.3x - 0.5x^2$
$0.6 \leq x \leq 1.0$	$\frac{\tan \beta_I(x)}{\tan \beta_I(0.7)} =$	$1.21 - 0.3x$

Table 3.2 Radial distribution of hydrodynamic pitch O'Brien (1962)

(6) After obtaining the hydrodynamic pitch angles at the different radii, one may calculate the local advance ratios including the induced velocity components:

$$\lambda_I = x \tan \beta_I \quad (3.16)$$

(7) Obtain the Goldstein factors K for each radius which are given as functions of $1/\lambda_I$, the non-dimensional radius x and the number of blades Z are obtained for instance from the following table and its corresponding curves in **Figure 3.5**, it shows an example of the curves to obtain K from the Goldstein Functions for Four-Bladed Propellers.

$$k = a + b \left(\frac{1}{\lambda_I} \right) + c \left(\frac{1}{\lambda_I} \right)^2 + d \left(\frac{1}{\lambda_I} \right)^3 \quad (3.17)$$

r/R	Number of Blades, $Z=4$			
	a	b	c	d
0.2	1.7496360E+00	-3.3573776E-01	5.0925408E-02	-2.6573427E-03
0.3	1.3368727E+00	-1.9570281E-01	3.6153845E-02	-2.2237762E-03
0.4	1.0046545E+00	-2.9904420E-02	7.6526800E-03	-5.3613057E-04
0.5	7.4438787E-01	1.0496193E-01	-1.5128205E-02	7.1173272E-04
0.6	5.0827870E-01	2.3900738E-01	-4.1976690E-02	2.5905205E-03
0.7	3.6886668E-01	2.7456838E-01	-4.3508161E-02	2.4397825E-03
0.8	2.1533333E-01	3.0709362E-01	-4.8083916E-02	2.8236208E-03
0.85	1.6254544E-01	2.8706294E-01	-4.1976690E-02	2.3682984E-03
0.9	9.4375750E-02	2.6828283E-01	-3.8787870E-02	2.2626263E-03
0.95	2.6442423E-02	2.2522765E-01	-3.3561774E-02	2.0916860E-03
0.975	3.0242424E-03	1.6694678E-01	-2.3643358E-02	1.4390054E-03

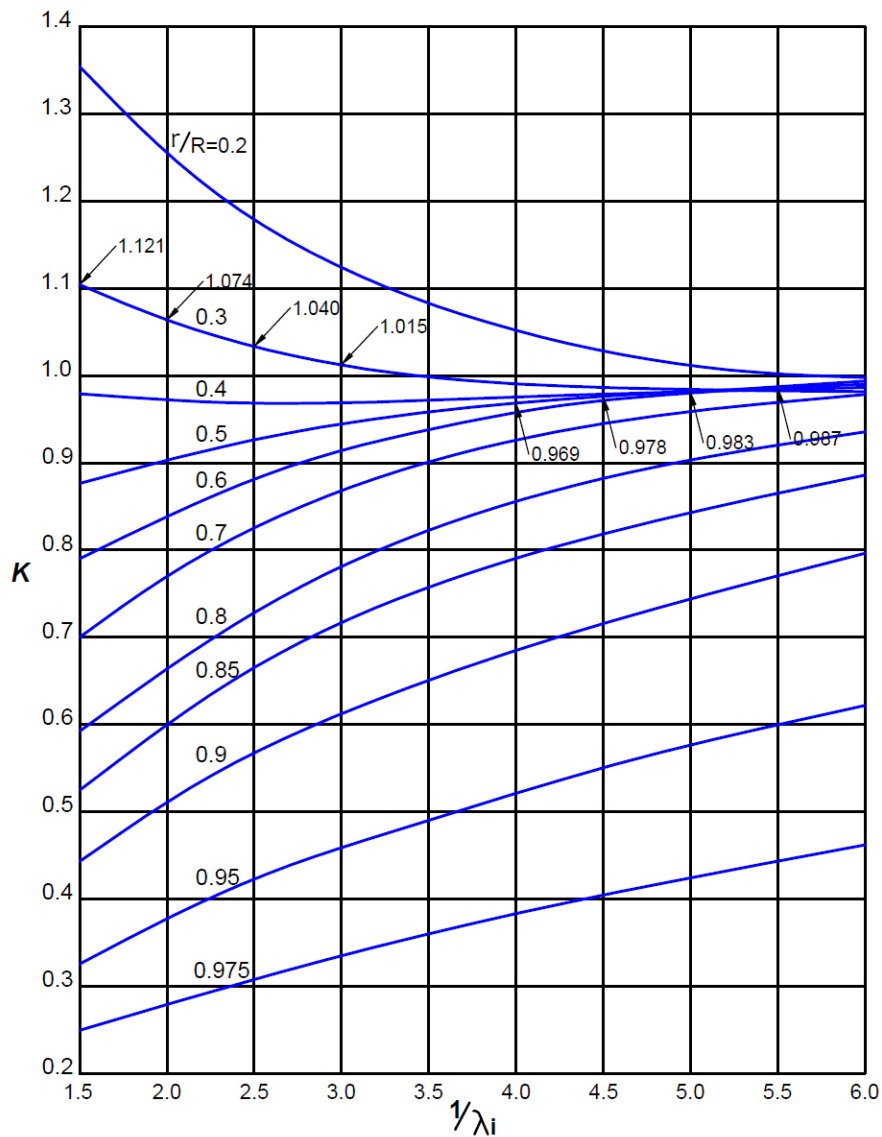


Figure 3.5 Goldein Functions (K) for Four-Bladed Propellers (**A propeller design method, 1955**)

(8) One may now calculate the radial distribution of the ideal thrust loading coefficient after including the Goldstein factor:

$$\frac{dC_{TLi}}{dx} = 8 \times k \frac{\frac{1}{2}u_t}{V_A} \frac{V_R}{V_A} \cos \beta_I \quad (3.18)$$

where:

$$\frac{\frac{1}{2}u_t}{V_A} = \frac{\tan \beta_I (\tan \beta_I - \tan \beta)}{\tan \beta (1 + \tan^2 \beta_I)} = \frac{\sin \beta_I \sin(\beta_I - \beta)}{\sin \beta} \quad (3.19)$$

and

$$\frac{V_R}{V_A} = \frac{\cos(\beta_I - \beta)}{\sin \beta} \quad (3.20)$$

The equation (3.18) could also be written in terms of a non-dimensional circulation defined by:

$$G = \frac{T}{\pi D V_A} = \frac{2 \times k}{Z} \frac{\frac{1}{2}u_t}{V_A} \quad (3.21)$$

then,

$$\frac{dC_{TLi}}{dx} = 4 Z G \left[\frac{1}{\tan \beta} - \frac{\frac{1}{2}u_t}{V_A} \right] \quad (3.22)$$

and the ideal thrust loading coefficient is obtained from the integration of (3.22)

$$C_{TLi} = \int_{x_b}^1 \frac{dC_{TLi}}{dx} dx \quad (3.23)$$

In this point the value of C_{TLi} must be equal to the initial value of C_{TLi} calculated from Eqn. (3.10) or Eqn. (3.12). If the two values of $CTLi$ are not in agreement, the value of η_i must be altered and the calculation repeated until the initial value of C_{TLi} from Eqns. (3.10) or (3.12) and the final value obtained from Eqn. (3.23) are in sufficiently close agreement. Eckhardt and Morgan (**A propeller design method, 1955**) suggest that the number of iterations to bring this about can be reduced by using the following empirical relation:

$$\eta_{i(k+1)} = \frac{\eta_{ik}}{1 + \frac{C_{TLi0} - C_{TLik}}{5 C_{TLi0}}} \quad (3.24)$$

where η_{ik} and $\eta_{i(k+1)}$ are the values of η_i for the k^{th} and $(k + 1)^{\text{th}}$ iterations, C_{TLi0} is the desired value of C_{TLi} , and C_{TLik} the value obtained, in the k^{th} iteration.

(9) Once the radial distribution of hydrodynamic pitch angle for a specified ideal thrust loading coefficient has been determined, the values of the product $C_L \frac{c}{D}$ at various radii can be obtained:

$$C_L \frac{c}{D} = \frac{4\pi}{Z} x k \sin \beta_I \tan(\beta_I - \beta) \quad (3.25)$$

c/D is obtained from the following table 3.4

(10) Determining the shape of the blade sections at the different radii and their pitch angles. Since The lift coefficient C_L depends upon the type of aerofoil section, and its camber ratio, thickness-chord ratio and the angle of attack, it is necessary to choose these geometrical parameters regarding the requirements of minimum risk of cavitation, adequate blade strength and minimum drag in order to obtain the desired values of $C_L \frac{c}{D}$ at different radii depending the chosen aerofoil used in propeller design via circulation theory.

The geometrical details of the various types of sections used in propellers designed by the circulation theory for NACA-16 and NACA-66 is shown in following Table 3.3.

	Mean Lines		Thick Distributions	
	NACA a=0.8 (modified)	NACA a=1.0	NACA-16	NACA-66 (modified)
x/c	$y_c(x)/f$	$y_c(x)/f$	$y_t(x)/f$	$y_t(x)/f$
0	0	0	0	0
0.0125	0.0907	0.097	0.1077	0.1044
0.025	0.1586	0.169	0.1504	0.1466
0.05	0.2711	0.287	0.2091	0.2066
0.075	0.3657	0.384	0.2527	0.2525

0.1	0.4482	0.469	0.2881	0.2907
0.2	0.6993	0.722	0.3887	0.4
0.3	0.8633	0.881	0.4514	0.4637
0.4	0.9614	0.971	0.4879	0.4952
0.5	1.0	1.0	0.5	0.4962
0.6	0.9785	0.971	0.4862	0.4653
0.7	0.889	0.881	0.4391	0.4035
0.8	0.7026	0.722	0.3499	0.311
0.9	0.3687	0.469	0.2098	0.1877
1	0	0	0.01	0.0333

Table 3.3 Mean Lines and Thickness distribution for NACA16 and NACA66,
(Abbot and Doenhoff, 1959)

where:

x = distance from leading edge along nose-tail line

c = section chord

t = section thickness

f = section camber

y_c = ordinate of mean line from nose-tail line

y_t = ordinate of section face (and back) from mean line

The leading edge radii of the two sections are as follows:

	NACA-16	NACA-66 modified
radius=	$0.4885 t^2/c$	$0.448 t^2/c$

The hydrodynamic characteristics of such sections are generally available in the form of diagrams giving $C_L/(t/c)$ for cavitation inception as a function of the minimum pressure coefficient $-C_{pmin}$ for various values of the thickness chord ratio t/c and the camber ratio f/c for "shock free entry" (or ideal angle of attack at which the suction pressure variation does not have a sharp peak). The hydrodynamic characteristics of section shapes used in propellers, are also given in the form of "bucket diagrams" which indicate the range of angles of attack for which the section will not cavitate for a given $-C_{pmin}$, as you can see in the Figure 3.6.

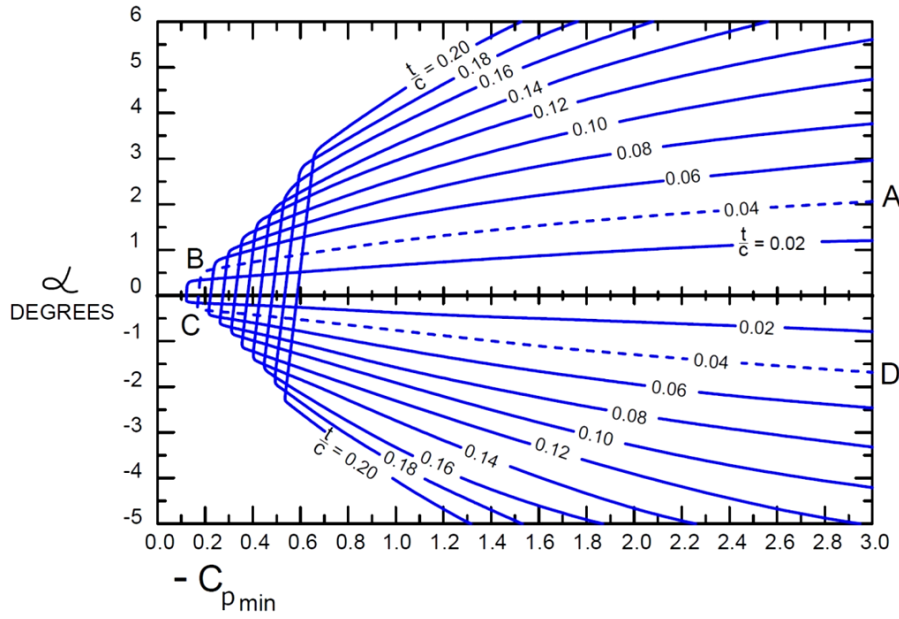


Figure 3.6 Minimum Pressure Envelopes for NACA-66

(11) Blade section geometry: After having selected the type of section to be used, one may use its hydrodynamic characteristics to determine the chord c , the thickness t and the camber f at the various radii r using the value of the minimum pressure coefficient calculated at each radius with the following formula:

$$-C_{p_{min}} = \frac{pA + \rho g (h - xR) - pV}{\frac{1}{2} \rho V_R^2} \quad (3.26)$$

The values of t/c and f/c are then determined so that the required value of C_L , c/D is obtained at each radius without exceeding the limiting value of $C_L/(t/c)$ for cavitation inception at the calculated $-C_{p_{min}}$. The value of $-C_{p_{min}}$ is sometimes reduced up to around 20 percent to allow for the non-uniform flow field. Sometimes it is necessary to fair these values to obtain a smooth variation due an "unfair" variation of f and c with radius r and it is recommended that t/c should not exceed 0.22. After having determined the fair values of c and t at each radius, the value of C_L can be calculated from Eqn. (3.25).

Another option is first to select a suitable blade thickness distribution satisfying a given strength criterion and a suitable blade width distribution, i.e. the variation of c with r . As the following

$$\frac{t(x)}{D} = (1 - x) \frac{t_0}{D} + x \frac{t_1}{D} \quad (3.27)$$

where $t(x)$ is the blade thickness at the non-dimensional radius x , t_0/D the blade thickness fraction and t_1 the tip thickness and a common value for t_1/D is 0.003.

Two standard blade width distributions 'used in propeller design are one used in the Troost B Series and one proposed by Morgan, Silovic and Denny (1968). These chord distributions are given by:

$$\frac{c(x)}{D} = \frac{c_1(x)}{Z} \frac{A_E}{A_O} \quad (3.28)$$

where the values of $C_I(x)$ are given in the following table 3.4

x	<i>Values of $c_I(x)$</i>	
	B Series	Morgan
0.20	1.662	1.6338
0.30	1.882	1.8082
0.40	2.050	1.9648
0.50	2.152	2.0967
0.60	2.187	2.1926
0.70	2.144	2.2320
0.80	1.970	2.1719
0.90	1.582	1.8931
0.95	1.274	1.5362
1.00	0.000	0.0000

Table 3.4 Blade Chord distribution

(12) A suitable distribution of skew to define the shape of the expanded blade in order to minimize unsteady propeller forces due to a non-uniform wake, the outline may also be selected at this stage.

A typical distribution of skew given by Morgan, Silovic and Denny is as follows:

$$\frac{skew(x)}{R} = R_S - [R_S^2 - (x - 0.2)^2]^{0.5} \quad (3.29)$$

where:

$$R_S = \frac{0.32}{skew(1)} + \frac{skew(1)}{2} \quad (3.30)$$

and

$$skew(1) = \frac{\theta_S}{57.3 \cos \beta_I(1)} \quad (3.31)$$

θ_S being the skew angle in degrees and $\beta_I(1)$ the hydrodynamic pitch angle at the blade tip.

Once the blade chord distribution has been selected, the value of C_L can be calculated at each radius from Eqn.(3.25). Normally, it is assumed that at the ideal angle of attack the drag coefficient is $C_D=0.008$ and this allows the lift-drag ratio at each radius to be calculated:

$$\tan \gamma = \frac{C_D}{C_L} = \frac{0.008}{C_L} \quad (3.32)$$

(13) Determine the thrust-loading coefficient for viscous flow as follow:

$$C_{TL} = \int_{x_b}^{1.0} \frac{dC_{TLi}}{dx} (1 - \tan \beta_I \tan \gamma) dx \quad (3.33)$$

At this point C_{TL} should agree sufficiently well with the initial value at the start of the design calculation obtained from Eqn. (3.8).

If the value of C_{TL} obtained from Eqn. (3.33) differs widely from the value obtained from Eqn. (3.8), the value of C_{TL} must be modified and the entire calculation starting from initial estimation of η_i repeated until a satisfactory agreement is obtained between the initial and final values of C_{TL} .

(14) After this, it is possible to determine the power coefficient:

$$C_P = \frac{P_D}{\frac{1}{2} \rho A_O V_A^3} = \int_{x_b}^1 \frac{dC_{TLi}}{dx} \frac{\tan \beta_1 + \tan \gamma}{\tan \beta} dx \quad (3.34)$$

The delivered power P_D obtained from this value of C_P must match the design delivered power of the ship propulsion plant; otherwise, the ship speed and the corresponding propeller thrust must be changed and the calculations repeated until the calculated C_P matches the delivered power available.

(15) Efficiency behind the hull is obtained as follow:

$$\eta_B = \frac{C_{TL}}{C_P} \quad (3.35)$$

(16) Design of the blade sections, once these iterative processes have converged to satisfactory values of C_{TL} and C_P , the camber ratio f/c and the ideal angle of attack α_i are determined at each radius from the corresponding values of C_L :

$$\frac{f}{c} = k_1 C_L \quad \alpha_i^0 = k_2 C_L \quad (3.6)$$

where k_1 and k_2 depend upon the type of mean line and are given in Table 3.5 including the **Correction Factor (μ)**

Mean Line	k_1	k_2	μ
NACA $\alpha = 0.8$	0.06790	1.54	1.05
NACA $\alpha = 0.8$ (modified)	0.06651	1.40	1.00
NACA $\alpha = 1.0$	0.06515	0	0.74
Circular Arc	0.07958	0	0.80

Table 3.5 Camber Ratio, Ideal Angle of Attack and Viscosity Correction Factor (μ)

The value of α_i should lie within the cavitation free zone as indicated in the "bucket diagram" illustrated in Fig. (3.6)

The maximum and minimum values of the angle of attack α for cavitation free operation with a given $-C_{pmin}$, t/c and f/c for blade sections with different types of mean line and thickness distributions may be determined using the following data based on material given in Breslin and Andersen (1994):

$$\alpha_{MAX} = a_1 \frac{f}{c} + a_2 \frac{t}{c} \sqrt{\left[-C_{pmin} + a_3 \frac{t}{c} + a_4 \frac{f}{c} \right]} \quad (3.37)$$

$$\alpha_{MAX} = a_1 \frac{f}{c} - a_2 \frac{t}{c} \sqrt{\left[-C_{pmin} + a_3 \frac{t}{c} + a_4 \frac{f}{c} \right]}$$

where the constants a_1 , a_2 , a_3 , a_4 depend on the mean line and the thickness distribution of the blade section and are given in Table 3.6

Mean line	Thickness distribution	a_1	a_2	a_3	a_4
$a=0.8$	NACA-16	22.6804	28.3183	-2.28	8.1820
$a=0.8$ modified	NACA-66 (modified)	21.0495	27.1163	-2.42	8.3550
$a=0.8$ modified	NACA-16	22.6804	28.3183	-2.28	8.3530
$a=1.0$	NACA-16	0	28.3183	-2.28	9.0662
$a=1.0$	NACA-66 (modified)	0	27.11631	-2.42	9.0662

Table 3.6 Coefficients of Minimum and Maximum Angles of Attack,
Breslin and Andersen (1994)

The values of f/c and a_i obtained from Table 3.5 are correct if the lift coefficient is due to a lifting line in inviscid flow. Since the propeller blades are like lifting surfaces, have a finite thickness and operate in a viscous flow, it is necessary to correct the values of camber ratio and angle of attack to account for lifting surface, thickness and viscosity effects.

Based on experience, the correction for viscosity for the NACA $a=0.8$ mean line, is very small. Blade sections with the NACA $a=0.8$ mean line and NACA-66 (modified) thickness distribution are therefore often preferred for the design of propellers.

For other types of sections, a small increase in the camber ratio or the angle of attack or both is necessary to obtain the required lift coefficient. This is possible using a method suggested by van Manen (1957) as follows:

$$\Delta\alpha^0 = 0.7 \frac{1-\mu}{\mu} k \frac{f}{c} \times 57.3 \quad (3.38)$$

$$\Delta\frac{f}{c} = 0.35 \frac{1-\mu}{\mu} k \frac{f}{c}$$

where μ is the viscous correction factor given in Table 3.5 and k is the Ludwig-Ginzler curvature correction factor which is a function of the number of blades, the blade area ratio, the non-dimensional radius and the hydrodynamic pitch angle.

(17) Lifting surface corrections may be applied using the factors due to Morgan, Silovic and Denny (1968):

$$\frac{f}{c} \text{ corrected} = k_c \frac{f}{c}$$

$$\alpha_i^0 \text{ corrected} = k_\alpha \alpha_i^0 \quad (3.39)$$

$$\alpha_t^0 = 57.3 k_t \frac{t_0}{D}$$

where:

k_c : lifting surface correction factors for camber ratio

k_α : lifting surface correction factors for angle of attack

α_t : is a correction to the angle of attack to account for the finite thickness of the blade

k_t : the corresponding factor and t_0/D the blade thickness fraction.

These correction factors, which are given in Table 3.7 for $Z=4$, have been derived under certain restricted conditions (such as constant hydrodynamic pitch over the radius, and NACA $a = 0.8$ mean line and NACA-66 thickness distribution), and it is not strictly correct to regard these factors as applicable in all cases.

		Number of blades = 4 Expanded blade area ratio = 0.5000 Skew angle = 10 degrees						
x	$\lambda_I :$	0.1000	0.2000	0.3000	0.4000	0.5000	0.6000	0.7000
0.2	k_a	2.5026	2.3229	2.1816	2.0786	2.0139	1.9875	1.9993
	k_c	1.9198	1.8014	1.7290	1.7028	1.7226	1.7886	1.9006
	k_t	0.7149	0.5356	0.3903	0.2790	0.2016	0.1582	0.1488
0.3	k_a	2.2003	2.1983	2.2008	2.2076	2.2189	2.2347	2.2548
	k_c	1.2921	1.2883	1.2975	1.3197	1.3550	1.4033	1.4647
	k_t	0.4565	0.3733	0.3033	0.2464	0.2028	0.1723	0.1549
0.4	k_a	1.9155	2.0267	2.1209	2.1981	2.2582	2.3013	2.3275
	k_c	0.9709	1.0347	1.0910	1.1399	1.1815	1.2156	1.2423
	k_t	0.2539	0.2409	0.2260	0.2093	0.1907	0.1704	0.1482
0.5	k_a	1.6481	1.8081	1.9421	2.0499	2.1317	2.1875	2.2172
	k_c	0.9562	1.0405	1.1095	1.1633	1.2019	1.2253	1.2335
	k_t	0.1074	0.1385	0.1586	0.1676	0.1656	0.1525	0.1284
0.6	k_a	1.5556	1.6800	1.7882	1.8801	1.9558	2.0152	2.0584
	k_c	1.0260	1.1075	1.1727	1.2217	1.2545	1.2710	1.2713
	k_t	0.0497	0.0850	0.1101	0.1252	0.1301	0.1249	0.1096
0.7	k_a	1.4797	1.5251	1.5721	1.6207	1.6710	1.7230	1.7766
	k_c	1.1490	1.2248	1.2835	1.3249	1.3491	1.3561	1.3460
	k_t	0.0307	0.0559	0.0748	0.0877	0.0944	0.0949	0.0893
0.8	k_a	1.3785	1.3087	1.2565	1.2217	1.2045	1.2047	1.2223
	k_c	1.3493	1.4030	1.4437	1.4712	1.4857	1.4871	1.4754
	k_t	0.0228	0.0379	0.0502	0.0596	0.0662	0.0699	0.0708
0.9	k_a	1.1158	0.8078	0.5715	0.4070	0.3142	0.2931	0.3437
	k_c	1.8914	1.8661	1.8463	1.8318	1.8227	1.8189	1.8206
	k_t	-0.0050	0.0169	0.0342	0.0468	0.0548	0.0581	0.0568

Table 3.7 Lifting surface correction factors

(18) The pitch angle at each radius is then obtained:

$$\varphi = \beta_I + \alpha_i + \alpha_t \quad (3.40)$$

and the pitch ratio at each radius becomes:

$$\frac{P(x)}{D} = \pi x \tan \varphi \quad (3.41)$$

3.4. Third stage: Analysis

In the final hydrodynamic analysis the propeller is analyzed in all operating conditions. In the analysis stage the propeller can be evaluated in several ways: computational analysis, experimental model tests and full scale tests. The analysis requires the detailed geometry of propeller, the effective wake distribution and operational conditions of the propeller. The experimental tests in towing tanks and tunnel cavitation are expensive, time consuming and for this reason analytical and numerical methods have been developed and used for the study of the propeller's behaviour in off design conditions.

The objectives of this stage are the evaluation of the hydrodynamic performances of propeller in steady and unsteady flow. Then, for a steady analysis, we can obtain:

- calculation of the open water characteristics
- calculation of the pressure distribution on propeller blades operating in uniform flow or in a radially varied circumferential mean flow

It would be normal to find out eventual problems related to the failure in getting the foreseen performance even in the early stages of the initial design process avoiding the risks of getting them during the most expensive stage of the experiments. Then, the reduction of the design durations and costs become feasible.

In my case, I will perform a 2D and a 3D analysis using FLUENT 6.3 to obtain the pressure on the blades and consequently the Thrust and Torque. The complete analysis and the results from the second stage will be explained in detail within the following Chapter 4.

3.4.1 Turbulence model

The chosen turbulence was *The Realizable k-epsilon turbulence model* because its reputation in the CFD industry due it is the simplest complete model of turbulence using two-equation models in which the solution of two separate transport equations allows the turbulent velocity and length scales to be independently determined. Robustness, economy and reasonable accuracy for a wide range of turbulent flows explain its popularity in industrial flow and heat transfer simulations.

4. ANALYSIS AND RESULTS

In the present chapter, the three stages of propeller design will be applied to a real ship. Starting with the traditional Wageningen-B series propeller diagrams in order to have a starting point for the next stage "preliminary design" using the lifting-line method with surface corrections and applying the data from this method to be used in the final stage "analysis" via CFD- RANS method, using the commercial code Fluent 6.3.

4.1 Definition of the problem

It was already established in section 3.2 that there are two types of design problems for free running propellers, then based on that definition our problem will be as follow:

- Given the engine power and propeller rpm, design the optimum propeller to maximize the ship speed.

The following table 4.1 give us the information provided by the customer or owner of the ship.

V_S	knot	17.4
L_{pp}	m	125
B	m	21.4
T	m	8.5
∇	m ³	14758
Engine type	-	MAN B&W 5 S46ME
Break Power	kW	6900 MCR
RPM	-	129
η_{shaft}	-	0.98

Table 4.1 Main characteristics of the ship and engine.

Within the main characteristics of the ship, it is necessary to have an estimation of the delivered power of the ship P_D based on a resistance prediction of the ship in calm water. In my case the resistance prediction of the ship has been given by ICEPRONAV or it could be also included in the propulsion study, in our case it has been given by an external designer, as shown in the following table:

V_S (knots)	R (kN)	w	t	η_R
15	297.30	0.3231	0.2324	1.049
16	346.49	0.3145	0.2189	1.046
17	422.28	0.3171	0.2224	1.041
18	570.92	0.3072	0.1910	1.037
19	748.21	0.3016	0.1842	1.027

Table 4.2 Resistance prediction of the ship in calm water

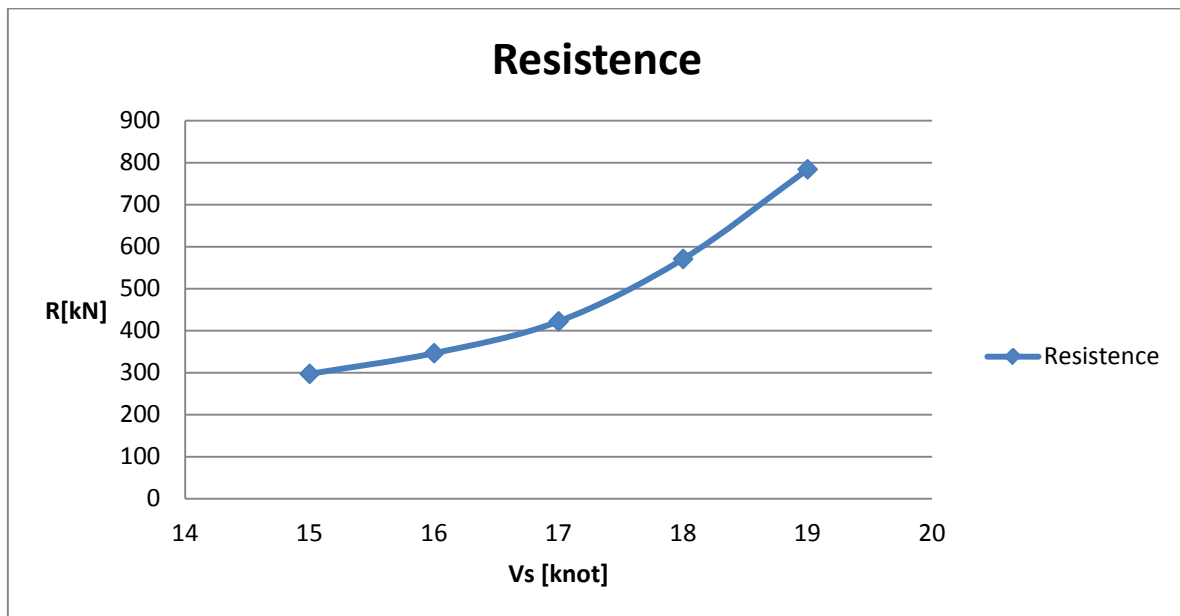


Figure 4.0 Prediction of the Resistance of the ship

The effective wave fraction is $w=0.3144$, and the radial variation of nominal wake is as follows:

$r/R :$	0.2	0.3	0.4	0.5	0.6	0.7	0.8	0.9	1.0
$w(x)=$	0.699	0.684	0.641	0.569	0.456	0.340	0.264	0.224	0.200

The optimum diameter for the propeller will be obtained using an EXCELL sheet with the formulation presented in section 2.2.1 by using the formulas (2.9), (2.10) and the table 2.2 related to the Wageningen-B series of propeller and once the diameter is obtained it must be verified that the diameter doesn't affect the minimum requires regarding the clearance between the tip of the propeller and the hull.

The number of blades Z has been established as 4 due the number of cylinders of the main engine which is 5 in order to avoid resonance.

The expanded area ratio A_E/A_0 is usually part of the optimization result and it may be restricted with respect to cavitation. We will use the criterion developed by Keller (1966):

$$\frac{A_E}{A_0} = \frac{(1.3 + 0.3Z)T}{(p_o - p_v)D^2} + k = \mathbf{0.71} \quad (3.4)$$

where:

$$T = \frac{R_T}{(1 - t)} = \mathbf{604.55 \text{ [kN]}} \quad (4.1)$$

R_T is the Total resistance of the ship in calm water at the service speed of the ship which is $V_S=17.4$ knots and the total resistance is $R_T=476.08[kN]$, Obtained from the curve of Resistance v/s V_S Figure 4.0

t : is thrust deduction fraction, which is 0.2125.

$(p_o - p_v)$ = atmospheric pressure minus vaporization pressure of water

$$(p_o - p_v) = (10^5 - 2300) \text{ [Pa]}$$

$k=0.15$, constant that depends on the type of vessel

Finally it is necessary to estimate the delivered power for the ship P_D . using the following formula:

$$P_D = P_B \cdot \eta_{shaft}(1 - SM) \quad (4.2)$$

where:

$$P_B: 6900 \text{ [kW]}$$

$$\eta_{shaft} = 0.98$$

$SM=15\%$, is the sea margin that does not include the generator load P_G explained in section 3.1

and the delivered Power is

$$P_D = \mathbf{5747.7 \text{ [kW]}}.$$

Using the formula (4.3) it is possible to estimate the required Torque which is:

$$Q = \frac{P_D}{2\pi \cdot n} = \frac{5747.7}{2\pi \cdot 2.15} = \mathbf{425.48 \text{ [kN} \cdot \text{m]}}$$

And finally it is also possible to estimate the Thrust loading coefficient and power coefficient, formulas (2.6), which is:

$$C_{Th} = \frac{T}{\rho V_A^2 D^2 \frac{\pi}{8}} = \mathbf{0.71}$$

$$C_P = \frac{P_D}{\rho V_A^3 D^2 \frac{\pi}{8}} = 0.73$$

4.2. First stage: Preliminary design

In preliminary design stage, a propeller of optimal efficiency is determined using the design charts based on model tests with series of propellers (such as the Wageningen B-series). The main characteristics of the propeller such as diameter, number of blades, rotation rate, etc. are fixed and this is a *starting point* for the propeller design using the circulation theory: lifting line and lifting surface theory.

4.2.1 Use of Wageningen-B series to obtain the optimum diameter D

As you have seen in section 3.2.2, to obtain the optimum diameter it is necessary to use the " B_P - δ_{OPT} " design chart, but this part will be done manually by replacing B_P by K_Q/J^5 and δ by J for different P/D curves. The explanation for using K_Q/J^5 and not other formula is the following:

Using the definition of P_D regarding the torque, it is possible to combine it with the open-water formula for K_Q Formula (2.2) as follow:

$$P_D = Q \cdot \omega \quad (4.3)$$

$$\omega : \text{angular velocity} \quad \omega = 2\pi \cdot n \quad (4.4)$$

then,

$$K_Q = \frac{Q}{\rho \cdot n^2 \cdot D^5} = \frac{P_D}{2\pi \cdot \rho \cdot n^3 \cdot D^5} \quad (2.2) \text{ and } (4.3)$$

finally using the formula of advance number J and replacing D in the last formula we have:

$$J = \frac{V_A}{n \cdot D} \quad (2.3)$$

$$\frac{K_Q}{J^5} = \frac{P_D \cdot n^2}{2\pi \cdot \rho \cdot V_A^5} \quad (4.6)$$

$$V_A = V_S(1 - w) \quad (2.4)$$

The right side of the last formula (4.6) is constant, then it is possible to use it to graph K_Q over J (Fig. 4.1), and then intersect this curve with the P/D curves explained in the following.

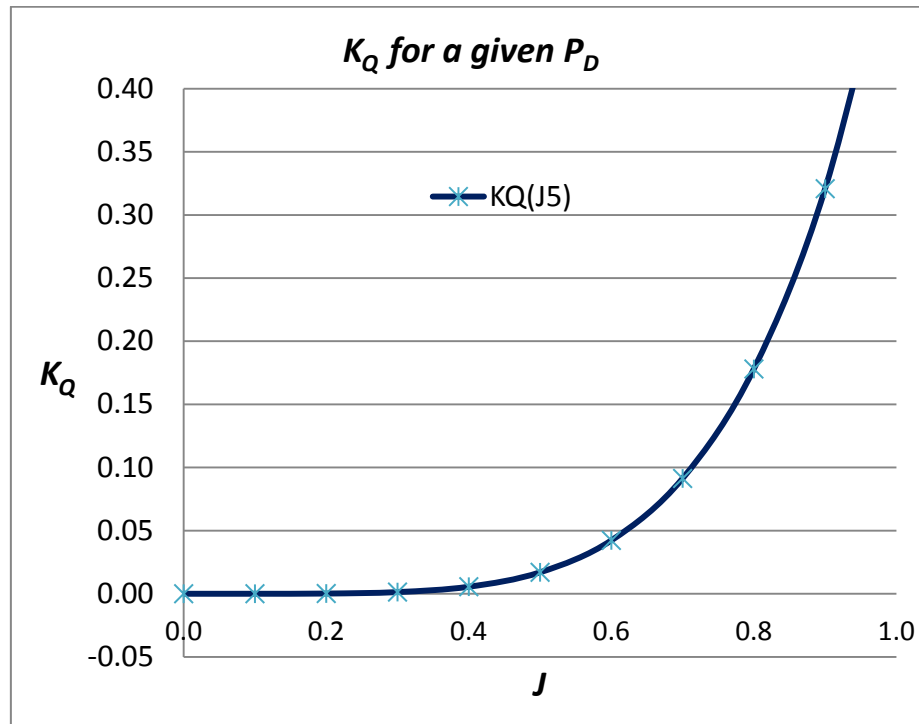


Figure 4.1 K_Q over J for a given P_D .

Normally, the optimum open water efficiency η_o and hence the optimum diameter D_{OPT} are located in range of P/D corresponding at $0.6 < (P/D) < 1.2$, then, four K_Q curves (corresponding to four ratios $P/D=0.6, 0.8, 1.0, 1.2$), will be obtained using the polynomial regression of K_Q made by van Oossanen Form. (2.9) explained in section 2.2.1, keeping constant $A_E/A_o=0.6$ and located on the same graph over J .

The result obtained using an EXCELL application made by myself based on the polynomial form of K_Q explained in the section 2.2.1 for different P/D curves can be seen in the following table 4.3

P/D	J=	0	0.1	0.2	0.3	0.4	0.5	0.6	0.7	0.8	0.9	1
1.2	$K_Q=$	0.08965	0.08589	0.08158	0.07675	0.07142	0.06560	0.05932	0.05259	0.04544	0.03788	0.02994
1.0	$K_Q=$	0.06353	0.06023	0.05646	0.05222	0.04753	0.04239	0.03682	0.03083	0.02444	0.01764	0.01046
0.8	$K_Q=$	0.04141	0.03867	0.03553	0.03198	0.02805	0.02373	0.01904	0.01398	0.00856	0.00279	-0.00332
0.6	$K_Q=$	0.02428	0.02216	0.01971	0.01695	0.01388	0.01051	0.00686	0.00293	-0.0012	-0.0057	-0.01041
$K_Q(J^5)=$		0.0000	0.00001	0.00017	0.00132	0.00556	0.01697	0.04224	0.09129	0.17798	0.32073	0.54317

Table 4.3 K_Q curves for different P/D ratios

In the following graph (Figure 4.2) it is possible to observe the four K_Q curves for different P/D and the K_Q curve from (4.6).

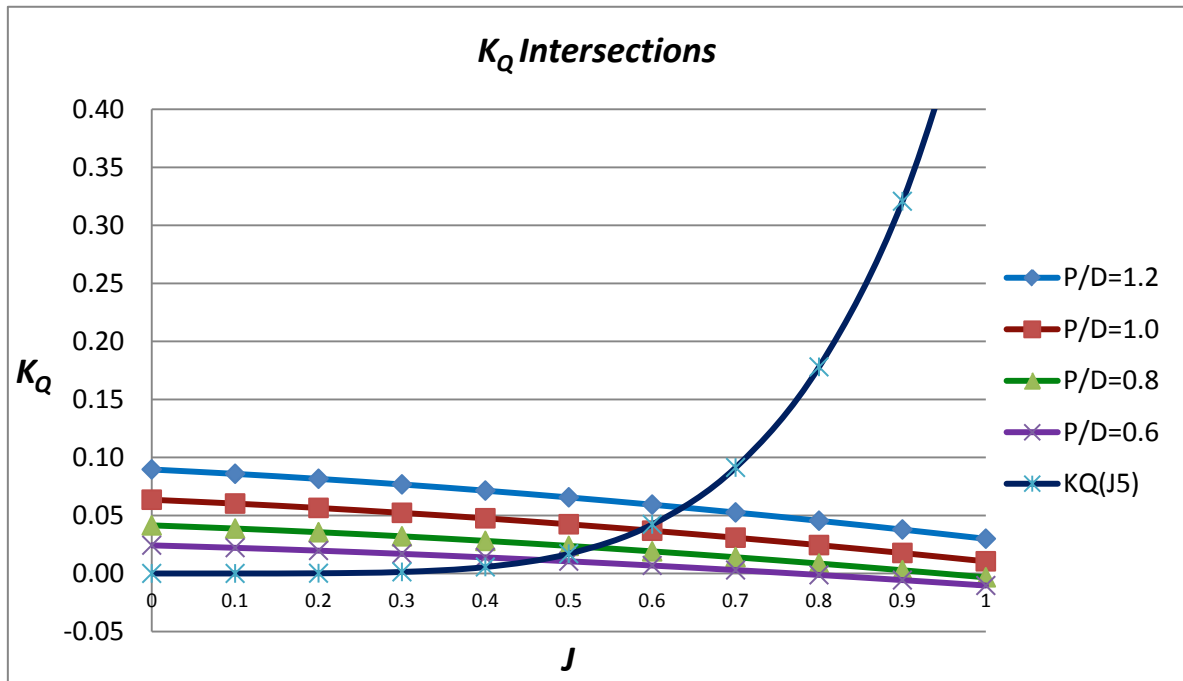


Figure 4.2 Intersections for K_Q curves

On this graph it is possible to define a range of intersection and then to zoom for instance the zone between $0.4 < J < 0.7$ in order to obtain the exact points of intersection as follow.

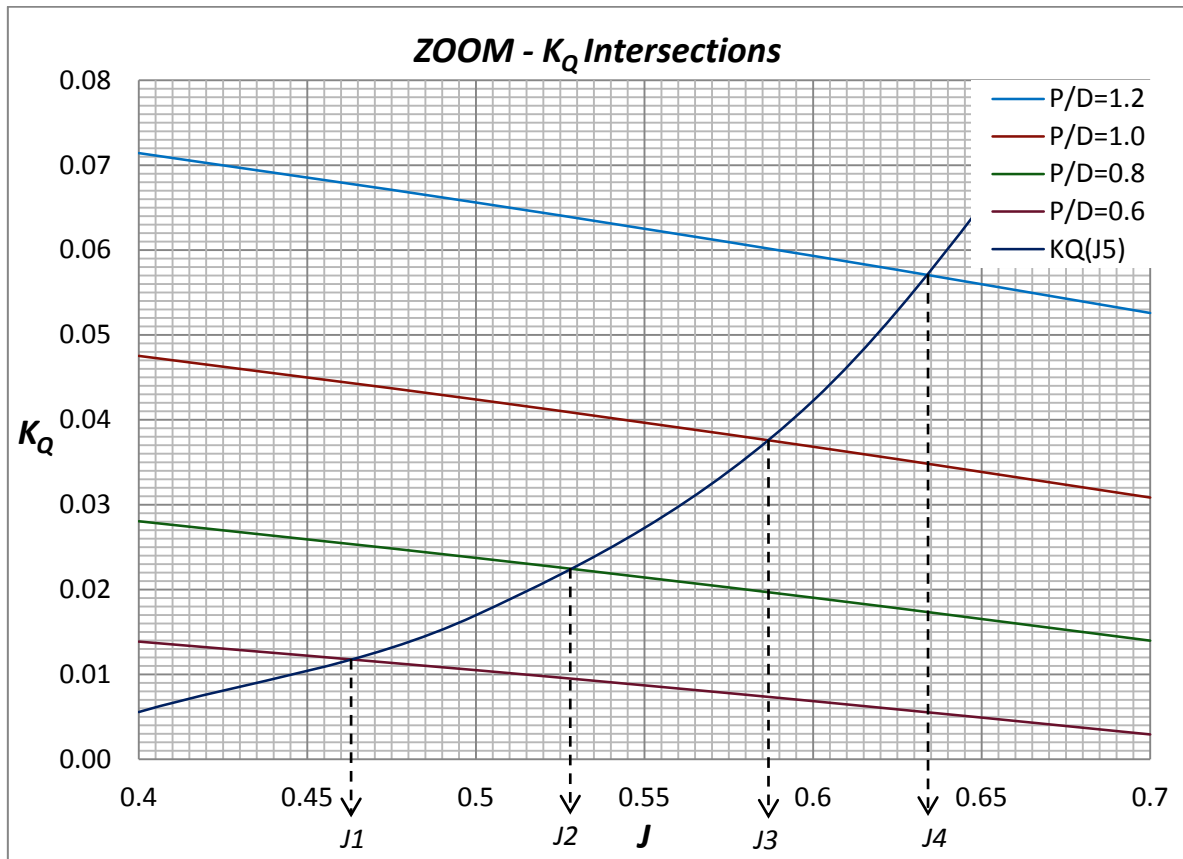


Figure 4.3 Intersections for K_Q curves Zoomed

Once the values for $J1$, $J2$, $J3$ and $J4$ of the intersection points with the P/D curves are obtained, they are replaced in the polynomial regression of K_Q and K_T made by van Oossanen, Formulas (2.9) and (2.10), then replacing these values for each J in the formula (2.3) the open-water efficiency η_o is obtained for each J corresponding to each P/D curve as follow:

$$\eta_o = \frac{K_T}{K_Q} \cdot \frac{J}{2\pi} \quad (2.5)$$

	$J1$	$J2$	$J3$	$J4$
P/D	0.6	0.8	1.0	1.2
$J=$	0.4625	0.5282	0.5863	0.6340
KT	0.0893	0.1586	0.2307	0.3037
KQ	0.0118	0.0224	0.0376	0.0571
$\eta_o=$	0.5568	0.5938	0.5722	0.5368

Table 4.4 Open-water efficiency η_o for each intersection J

Now, the next step is to find the Maximum open-water efficiency η_o from the graph in the Fig.4.3 made of the values obtained in the previous step, where the open-water efficiency η_o

are graphed against $J1$, $J2$, $J3$ and $J4$. The Maximum open-water efficiency will be the highest point of the curve, and from that point the optimum value of J is also obtained.

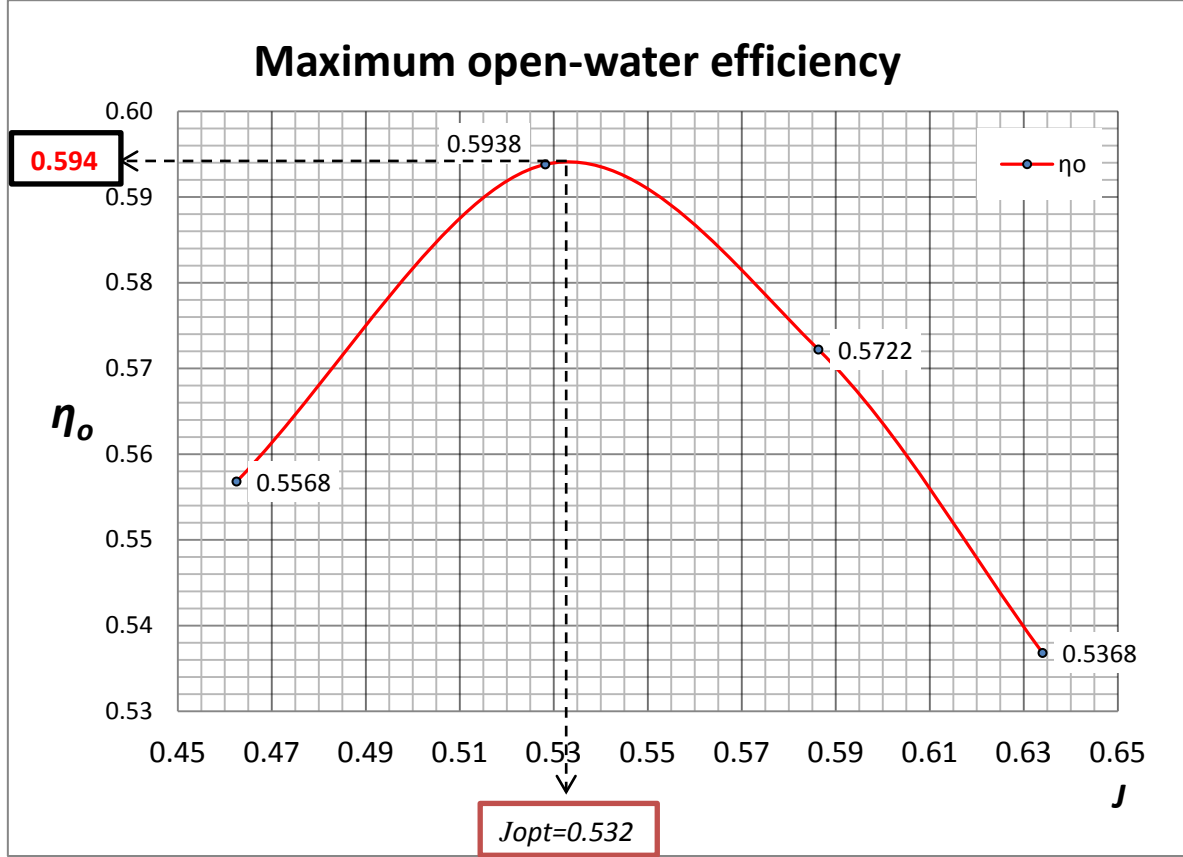


Figure 4.4 Optimum J and maximum open-water efficiency

At this point, using the Formula (2.3) it is possible to find the optimum Diameter D_{OPT} replacing J_{OPT} , n , and V_A on it, as follow:

$$J = \frac{V_A}{n \cdot D} \quad (2.3)$$

where:

$$J_{OPT} = 0.532$$

$$n = 2.15 \text{ rps}$$

$$V_A = 17 \cdot 0.5144 \cdot (1 - 0.3171) = 5.72 \text{ [m/s]} \quad (2.4)$$

Then, the optimum diameter is $D_{OPT} = 5.21 \text{ m}$.

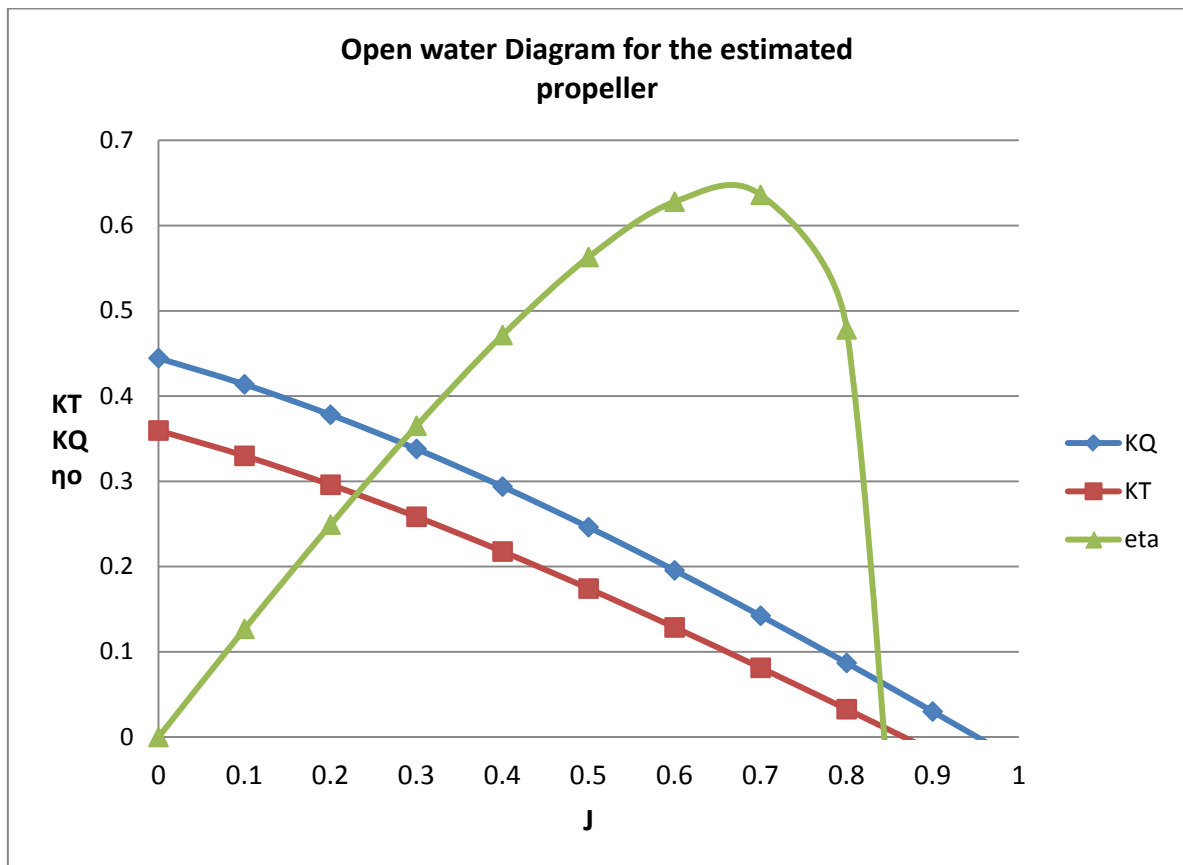
Finally, using the Table 4.2 it is possible to find the optimum P/D ratio by interpolating the values which surround J_{OPT} , as follow:

Interpolation		
P/D		
	P/D	
J3=	0.5863	1
J_{OPT}=	0.532	0.81
J2=	0.5282	0.8

P/D_{optim}

And now, using D_{OPT} and the optimum P/D we can obtain the mean pitch which is $P=4.22m$.

After obtaining the previous data, it is possible to use the Lifting-line theory with surface corrections to obtain the geometry of the propeller. The following diagram correspond to the open water characteristics of the propeller with the previous dimensional characteristics, obtained with the EXCELL application.



4.3. Second stage: Detail design phase

In this stage, *the lifting line theory with lifting surface corrections method* explained in 3.3.1 will be used. This method has been implemented in a code developed at UGAL University by Prof. Amoralities. This code has been used to obtain the parameters of the propeller geometry in order to perform 2D and 3D RANS analysis in the *third stage: Analysis*.

4.3.1 Design of the non-dimension relations of the blade sections.

Using the code developed at UGAL based on *lifting line theory with lifting surface corrections method*, I will obtain the complete geometry of the propeller based on the non-dimension relations for the blade sections at different radii for the expanded outline of the blade. These relations are:

P/D : Pitch ratio

c/D :Chord ratio

t/D :Thickness ratio

f/c :Camber ratio

Furthermore, from this method it is possible to obtain the angle of attack, pitch angle and the tangential speed at each radius.

The main steps in the *lifting line theory with lifting surface corrections method* are:

1. Collection of the necessary design data.
2. Determination of the correct hydrodynamic pitch angle.
3. Determination of the coefficient of lift (C_L), blade sections, thickness ratios (t/D) and camber ratios (f/c) from cavitation considerations.
4. Correction to camber from lifting-surface theory (2).
5. Correction to pitch from lifting-surface theory (3), from the mean line in ideal flow, and from viscous flow.
6. Check of power and of- original approximations.

Once the relations are obtained the next step is to generate the geometry of all the section at each radius. This step will be explained in the following section 4.3.2.

Without knowing the algorithm implemented in the code at UGAL, I can nevertheless, to figure out the flow chart of the *lifting line theory with lifting surface corrections method* that is implemented in the code, as you will see in the following Figure 4.5, finally taking in consideration that the optimum diameter is $D=5.21m$, then the results are in the following table 4.5

r/R	P: Pitch [m]	c: Chord [m]	t:Maximum Thickness [m]	f: Maximum Camber [m]	α deg	β_I deg	V_R m/s
0.2	3.8358	1.5589	0.2279	0.0000	2.0414	47.4805	5.4911
0.3	4.0883	1.7254	0.1956	0.0752	3.5690	36.2120	10.6739
0.4	4.1043	1.8748	0.1656	0.0549	2.8417	29.2417	14.2248
0.5	4.1201	2.0006	0.1373	0.0468	1.9651	24.7576	17.8798
0.6	4.1954	2.0922	0.1112	0.0401	1.3323	21.8002	21.6217
0.7	4.2588	2.1297	0.0868	0.0345	0.8379	19.5527	25.3394
0.8	4.2675	2.0725	0.0634	0.0299	0.4495	17.6019	28.9367
0.9	4.2227	1.8064	0.0416	0.0264	0.0926	15.9026	32.4495
1.0	4.2220	0	0.0208	0.0104	0.0000	14.4639	35.9333

Table 4.5 Main dimensions of the profile obtained from Lifting line theory with surface corrections

The complete results of the Lifting-line theory with surface corrections can be found in the APPENDIX A1

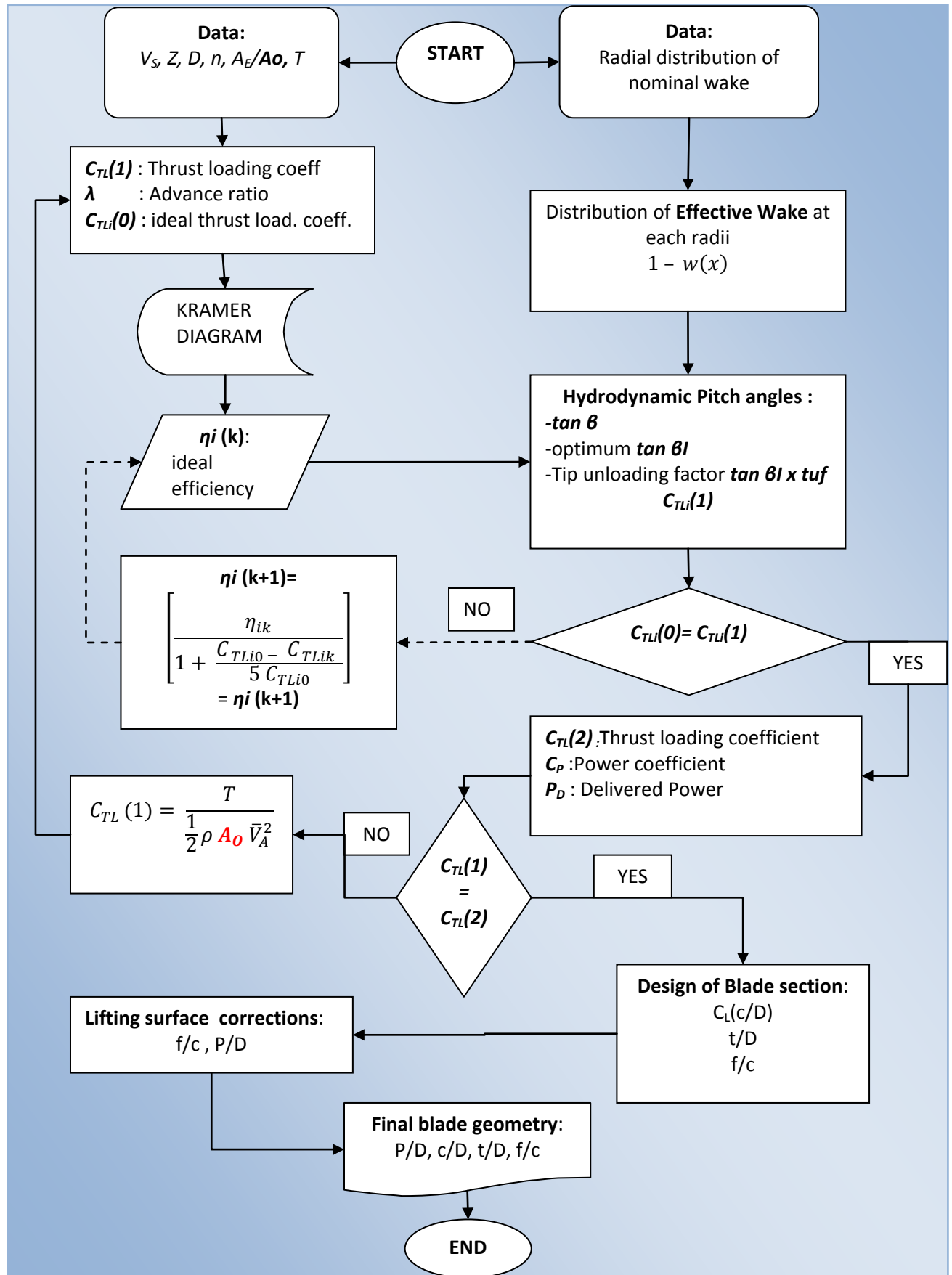


Figure 4.5 Flowchart of the Lifting line theory with surface corrections

4.3.2. Generation of the section geometry

The mean line or camber line (f) is the locus of the mid-points between the upper and lower surfaces when measured perpendicular to the camber line. The ends of the camber line are called the leading and trailing edges of the aerofoil and the straight line joining these two points is termed the chord line (c). The distance between the leading and trailing edges when measured along the chord line is termed the chord length (c) of the section. The camber of the section is the maximum distance between the mean camber line and the chord line, measured perpendicular to the chord line. The aerofoil thickness (t) is the distance between the upper and lower surfaces of the section, usually measured perpendicularly to the chord line although strictly this should be to the camber line.

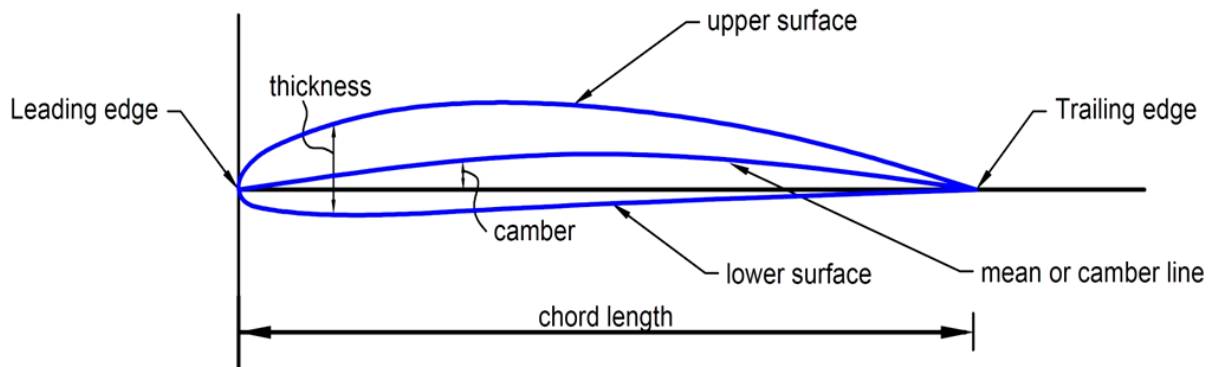


Figure 4.6 General definition of an aerofoil section

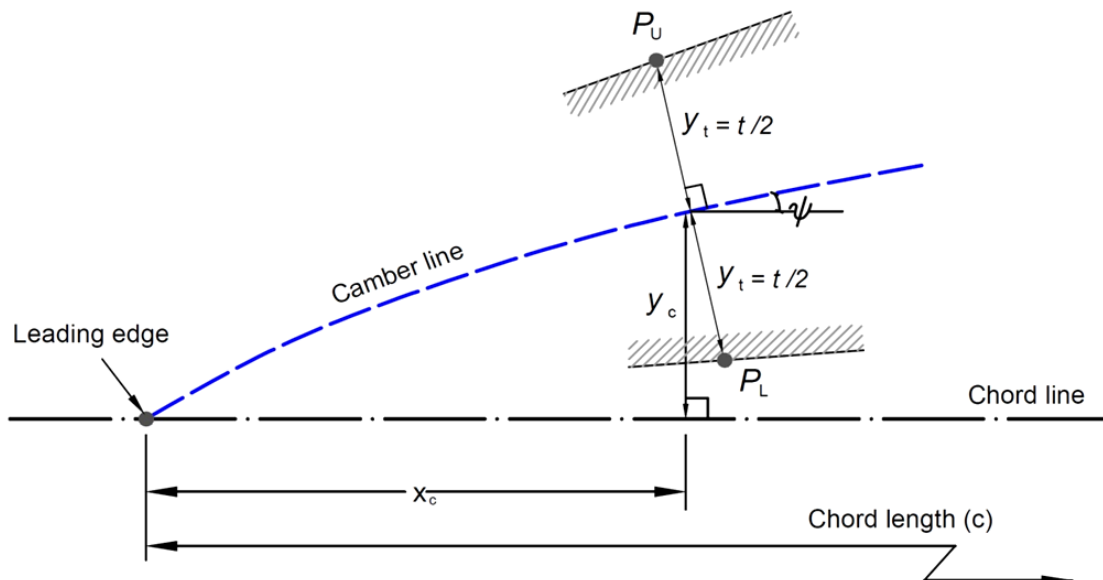


Figure 4.7 Aerofoil section definition

The following **Table 4.6** shows the typical distribution for the airfoil NACA-66(modified), which was used to define the section geometry of the blade, where y_c is the camber in per cent of the maximum camber shown in table 4.5 and y is the thickness in per cent of the maximum thickness shown in table 4.5 as well.

	Distribution	
chord	Camber	thickness
x/c	y_c/f_{max}	y/t_{max}
0	0	0
0.0025	0.0235	0.0445
0.005	0.0423	0.0665
0.0075	0.0595	0.0812
0.0125	0.0907	0.1044
0.025	0.1586	0.1466
0.05	0.2715	0.2066
0.075	0.3657	0.2525
0.1	0.4482	0.2907
0.15	0.5869	0.3521
0.2	0.6993	0.4
0.25	0.7905	0.4363
0.3	0.8635	0.4637
0.35	0.9202	0.4832
0.4	0.9615	0.4952
0.45	0.9881	0.5
0.5	1	0.4962
0.55	0.9971	0.4846
0.6	0.9786	0.4653
0.65	0.9434	0.4383
0.7	0.8892	0.4035
0.75	0.8121	0.3612
0.8	0.7027	0.311
0.85	0.5425	0.2532
0.9	0.3586	0.1877
0.95	0.1713	0.1143
0.975	0.0823	0.0748
1	0	0.0333

Table 4.6 Camber and thickness distribution for aerofoil NACA-66(modified)

With the information obtained until now it is possible to draw the section edges at each radii as follow:

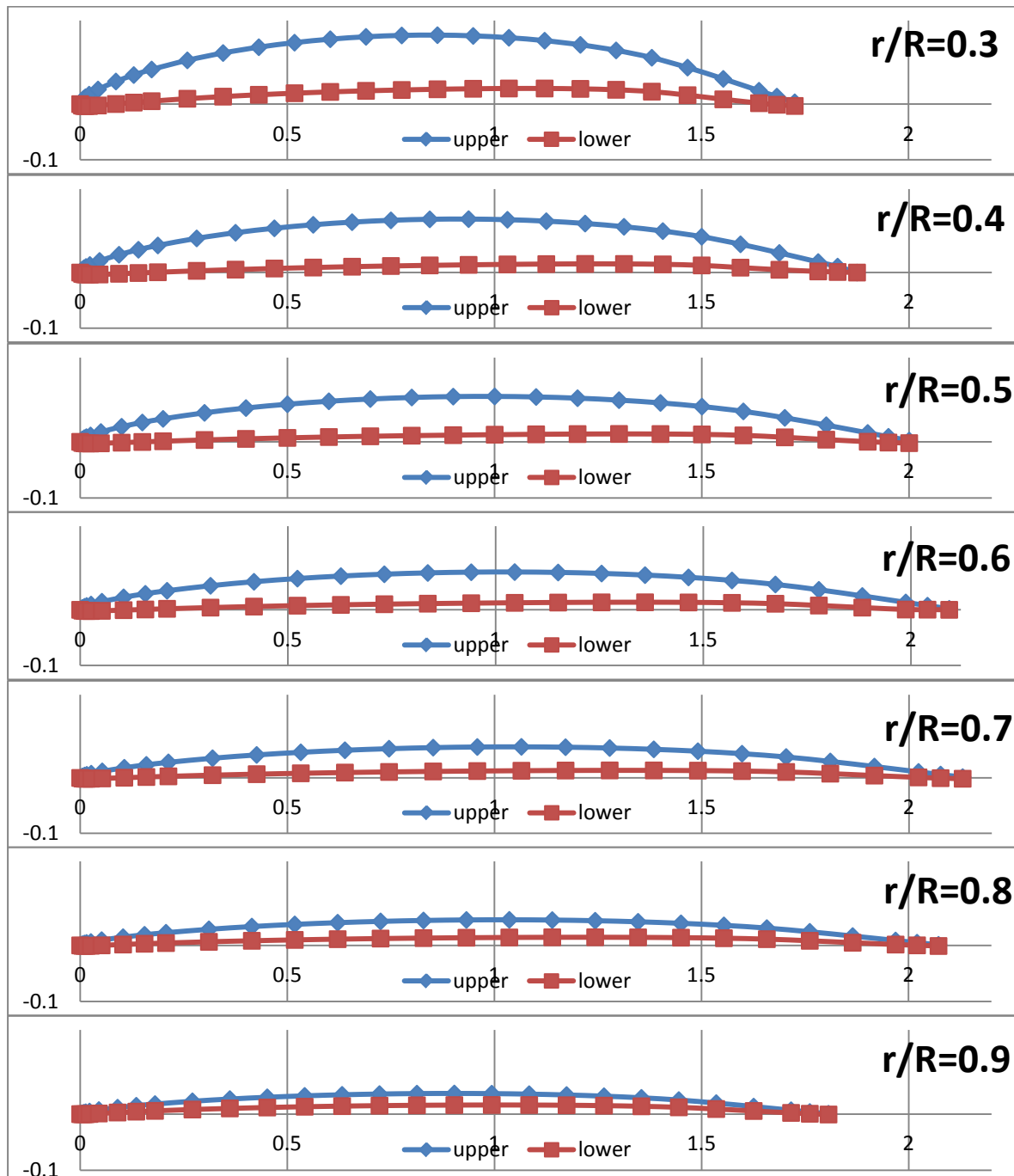


Figure 4.8 Definition of the edges at each radius.

4.3.3 Result of the lifting-line with surface corrections method

In addition to the geometry of the aerofoils shown in the previous section, this method gives the Thrust, Torque and thrust coefficient C_T , which are:

$$\begin{aligned} \mathbf{T} &= 595.68 \quad [\text{kN}] \\ \mathbf{Q} &= 442.14 \quad [\text{kN-m}] \\ \mathbf{C_T} &= 0.70 \quad \text{Thrust coefficient} \end{aligned}$$

This results can now be compared with the results obtained in section 4.1: *Definition of the problem*. in the following table, where the column "Estimated" correspond to the values obtained by using the formulas and the column "Computed" correspond to the result obtained by the Lifting-line method with surface corrections.

	Estimated	Computed	Difference	
C_T	0.71	0.70	0.01	1.41% less than estimated

4.4. Third stage: Analysis of the design

The present stage will begin performing a 2D numerical analysis in Fluent in order to compare the results with the ones from the second stage by analyzing the blade's sections separately in order to obtain the total thrust coefficient of the blade and then compare it with the previous results.

Then, a 3D numerical analysis will be performed in Fluent in order to obtain the Thrust, Torque and the open water propeller diagram.

4.4.1 Numerical Analysis in 2D of the geometry of blade's sections in Fluent

After obtaining the geometry of each blade section we can perform a numerical analysis for each one of the section in order to obtain the lift and drag coefficients to be used to calculate the Thrust loading coefficient.

The geometry of the section will be introduced in the pre-processor software Gambit 2.4.6 importing the section as two groups of vertices with coordinates in 2D and then with the geometry tools of Gambit the two edges and the surface will be created.

The fluid domain has been chosen based in several numerical studies about airfoils or hydrofoils. The following figure shows the typical fluid domain for airfoils analysis.

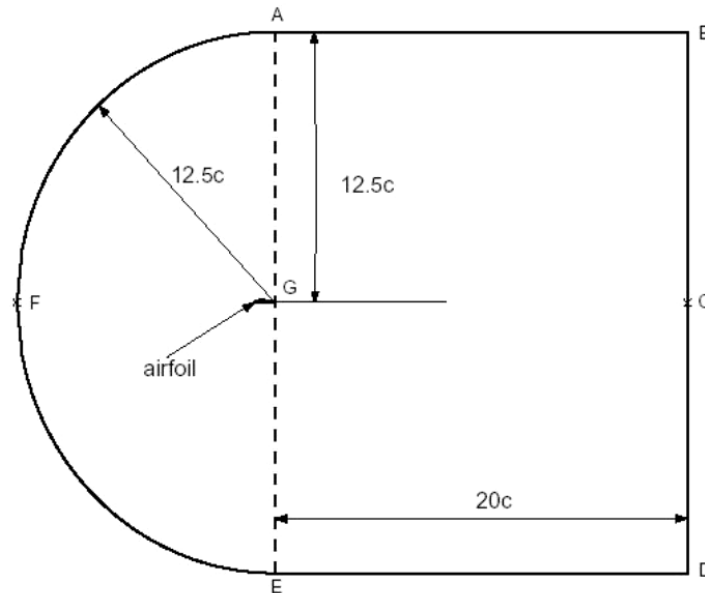


Figure 4.9 Typical Fluid domain in 2D for the analysis of an airfoil

Where c is the chord length of the airfoil.

Once we have created the fluid domain, the next step is to create the meshing, but first it necessary to subtract the region of the airfoil from the fluid domain surface. After that, we start meshing the all the external boundaries and for the airfoil a boundary layer tool will be applied in order to make easier the meshing around the airfoil Fig. 4.10

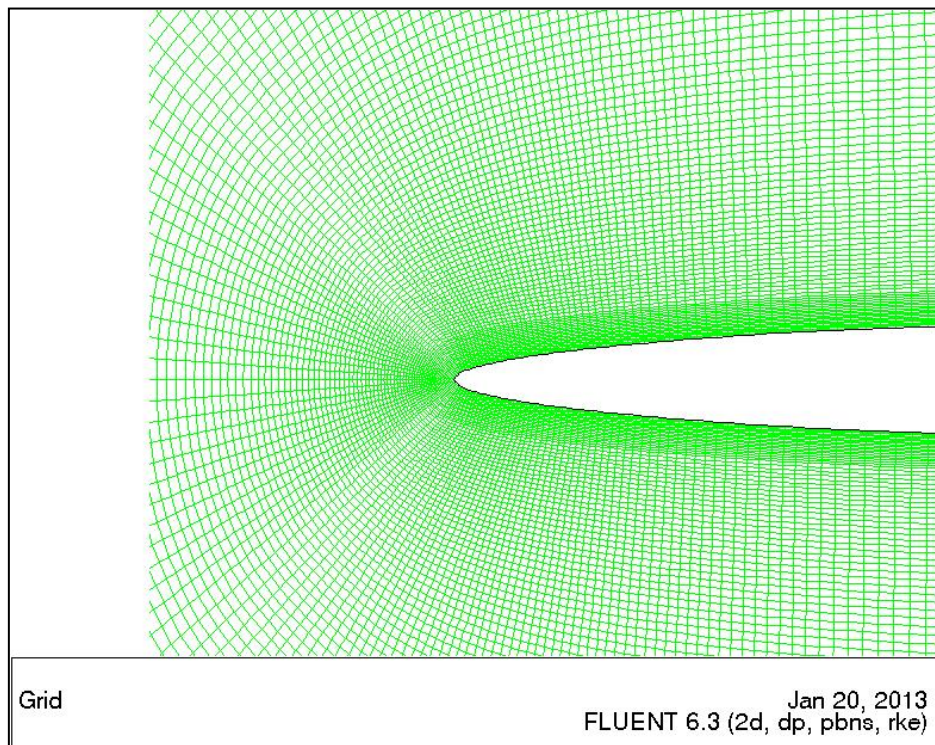


Figure 4.10 Boundary layer applied to the airfoil at $r/R=0.2$

And the following Fig. 4.10 shows the entire meshing of the fluid domain

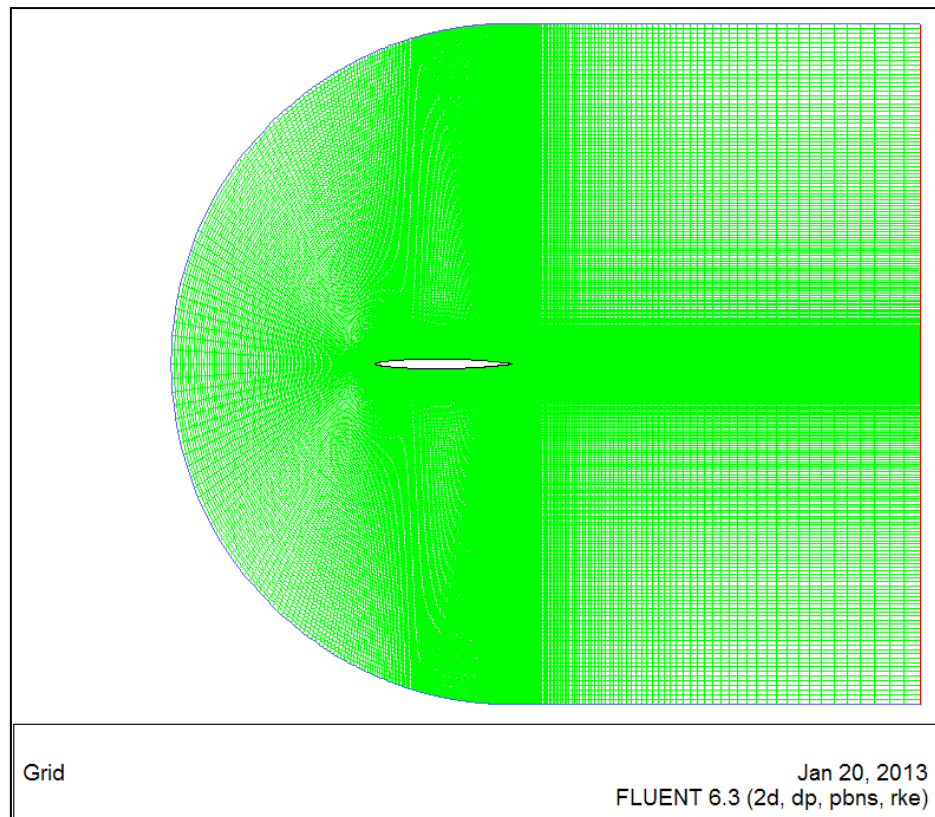


Figure 4.11 Complete meshing of the fluid domain for airfoil at $r/R=0.2$.

Taking the Fig. 4.9 as reference the boundary layers will be created as follow : the lines AB, DE, EF and FA will be defined as Velocity-Inlet; the lines BC and CD will be defined as Pressure-Outlet; and the edges of the airfoil will be defined as Wall.

The speed and the angle of attack for each section was obtained from the Lifting-line theory and the results are in the table 4.5. To set up the speed and the angle of attack the airfoil was modelled in Gambit with 0° angle of attack respect to the x direction and once the model was set-up in Fluent, the speed was introduced in components x and y.

The turbulent model and mesh size was chosen based in the study "*Evaluation of the turbulence models for the simulation of the flow over a NACA-0012 airfoil*" by Eleni, Athanasiuos and Dionissios, 2012 [Ref.19]. This study revealed two important things.

-The first is the effect of the mesh on the solution: generally the numerical solution becomes more accurate as more nodes are used and also this influences the increase the computer memory and computational time. Based on this, an airfoil studied at stall angle of 16° using a C-type topology with quadrilateral cells got same results from the number of cells was 80000. So, in all my meshes I got more than 80000 cells.

-The second is the model of turbulence: analyzing the airfoil at angles of attack between 0° and 20° the results are practically the same for small angles of attack ($\alpha^\circ < 4^\circ$) by comparing the empirical data from Abbot [Ref.20] and the following models of turbulence in Fluent: k-epsilon Realizable, Spalart-Allamas and k-omega SST. Then, since the maximum angle of attack to analyzed in my study is $\alpha^\circ = 3.57^\circ$ for the airfoil at $r/R=0.3$ the chosen turbulence model was the k-epsilon Realizable because of its robustness, economy and reasonable accuracy for a wide range of turbulent flows.

The results will be shown in the table 4.7 and the contours of pressures will be shown in the following set of pictures each one corresponding to one of the section blade.

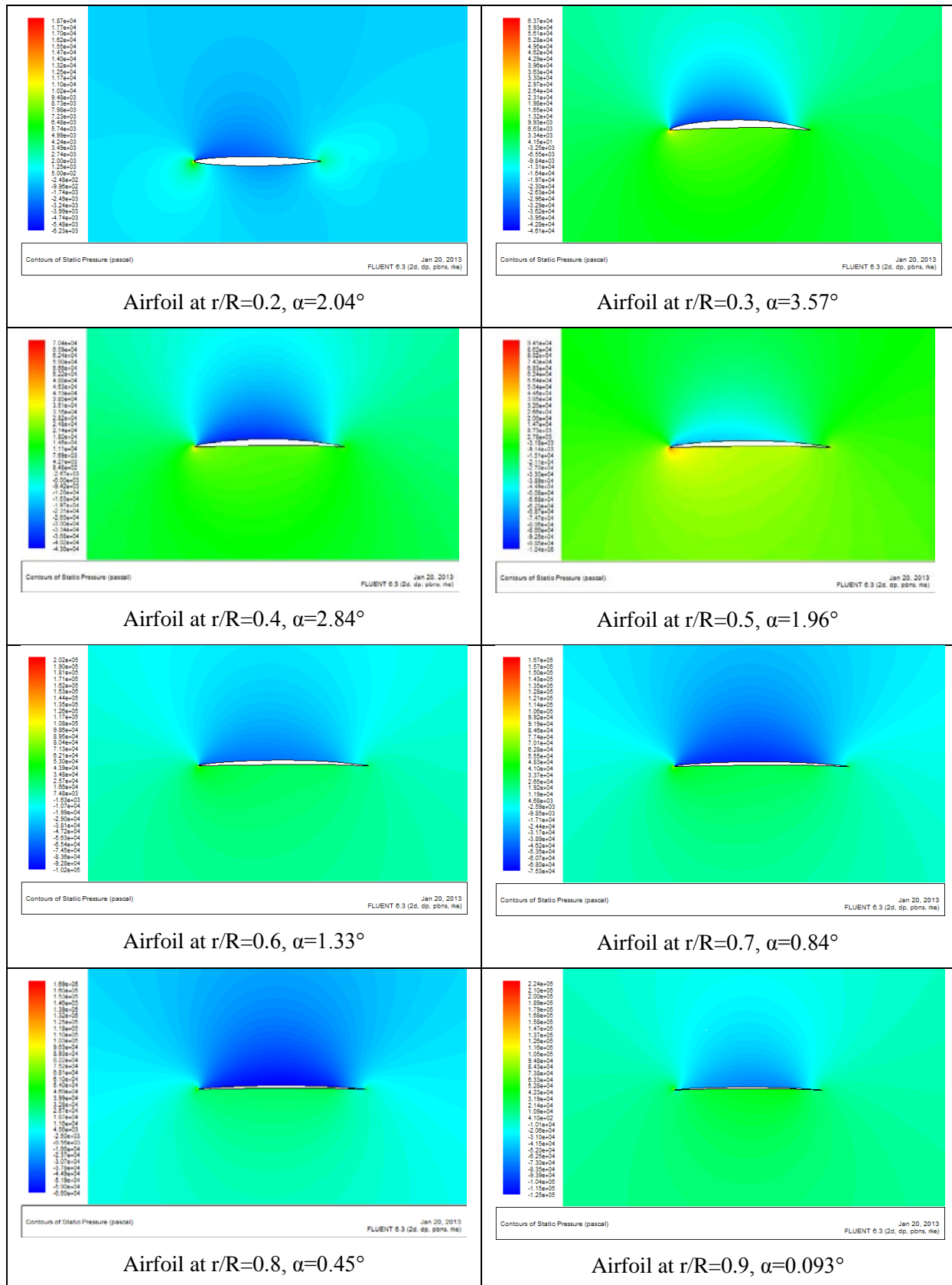


Figure 4.12 Contours of Static pressure for each section

The results obtained in Fluent are C_L and C_D , with these values it is possible to compute the total thrust of the blade and therefore the total thrust of the propeller.

Based on the Blade element theory Formula 4.7, it is possible to obtain dT at each section and then using the Simpson's rule we can integrate all the dT and obtain the total thrust of the propeller.

r/R	FLUENT 2D		β				
	C_L	C_D	rad	C_T	dT	SF	SFxdT
0.2	0.0586	0.0051	0.828	0.035828962	0.86	1	0.863107825
0.3	0.3573	0.0030	0.6329	0.286476365	28.86	4	115.4459527
0.4	0.2494	0.0028	0.5197	0.215100971	41.82	2	83.63990263
0.5	0.2355	0.0028	0.432	0.212646467	69.70	4	278.803107
0.6	0.1868	0.0028	0.3808	0.172367773	86.40	2	172.8075881
0.7	0.1462	0.0027	0.341	0.136907323	95.95	4	383.7882071
0.8	0.1085	0.0023	0.307	0.102773591	91.40	2	182.8091551
0.9	0.0793	0.0025	0.277	0.075604515	73.70	4	294.8027547
1	0	0	0.252	0		1	0
						Σ	1512.959775
						\int	131.3753405
Total Thrust =						$\times 4 =$	525.501[kN]

Table 4.7 Total Thrust computed by blade element theory and 2D CFD analysis.

where:

dT is the Thrust generated by the blade element with a span equal to $dr=0.1R$, it means the blade element is assumed with a span of 0.2605 m. and without having the influence of the variation of pitch along the span.

$$dT = \frac{1}{2} \rho \cdot c \cdot V_R \cdot (C_L \cos \beta - C_D \sin \beta) dr \quad (4.7)$$

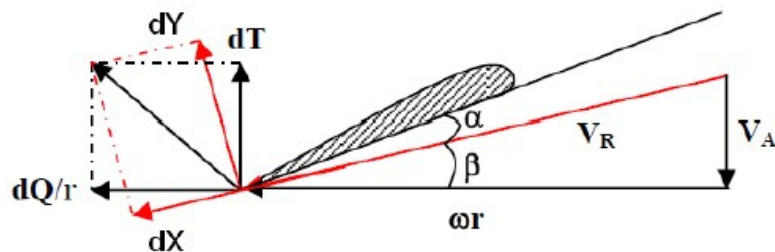


Figure 4.13 Thrust and Torque of the blade element

The same procedure is followed in order to obtain the Total Torque

r/R	FLUENT 2D		β			
	C_L	C_D	rad	C_Q	dQ	SFxdQ
0.2	0.0586	0.0051	0.8286	0.0466	0.5851	0.5851
0.3	0.3573	0.0030	0.6320	0.2135	16.8113	67.2454
0.4	0.2494	0.0028	0.5193	0.1262	25.5568	51.1136
0.5	0.2355	0.0028	0.4321	0.1011	43.1750	172.7000
0.6	0.1868	0.0028	0.3804	0.0719	56.3516	112.7032
0.7	0.1462	0.0027	0.3412	0.0515	65.7829	263.1316
0.8	0.1085	0.0023	0.3072	0.0350	64.8391	129.6782
0.9	0.0793	0.0025	0.2775	0.0241	55.0587	220.2347
1	0	0	0.2524	0	0	0
					Σ	1017.392
					\int	88.344
Total Torque Q					$\times 4 =$	353.374 [kN-m]

Table 4.8 Total Torque computed by blade element theory and 2D CFD analysis.

Here dQ is also defined in the blade element theory as follow:

$$dQ = \frac{1}{2} \rho \cdot c \cdot V_R \cdot (C_L \sin \beta + C_D \cos \beta) r dr \quad (4.8)$$

and for both formulas (4.7) and (4.8), we have:

c : chord of the airfoil

V_R : Incident velocity

r : distance from the axis to the blade element

ρ : density of the fluid

Now the same method will be used to obtain the Thrust and the Torque, but using the data generated by the Lifting-line CODE in order to establish it accuracy.

r/R	Lifting CODE		β							
	C_L	C_D	rad	CQ	dQ	SF	SFxdT	CQ	dQ	SFxdQ
0.2	0.0000	0.0099	0.8286	-0.0073	-0.1758	1	-0.1755	0.0066	0.08397	0.08397
0.3	0.4303	0.0093	0.6320	0.3417	34.4238	4	137.6952	0.2617	20.6056	82.4224
0.4	0.3588	0.0089	0.5193	0.3071	59.7003	2	119.4006	0.1858	37.6424	75.284
0.5	0.2810	0.0087	0.4321	0.2515	82.4457	4	329.7827	0.1255	53.6129	214.451
0.6	0.2150	0.0085	0.3804	0.1965	98.4844	2	196.9688	0.0877	68.7413	137.482
0.7	0.1608	0.0084	0.3412	0.1487	104.2228	4	416.8912	0.0617	78.8887	315.554
0.8	0.1199	0.0083	0.3072	0.1118	99.4115	2	198.8230	0.0441	81.8662	163.732
0.9	0.0893	0.0082	0.2775	0.0836	81.5295	4	326.1180	0.0323	73.9452	295.781
1	0	0	0.2524	0	0	1	0	0	0	0
						Σ	1725.5			
						\int	149.83			
								Σ	1284.8	
								\int	111.56	
						Total Thrust = 599.33 kN		Total Torque Q = 446.25 Kn-m		

The result of this technique using element blade theory and integration by Simpson's rule seems to be suitable having good results for C_L and C_D from the lifting-line with surface correction method, because in the other hand, the results for C_L and C_D from Fluent 2D analysis could not obtain good result having a difference for Thrust of 12% less and for Torque 20% less than the result obtained the same technique but with the coefficients C_L and C_D obtained from the lifting-line method.

4.4.2 Numerical Analysis in 3D of the entire propeller in Fluent

Having, therefore, defined the basis of section geometry, it is possible to define the 3D coordinates for any point P on the surface of the aerofoil section. There is a mathematical method to define the points of a blade in the 3D space considering the pitch angle, angle of attack and the position over its radius. This method was implemented in the code of Prof. Amoraritei and the result is a data file with the coordinates of all the points of every blade edge at each radii, as is shown in the following Figure 4.8, however, this method is explained more in detail in the book: *Marine Propellers and Propulsion*, **J. Carlton**, [Ref.20].

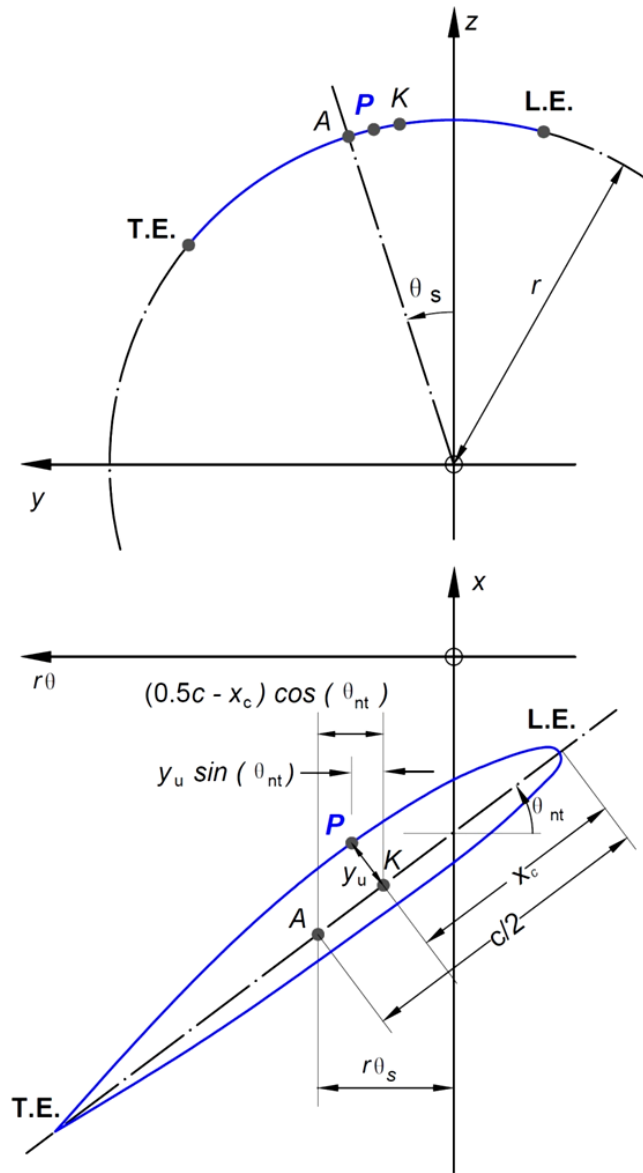


Figure 4.14 Definition of an arbitrary point p on a propeller blade surface. (CARLTON)

Where the equations defining the point P about the local reference frame Fig. 4.14 (down) are given by:

$$x_p = -[i_G + r\theta_s \tan(\theta_{nt}) + (0.5c - x_c)\sin(\theta_{nt}) + y_{u,L} \cos(\theta_{nt})] \quad (4.9)$$

$$y_p = r \sin \left[\theta_s - \frac{180[(0.5c - x_c) \cos(\theta_{nt}) - y_{u,L} \sin(\theta_{nt})]}{\pi r} \right] \quad (4.10)$$

$$z_p = r \cos \left[\theta_s - \frac{180[(0.5c - x_c) \cos(\theta_{nt}) - y_{u,L} \sin(\theta_{nt})]}{\pi r} \right] \quad (4.11)$$

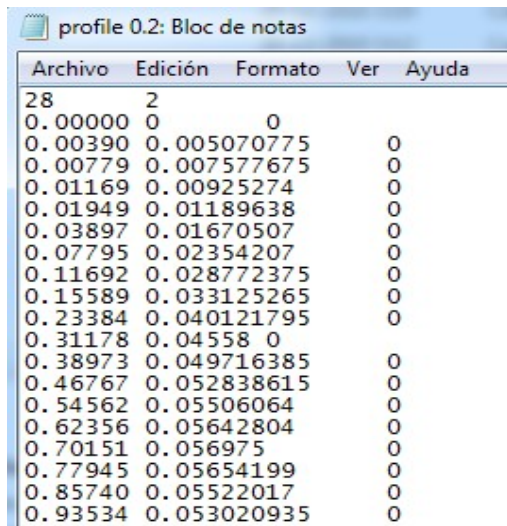
And to convert these to the global reference frame Fig. 4.8 (up) we simply write the transformation:

$$\begin{bmatrix} X_p \\ Y_p \\ Z_p \end{bmatrix} = \begin{bmatrix} 1 & 0 & 0 \\ 0 & \cos \phi & -\sin \phi \\ 0 & \sin \phi & \cos \phi \end{bmatrix} \begin{bmatrix} x_p \\ y_p \\ z_p \end{bmatrix} \quad (4.12)$$

where ϕ is the angle between the reference frames

4.4.1 Generation of the 3D propeller and fluid domain

Using the coordinates generated by the lifting-line theory in a data file, the geometry is imported in the pre-processor software GAMBIT 2.4.6 as groups of lines made of points (vertices) and choosing the option of generating the edges automatically what I obtained is all the blades edges as shown in Figure 4.15.



Archivo	Edición	Formato	Ver	Ayuda
28	2			
0.00000	0	0		
0.00390	0.005070775		0	
0.00779	0.007577675		0	
0.01169	0.00925274		0	
0.01949	0.01189638		0	
0.03897	0.01670507		0	
0.07795	0.02354207		0	
0.11692	0.028772375		0	
0.15589	0.033125265		0	
0.23384	0.040121795		0	
0.31178	0.04558	0		
0.38973	0.049716385		0	
0.46767	0.052838615		0	
0.54562	0.05506064		0	
0.62356	0.05642804		0	
0.70151	0.056975		0	
0.77945	0.05654199		0	
0.85740	0.05522017		0	
0.93534	0.053020935		0	

This picture of the data file shows only one part of the coordinates of the vertices. The number "28" indicate that there are 28 points which belong to one group or line and the number "2" indicates that there are two groups or in this case two lines corresponding to the upper and lower faces of the airfoil.

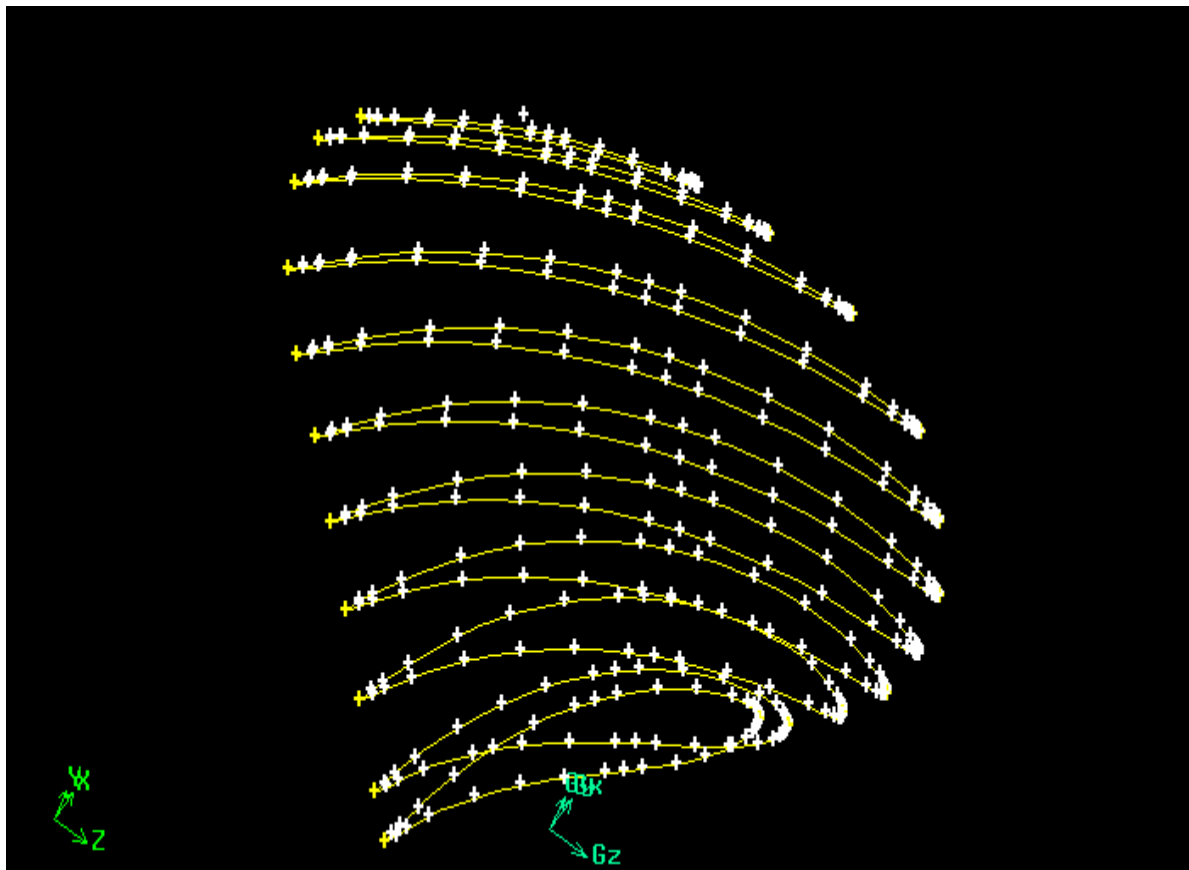


Figure 4.15. Geometry of the single blade generated in GAMBIT.

The next step is to create the volume of the blade using the commands of GAMBIT, then, the blade must be copied in order to create the complete propeller and create the shaft as you can see in the following Figures 4.16. and 4.17

Before to create the volume it is necessary to create the three surfaces that will wrap the blade's sections. One for the "face" side of the propeller, the second for the "back" side of the propeller and the third one is to "close" the surface connected to the HUB.

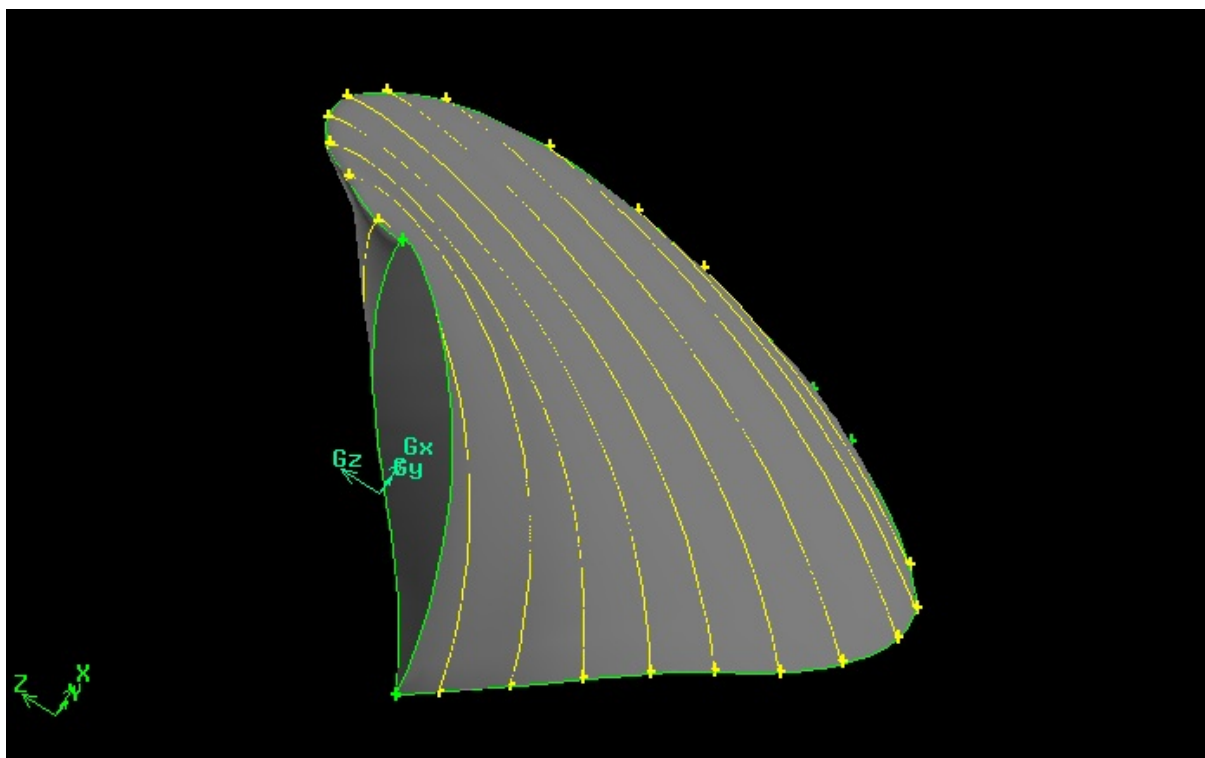


Figure 4.16. Volume created of the single blade

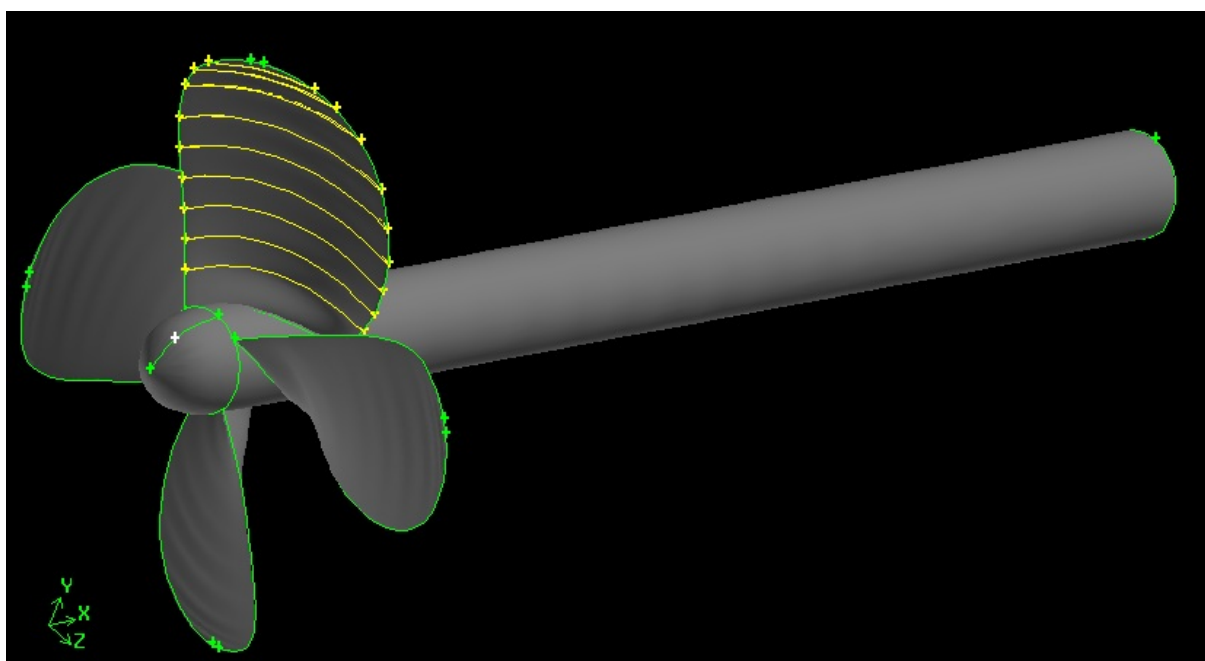


Figure 4.17. Final Volume of the propeller

The fluid domain will be cylindrical with the following dimensions: upstream length is taken as $2D$, downstream length is $5D$ and zone diameter is $3D$, as shown in Figure 4.18. where D is the diameter of the propeller.

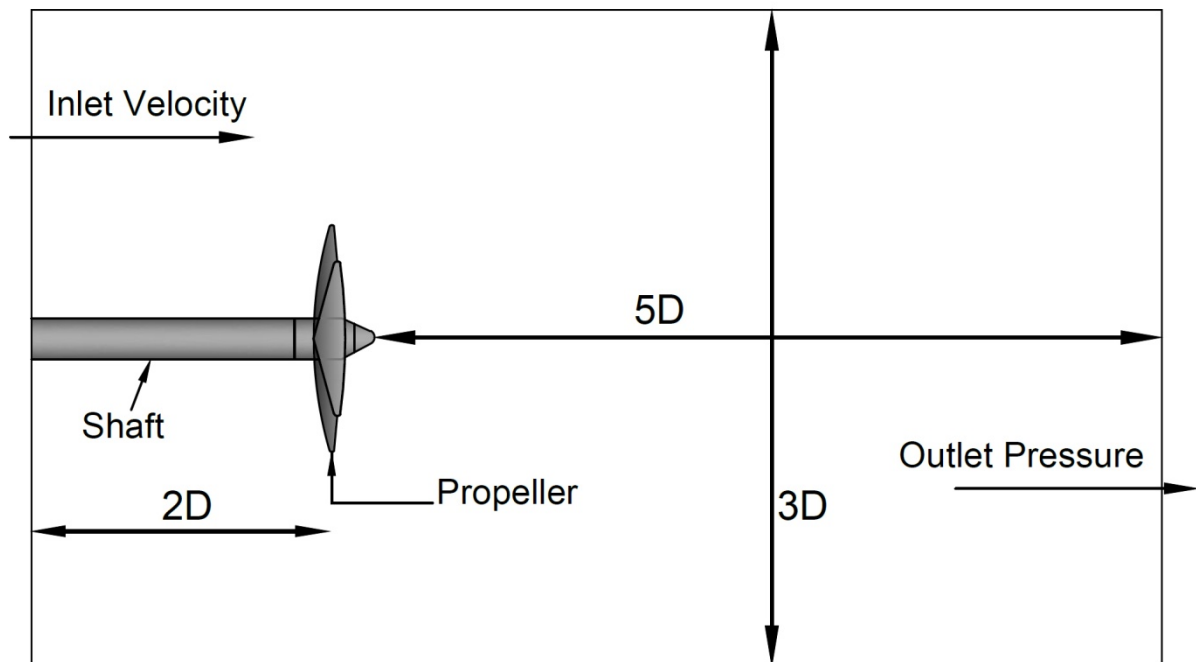


Figure 4.18 Scheme of the propeller and fluid domain

After the fluid domain is created it is necessary to subtract the propeller volume from the cylinder. Then, a Size Function will be used in order to make the mesh automatically starting from the propeller surface. The parameters of the size function are the following:

Angle : 20° of the tetrahedral element

Growth rate : 1.2

Max. size : 300 maximum size of the element in mm

Min. size : 10 minimum size of the element in mm

The meshing regarding the Size Function produced 1.559.103 tetrahedral elements or Cells, 3.141.592 Faces and 271.449 Nodes and the size of the mesh file was 182 Mb.

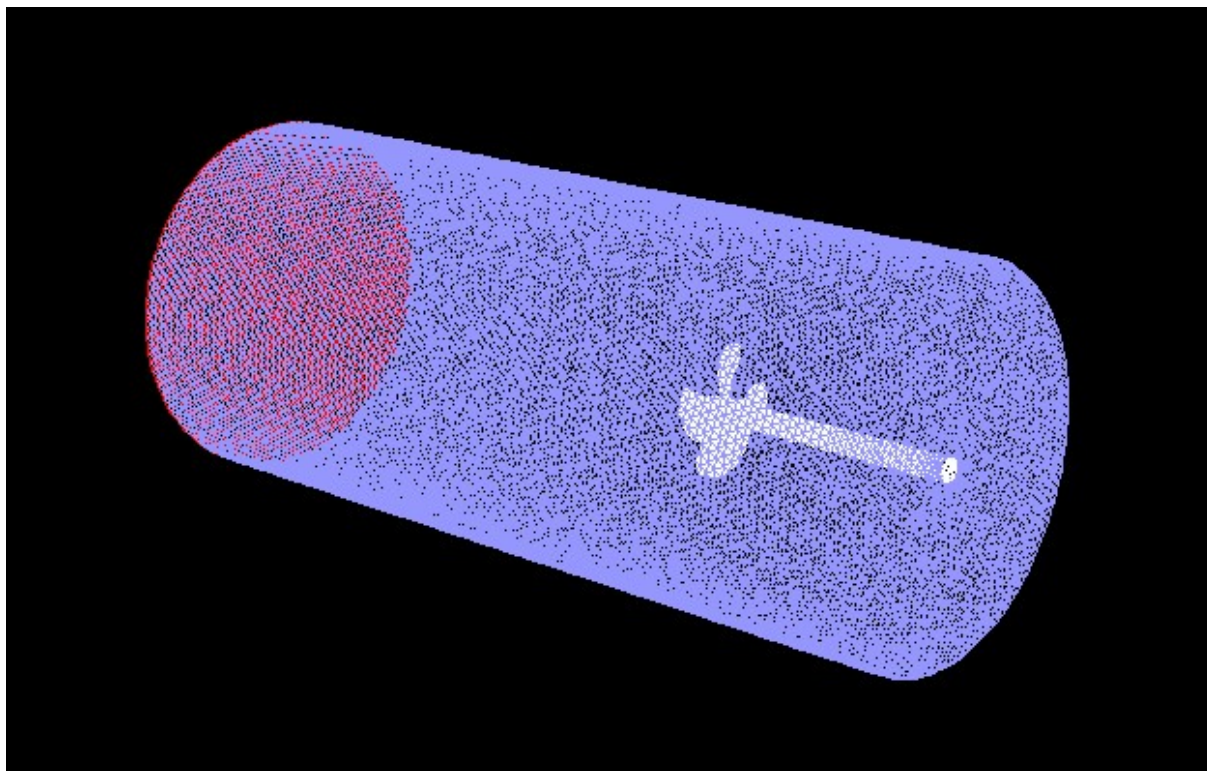


Figure 4.19a Final meshing of the fluid domain and the propeller

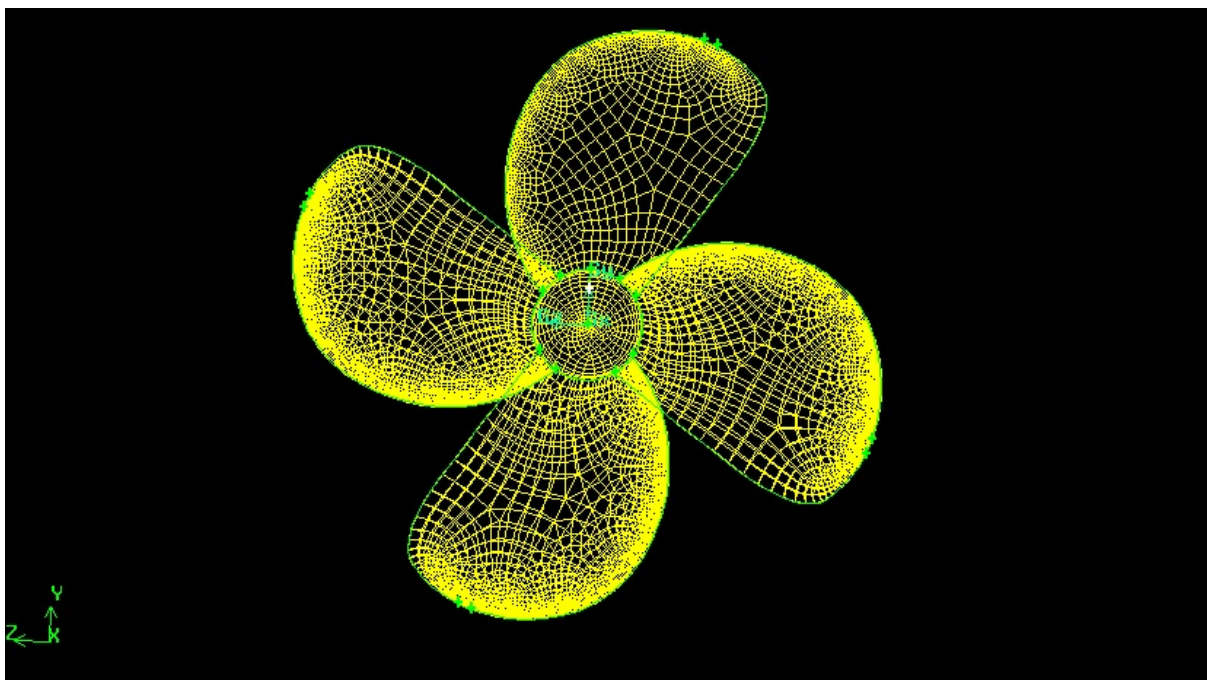


Figure 4.19b Final meshing of the propeller

4.4.2 Setting up of the RANS analysis in Fluent

The chosen solver has been Pressure Based with Implicit formulation of linearization. The Boundary conditions are three: the velocity inlet, pressure outlet and taking the propeller surface as Stationary Wall with No slip Shear condition.

The effect of the rotational movement of the propeller has been applied to the Fluid Zone and keeping the propeller stationary. The motion type of the fluid will be Moving Reference Frame rotating at the angular speed of 129 R.P.M.

The effect of the viscosity will be performed but the turbulent model k-epsilon Realizable with standard Wall Functions based on the good results obtained in one example of the book "*Computational Fluid Dynamics: a practical approach*, Jiyuan, Guan, Chaoqun 2008. Pgs 265-270" applying this model to an Hydrofoil.

The pressure-velocity method has been chosen as SIMPLE, because it is applicable in steady state flow.

The discretization method will be Second Order for Pressure and Second Order Upwind for the Momentum, Turbulent Kinetic Energy and Turbulent Dissipation Rate.

4.5. Post-Processing and Results

First, one analysis will be performed to compare the result with the one from the lifting-line theory obtained in section 4.3.3. Then, the K_T , K_Q and η_o diagram will be developed and compared with the theoretical diagram.

4.5.1. Thrust and Torque for operational speed V_S

The data used for this analysis has been the same used in the **Preliminary design** with lifting-line method.

$$V_s = 17.4 \text{ Knots,} = 8.95 \text{ [m/s]}$$

$$V_A = 6.14 \text{ [m/s]}$$

$$\text{RPM} = 129$$

Then, after 740 iterations as it is shown in figure 4.20, the axial forces on all the zone of the propeller which is interpreted as Thrust are:

Pressure Force [N]	Viscous Force [N]	Total force [kN]
593802.48	-4742.9946	= 589.059

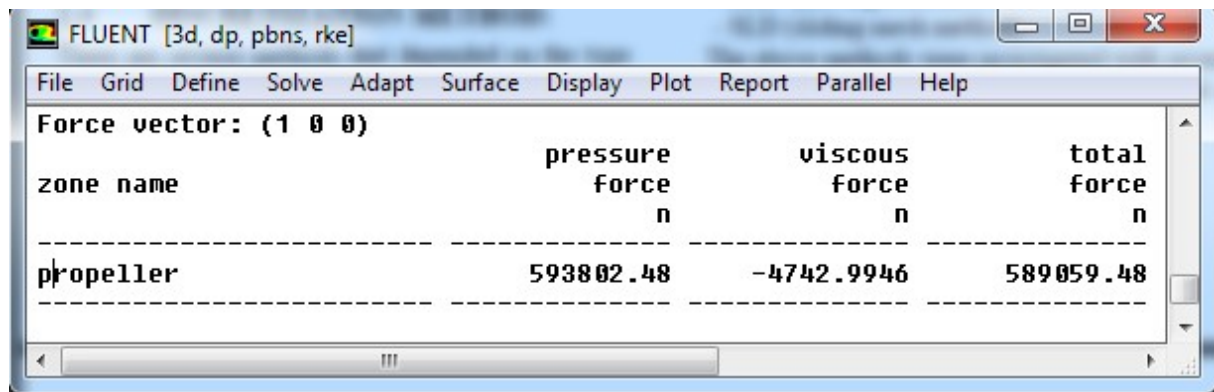


Figure 4.20 Report of the force in the "x" direction

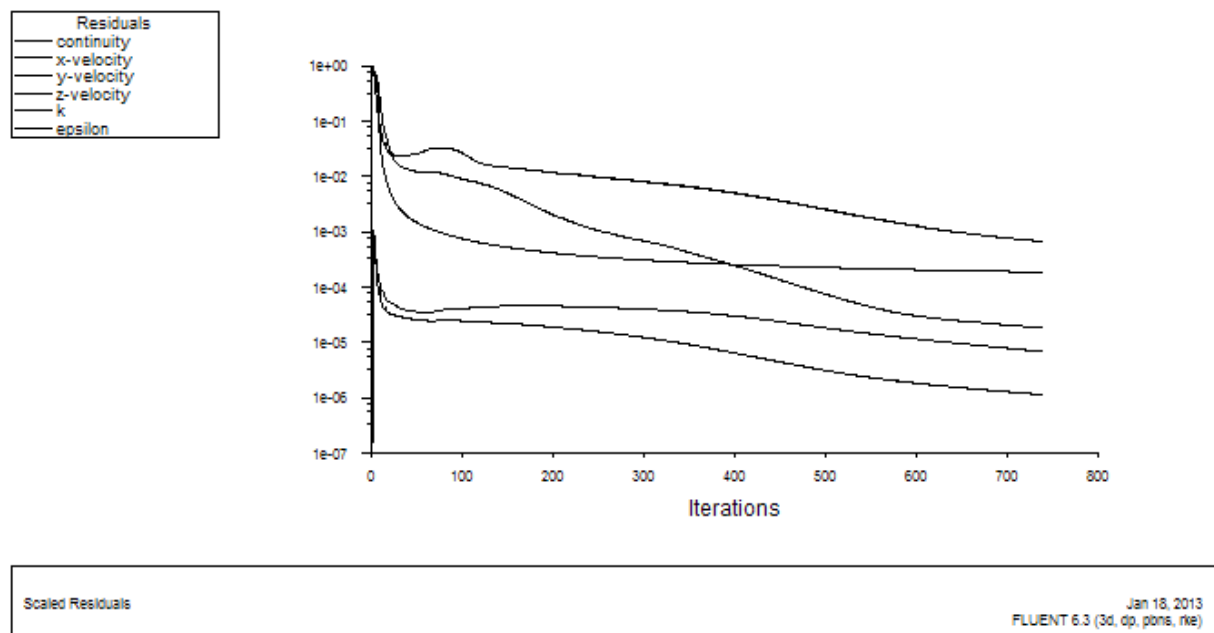


Figure 4.21 Convergence at iteration 740

The moment produced by the rotation of the fluid around the propeller surface will be interpreted as the Torque, and the result is:

Pressure Moment [N-m]	Viscous Moment [N-m]	Total Moment [kN-m]
402516.4	14888.16	= 417.40

The difference between the Lifting-line method and RANS method will be shown in the following table in terms of per cent:

	Lifting-line	RANS	difference	difference
	kN	kN	kN	%
T =	595.68	589.06	6.62	1.11% less than Lifting-line
Q =	442.14	417.4	24.74	5.6 % less than Lifting-line

The big difference in the Torque estimation could be due not only to the turbulence model but also due to the parameters defined in the used turbulence *model k-epsilon Realizable with standard Wall Functions*.

Another factor that could have influenced the torque is type of rotational analysis applied in the performance by rotating the fluid and not the surface of the propeller.

4.5.2. Analysis of the velocity and pressure field

Based on the wing theory and the distribution of pressure over an aerofoil and the momentum theory, despite it has no value in propeller design, it possible to explain graphically the results obtained in the previous section 4.5.1. using, as well, some tools of the post-processing part of Fluent. The theoretical behaviour of the flow regarding the momentum theory establishes that the pressure in the fluid suffers a decrease when it approaches the propeller, which is represented as an actuator disk. Within the decrease in the pressure there is an increase in the speed of the fluid when it comes closer to the propeller. The decreasing in the pressure continues up to the propeller and at that moment the pressure turns abruptly into an increase

of the pressure due the tangential shear stress produced by the blades, as shown in the Figure 4.22, where the fluid flows from right to the left.

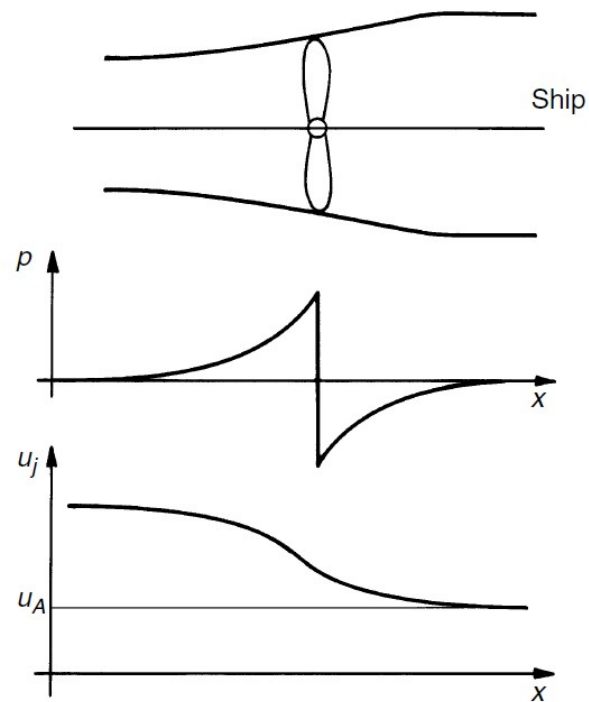


Figure 4.22. Representation of the momentum theory. (Bertram, 2000) where u_A and u_j are the speeds before and after the propeller.

Using the post-processing part of Fluent it is possible to observe this phenomena analyzing the distribution of pressure over the both sides of the blades propeller. The following figures 4.23 and 4.24 shows the pressures on the sides by a colored contours tool.

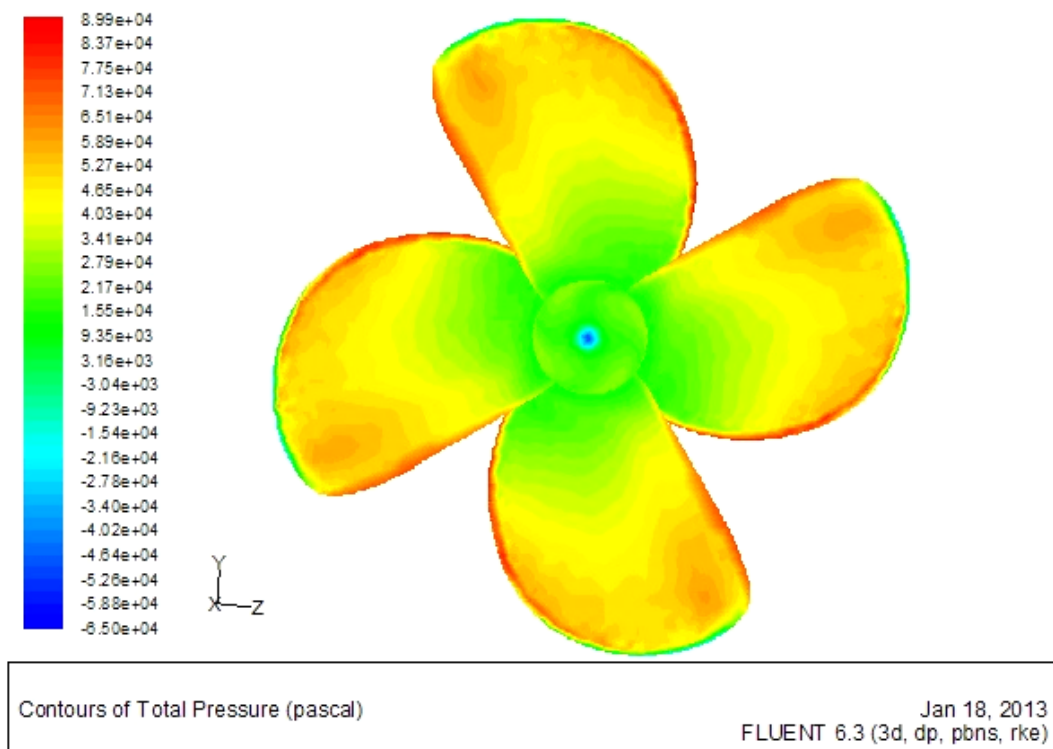


Figure 4.23 Distribution of pressure over the face side of the propeller at $J=0.53$

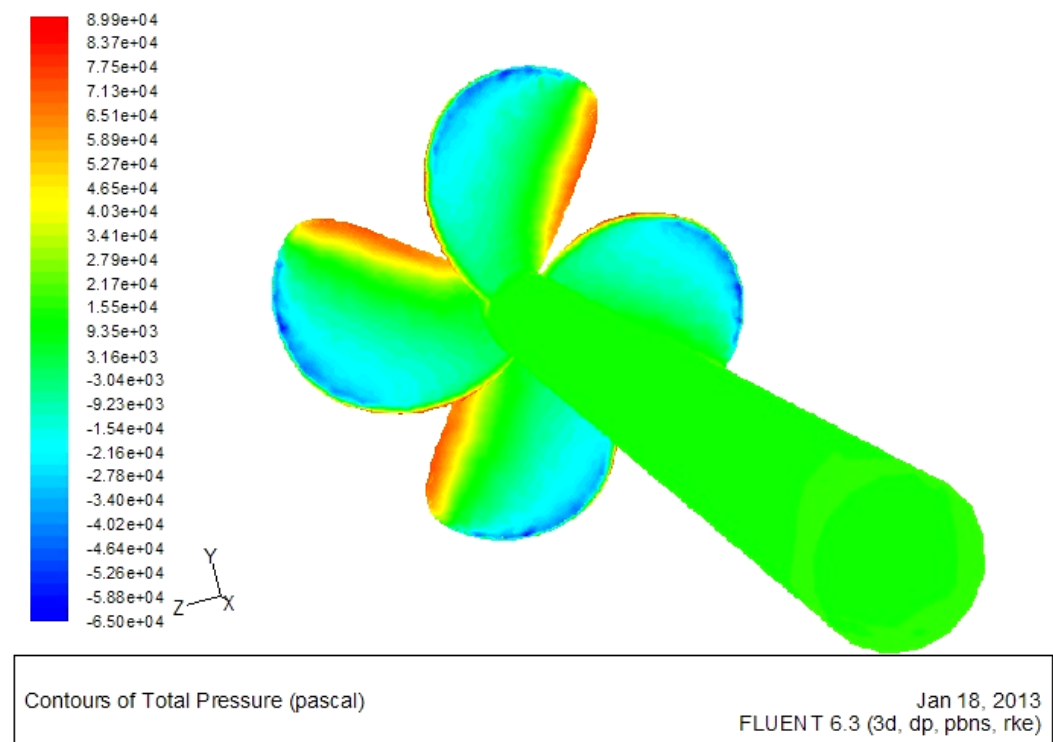


Figure 4.24 Distribution of pressure over the back side of the propeller $J=0.53$

The previous two pictures evidence the fact of the difference of pressure at both sides of the propeller. In the Fig. 4.23, the yellow colour indicates a positive pressure over most of the face side, in the other hand, in the Fig. 4.24. the light blue color indicates a negative pressure over the back side of the propeller. Consequently, we can say as well, that the positive pressure is pushing the blades in the fore direction and the negative is pulling the blades in the same direction as described in the wing's theory about pressure distribution over an aerofoil, that establish this in the following Figure 4.25. where the blue arrows mean negative pressure and the red ones mean positive pressure.

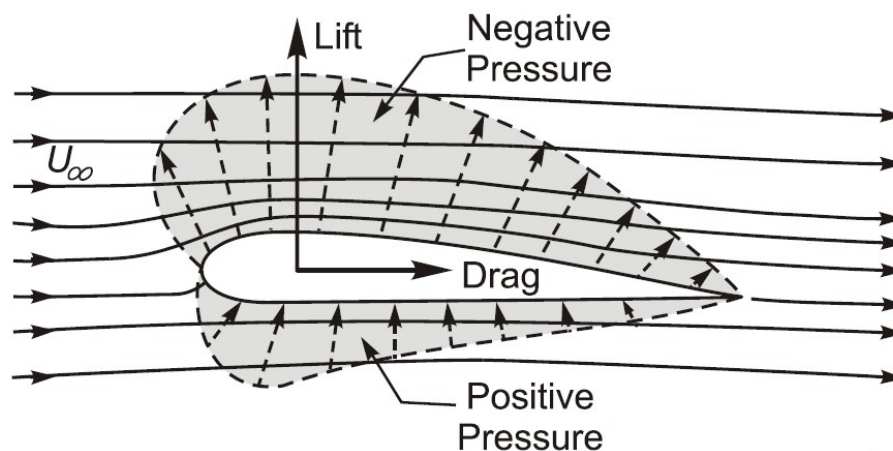


Figure 4.25 Idealized Pressure distribution over an aerofoil without turbulence.

Another application of the post-processing part of Fluent is the generation of pathlines of the fluid's flow characteristics like the velocity, pressure, viscosity, etc. The following Figure 4.26, has been made by two images created in Fluent post-processor. The two images have been located in one in order to appreciate the effect of the propeller on the fluid slipstream and its relation with the momentum theory as well.

The pathlines indicates the path followed by the slipstream regarding the relative velocity of the fluid before and after passing the propeller under the effect of the propeller acceleration.

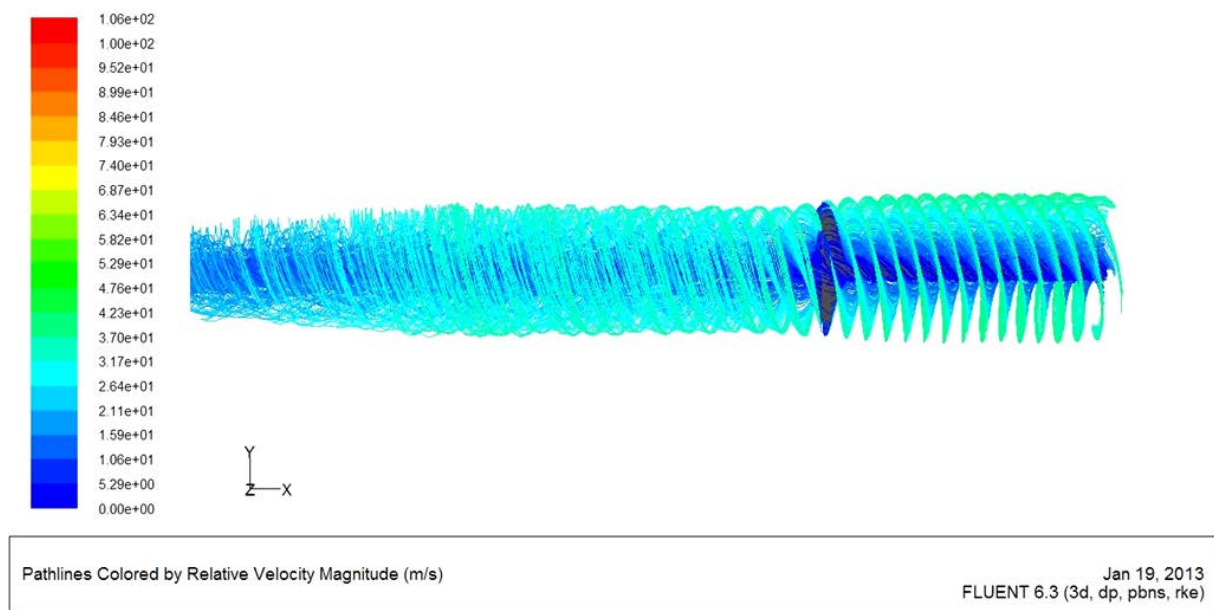


Figure 4.26 Effect of the propeller on the velocity slipstream

Another interesting tool, despite it is not used in propeller design, is the visualization of the Turbulence Viscosity and how it is dissipated into the fluid. The following Figure 4.27 represent this dissipation of the turbulence.

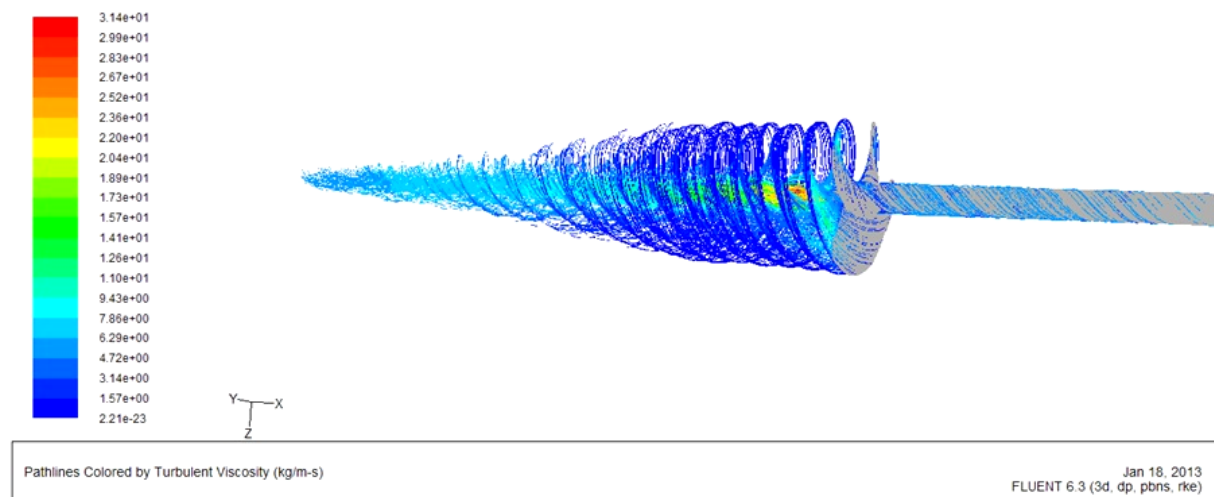


Figure 4.27. Dissipation effect of the turbulence.

4.5.3. Develop of the K_T , K_Q and η_o Diagrams.

The following table 4.9 shows the diagram of the propeller based in the results obtained with the polynomial form for K_T and K_Q of the Wageningen B-series shown in the section 2.2.1.

	Theoretical Open water										
J	0	0.1	0.2	0.3	0.4	0.5	0.6	0.7	0.8	0.9	1
K_{to}	0.3520	0.3248	0.2935	0.2584	0.2200	0.1787	0.1351	0.0894	0.0422	0.0062	0.0553
$10K_{Qo}$	0.4306	0.4027	0.3707	0.3347	0.2946	0.2507	0.2030	0.1516	0.0965	0.0379	0.0242
η_o	0.0000	0.1284	0.2520	0.3686	0.4753	0.5673	0.6353	0.6570	0.5561	0.2355	3.6378

Table 4.9 Theoretical values of K_T and K_Q of Wageningen-B series.

In the following table 4.10 it is found the result of Thrust and Torque for the range of J between 0 and 1. obtained using RANS numerical analysis in Fluent and below the K_T and K_Q obtained from the Thrust and Torque

	k-e realizable estándar										
J	0	0.1	0.2	0.3	0.4	0.5	0.6	0.7	0.8	0.9	1
$Va[m/s]$	0	1.120	2.240	3.360	4.480	5.600	6.720	7.841	8.961	10.081	11.201
$T[kN]$	1337.99	1199.52	1074.58	941.1	797.53	645.73	486.41	318.97	138.55	-64.68	-299.9
$Q[kN-m]$	860.08	779.36	705.46	628.59	546.82	460.15	368.41	271.25	165.87	45.97	93.69
K_T	0.3833	0.3436	0.3078	0.2696	0.2285	0.1850	0.1393	0.0914	0.0397	0.0185	0.0859
$10K_Q$	0.4729	0.4285	0.3879	0.3456	0.3006	0.2530	0.2026	0.1491	0.0912	0.0253	0.0515
η_o	0	0.1276	0.2526	0.3724	0.4837	0.5818	0.6569	0.6826	0.5541	1.0500	2.6542

Table 4.10 Values of K_T and K_Q obtained numerically via RANS

In the following table it is possible to observe the difference in percentage of the numerical data respect to the theoretical

k-e realizable standard v/s theoretical result											
<i>J</i>	0	0.1	0.2	0.3	0.4	0.5	0.6	0.7	0.8	0.9	1
%KT	8.87 %	5.78%	4.89 %	4.34 %	3.85 %	3.48 %	3.15%	2.19%	- 5.87%	197.31 %	55.23%
%K Q	9.83 %	6.41%	4.63 %	3.27 %	2.04 %	0.90 %	- 0.24%	- 1.63%	- 5.53%	-33.31%	112.75 %
% η_o	0.00 %	- 0.59%	0.25 %	1.04 %	1.78 %	2.56 %	3.39%	3.89%	- 0.36%	345.81 %	-27.04%

Table 4.11 Comparative table between theoretical and numerical results.

In the three previous tables it is possible to observe that the last two speeds give useless information in my study, because they correspond to another type of situation of flow direction and will not be considered for the following compares, taking into account only the range for *J* between 0 and 0.8.

Finally, both tables 4.9 and 4.10 are plotted in order to compare the curves. The blue curve is made of the theoretical result and the red curve indicates the result obtained in the numerical simulation.

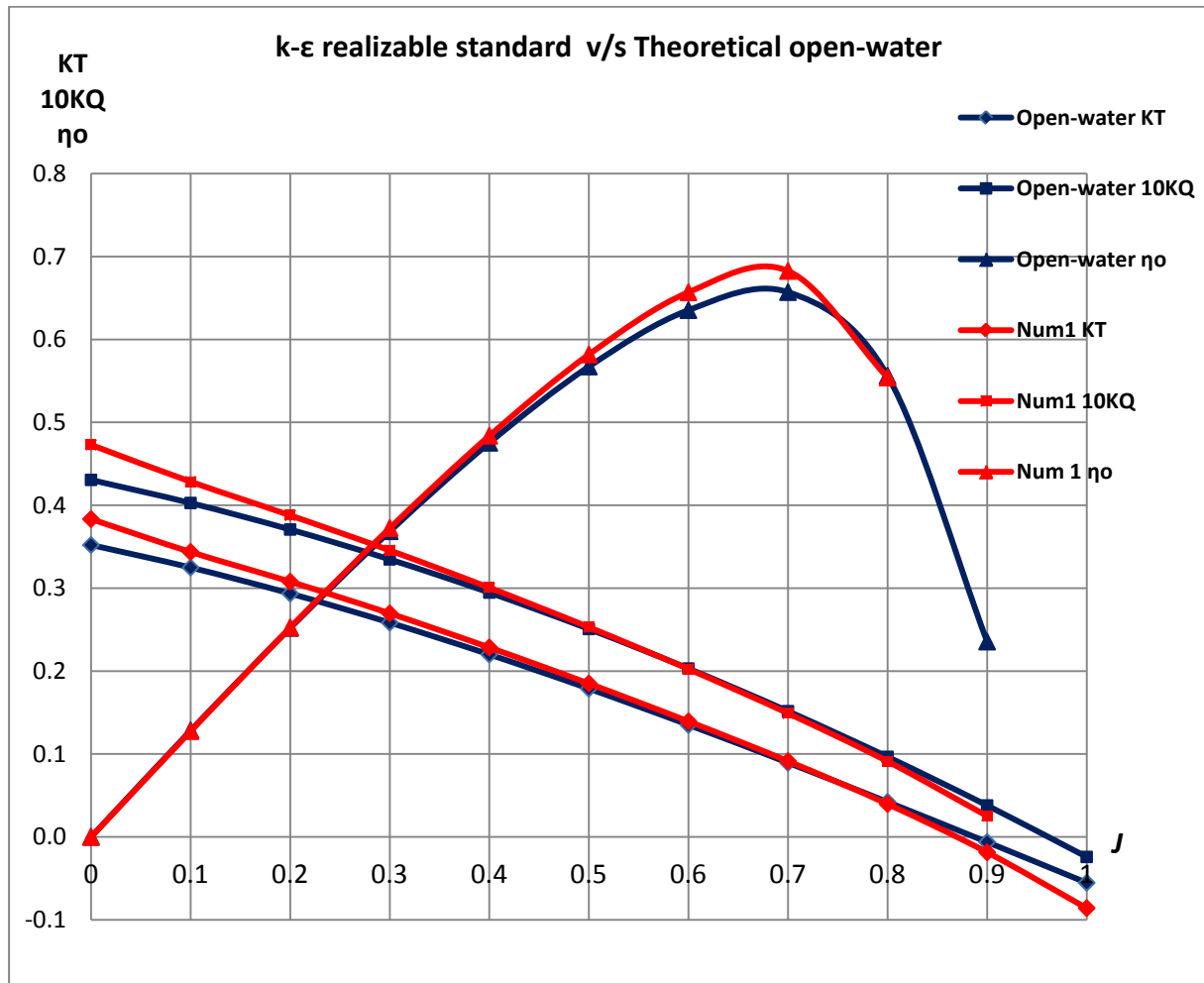


Figure 4.28. K_T and K_Q diagram comparing RANS method and Wageningen-B series chart.

Interpolating the values from the table 4.11 for the optimum $J_{opt}=0.53$ we can obtain the difference of the Numerical analysis respect to the result obtained from the Wageningen-B series chart.

J	0.5	0.53	0.6
% K_T	3.48%	3.36%	3.15%
% K_Q	0.90%	0.56%	0.24%

From this interpolation we can say that the RANS prediction obtained just a little over predicted values for K_T and K_Q .

Then using the formulas 2.1 and 2.2 to obtain K_T and K_Q from the results obtained with lifting-line theory it is possible to compare with the theoretical from Wageningen-B series chart. The following data was obtained in 4.3.3 with the lifting-line method.

$$\begin{aligned} \mathbf{T} &= 595.68 \quad [\text{kN}] \\ \mathbf{Q} &= 442.14 \quad [\text{kN-m}] \\ \mathbf{C}_T &= 0.70 \quad \text{Thrust coefficient} \end{aligned}$$

Using the formulas 2.1 and 2.2 we obtain:

$$\begin{aligned} K_T &= \frac{T}{\rho \cdot n^2 \cdot D^4} = 0.17 \\ 10xK_Q &= \frac{Q}{\rho \cdot n^2 \cdot D^5} = 0.243 \\ \eta_0 &= \frac{K_T}{K_Q} \cdot \frac{J}{2\pi} = 0.59 \end{aligned}$$

in the other hand we need to interpolate the values from the Wageningen-B series result.

J	0.5	0.53	0.6	Difference regarding lifting-line method
K_{to}	0.1787	0.166	0.1351	0.4% less
10K_{Qo}	0.2507	0.236	0.2030	0.7% less
η_o	0.5673	0.59	0.6353	0% of difference

After this last comparison, it is possible to confirm that the lifting-line method with surface corrections was more accurate than the analysis via CFD with k-epsilon realizable standard turbulent model.

The last diagram and the last results for torque and thrust reveals that the best prediction using the 3D RANS analysis in fluent using the turbulent model k-epsilon realizable standard was for the advance ratio $J=0.53$ which is the optimum J estimated, and the difference increases toward the extremities of the diagram.

5. CONCLUSIONS

First of all, the propeller design process is complete only after several optimizations and after that when a propeller model is tested in a towing tank or cavitation tunnel, but the last test is in a trial test of the ship, at that moment the propeller will be completely evaluated and the process of propeller design will finish only if the results agree with the estimated ones. Then, it is possible to establish if the method was the correct. In our case, without a model test, the best parameters to be compared are based on the propeller series charts such as Wageningen-B series due its extended used in the propeller design. This is the main reason to find good practices and techniques using CFD simulation in the propeller design field, it means to establish good procedures in order to decrease the dependence of the propeller model in a towing tank.

The 2D analysis in Fluent was originally thought to learn how to use this software get use to it and it was unexpected to get results for Thrust and Torque, then even these results were not totally good is a good starting point for future analysis with the technique applied on it.

The lifting-line theory with surface corrections has been proved to be the best option in the propeller design field due to its really accurate results compared with the RANS method using the same propeller geometry. Nevertheless, this comparison only regards the k-epsilon realizable standard method for turbulence and it should be noted, that there are more sophisticated model of turbulence, but k-epsilon was chosen due to its good reputation in the CFD industry.

There is no correlation in the differences between RANS analysis and the lifting line theory, I mean it is very probable that this differences change from one case to another or from one propeller to another, and that's why there still much more investigation to do with CFD simulation regarding the propeller design process.

It is very important to achieve good results starting with open water analysis or steady flow analysis, because in the end the final aim is to achieve good results in unsteady flows.

6. REFERENCES

- [1] Morgan, W. 1956, *A propeller design method*. New York, SNAME
- [2] Ghose and Gokarn, 2004 *Basic Ship Propulsion*. Kharagpur, Allied Publishers
- [3] Carlton, J. 2007 *Marine Propellers and Propulsion*, USA, Elsevier.
- [4] Bertram, V. 2000, *Practical ship hydrodynamic*, ISBN0-75064851-1, Great Britain.
- [5] Breslin, J., Andersen, P. 1996 *Hydrodynamics of ship propellers*, University of Cambridge, United Kingdom
- [6] Jiyuan Tu, Yeoh and Liu 2008, *Computational Fluids Dynamics: A practical approach*, University of Texas, Elsevier
- [7] Kerwin, J. and Hadler, J. 2010, *Propulsion*. USA, SNAME
- [8] Kerwin, J., and Lee, C.-S., 1978, *Prediction of Steady and Unsteady Marine Propeller Performance by Numerical Lifting-Surface Theory*, Trans. The Soc. of Naval Architects and Marine Engineers, 88.
- [9] Uto, S. and Kodama, Y. 1992, *Application of CFD to the Flow Computation around a Marine Propeller –Grid Generation and Inviscid Flow Computation using Euler Equations*, J. Kansai Society of Naval Architects, No. 218, pp. 171-180,
- [10] Funeno, I. and et al. 1999, *Analysis of Steady Viscous Flow around a Highly Skewed Propeller*, J. Kansai Society of Naval Architects, No. 231, pp. 1-6,
- [11] Martínez-Calle, Julián, 2002 *AN Open Water Numerical Model for a Marine Propeller: a Comparison with Experimental Data*, *Proceedings of the ASME FEDSM'02 2002 Joint USEuropean Fluids Engineering Summer Conference* July 14-18, Montreal, Canada
- [12] Yoshihisa TAKEKOSHI, 2003 *Simulation of Steady and Unsteady Cavitation on a Marine Propeller Using a RANS CFD Code*, Fifth International Symposium on Cavitation (CAV2003) Osaka, Japan, November 1-4,
- [13] Shin Hyung Rhee *2004, Evangelos Koutsavdis, *Two-dimensional simulation of unsteady marine propulsor blade flow using dynamic meshing techniques*, Fluent Inc., 10 Cavendish Ct., Lebanon, NH 03766, USA,
- [14] Amoraritei, M., 2006 *Numerical simulation and analysis of flow around marine propeller*, *International Conference on Fluid Flow Technologies*, September 6-9,
- [15] Amoraritei, M., 2010 *Theoretical study on propulsive performances and exciting forces induced by ship propeller*, The annals of "Dunarea de jos" UGAL fascicle XI-Shipbuilding, ISSN 1221-4620,.
- [16] Nakisa and Abbasi, 2010 *Assessment of marine propeller hydrodynamic performance in open water via CFD*, The International Conference on Marine Technology,
- [18] Amoraritei, M. 2012, *Lectures of ship propulsion*. UGAL
- [19] Eleni, D., Athanasios and Dionisios 2012, *Evaluation of the turbulence models for the simulation of the flow over a National Advisory Committee for Aeronautics (NACA) 0012 airfoil*, Greece, University of Patras.

[20] Abbot, Ira, 1959 *Theory of wings sections*, New York, NASA

APPENDIX A1**PROGRAM PROIECTARE ELICE TEORIA LINIEI PORTANTE****DATE INTRARE**

Putere motor	6900.000/	9387.755	[KW/CP]
Diametru elice	5.210		[m]
Turatie elice	129.000/	2.150	[rpm/rps]
Numar pale	4		
Densitate apa	1025.000		[kg/m3]
Sigma material	590.000		[N/mm2]
Rezerva la cavitate	45.000		
Imersiune ax	5.450		[m]
Coef.sig.rez.mat.	10.000		
Grosime relativa varf	0.004		[mm]
Skew	21.000		[grade]
Randament linie axe	0.980		
Coef.utilizare putere	0.850		

Vit [Nd]	Rez[kN]	Coef siaj	Coef suct	Rand rot
15.00	297.3	0.3231	0.2324	1.0410
16.00	346.5	0.3145	0.2189	1.0460
17.00	422.3	0.3171	0.2224	1.0410
18.00	570.9	0.3072	0.1910	1.0370
19.00	784.2	0.3016	0.1842	1.0270

Siajul mediu pe raza

0.2000 0.3000 0.4000 0.5000 0.6000 0.7000 0.8000 0.9000 1.0000

0.6990 0.6840 0.6410 0.5690 0.4560 0.3400 0.2640 0.2240 0.2000

Contur standard (Troost)

Grosimile nu sunt impuse

REZULTATE

Viteza de proiectare	17.3769/	8.939	[Nd]/[m/s]
Coeficient siaj	0.3144		
Coeficient suctiune	0.2125		
Randament rotativ	1.0395		
Rezistenta inaintare	468.7849/	47.7864	[kN]/[tf]
Impingere	595.6804/	60.7218	[kN]/[tf]
Moment	442.1409/	45.0704	[kNm]/[tfm]
Coeficient impingere	0.1706		
Coeficient moment	0.0243		
Randament elice	0.6086		
Avansul relativ	0.5471		
Coef.imping.dat	0.7001		
Coef.imping.calculat	0.7002		
Putere	5745.59/	7814.00	[kW]/[CP]
Raport disc	0.7175		
Pas mediu	4.1956		

r/R tg tgb be circ ua/vr ut/vr vr

0.2000	0.5411	1.0906	0.8287	0.0000	0.7084	0.8737	5.4911
0.3000	0.3711	0.7322	0.6320	0.0618	0.6096	0.4965	10.6739
0.4000	0.3006	0.5598	0.5104	0.0691	0.6422	0.3933	14.2248
0.5000	0.2703	0.4612	0.4321	0.0645	0.5742	0.2857	17.8798
0.6000	0.2643	0.4000	0.3805	0.0532	0.4387	0.1861	21.6217
0.7000	0.2609	0.3552	0.3413	0.0412	0.3194	0.1175	25.3394
0.8000	0.2480	0.3173	0.3072	0.0315	0.2533	0.0817	28.9367
0.9000	0.2297	0.2849	0.2776	0.0220	0.2223	0.0638	32.4495
1.0000	0.2117	0.2579	0.2524	0.0000	0.2056	0.0532	35.9333

r/R	M.rez	c.cav	cl.c/D	cl.c	cl	cd
0.2000	0.0028	9.6127	0.0000	0.0000	0.0000	0.0099
0.3000	0.0024	2.4992	0.1425	0.7425	0.4303	0.0093
0.4000	0.0018	1.3819	0.1291	0.6726	0.3588	0.0089
0.5000	0.0012	0.8587	0.1079	0.5621	0.2810	0.0087
0.6000	0.0007	0.5763	0.0863	0.4499	0.2150	0.0085
0.7000	0.0003	0.4116	0.0657	0.3424	0.1608	0.0084
0.8000	0.0001	0.3095	0.0477	0.2485	0.1199	0.0083
0.9000	0.0000	0.2413	0.0310	0.1613	0.0893	0.0082
1.0000	0.0000	0.1928	0.0000	0.0000	0.0000	0.0000

r/R	Gros	lat(r)	lat(c)	lat	curb	pas
0.2000	0.2279	0.6138	0.1613	1.5589	0.0000	3.8358
0.3000	0.1956	0.7229	0.7932	1.7254	0.0752	4.0883
0.4000	0.1656	0.7508	1.3058	1.8748	0.0549	4.1043
0.5000	0.1373	0.7143	1.6917	2.0006	0.0468	4.1201
0.6000	0.1112	0.6299	1.9417	2.0922	0.0401	4.1954
0.7000	0.0868	0.5137	2.0422	2.1297	0.0345	4.2588
0.8000	0.0634	0.3795	1.9699	2.0725	0.0299	4.2675
0.9000	0.0416	0.2358	1.6698	1.8064	0.0264	4.2227
1.0000	0.0208	0.0022	0.5936	0.0000	0.0104	4.2220

coeficientii de corectie

r/R	kc	ka	kt
0.2000	2.0905	2.5642	0.6545
0.3000	1.4909	3.1328	0.4786
0.4000	1.2030	3.2435	0.3365
0.5000	1.2268	2.8963	0.2282
0.6000	1.3139	2.6159	0.1494
0.7000	1.4820	2.1974	0.0942
0.8000	1.7692	1.4479	0.0584
0.9000	2.4057	-0.1625	0.0369
1.0000	3.3916	-2.6337	0.0296

valori unghiuri profil

r/R	alfa	be	gama	vr
0.2000	2.0414	47.4805	49.5219	5.4911
0.3000	3.5690	36.2120	39.7809	10.6739
0.4000	2.8417	29.2417	32.0835	14.2248
0.5000	1.9651	24.7576	26.7227	17.8798
0.6000	1.3323	21.8002	23.1324	21.6217
0.7000	0.8379	19.5527	20.3906	25.3394
0.8000	0.4495	17.6019	18.0514	28.9367
0.9000	0.0926	15.9026	15.9952	32.4495
1.0000	0.0000	14.4639	0.0000	35.9333